

AD-A070 935

PRATT AND WHITNEY AIRCRAFT GROUP WEST PALM BEACH FL 6--ETC F/G 20/11  
STRUCTURAL LIFE PREDICTION AND ANALYSIS TECHNOLOGY.(U)

DEC 78 T A CRUSE, T G MEYER

F33615-75-C-2063

UNCLASSIFIED

PWA-FR-10896

AFAPL-TR-78-106

NL

1 OF 2  
AD  
A070935



2  
B.S.

LEVEL

AFAPL-TR-78-106

AD A070935

# STRUCTURAL LIFE PREDICTION AND ANALYSIS TECHNOLOGY

**Authors:**

T. A. Cruse and T. G. Meyer  
Pratt & Whitney Aircraft Group  
Government Products Division  
Box 2691, West Palm Beach, Fla 33402

**DECEMBER 1978**

**Final Report      October 1975 - November 1978**

**Approved for Public Release; Distribution Unlimited**

**Prepared for**  
**Air Force Aero Propulsion Laboratory**  
**Air Force Wright Aeronautical Laboratories**  
**Air Force Systems Command**  
**Wright-Patterson Air Force Base, Ohio 45433**

DDC  
RECEIVED  
JUL 9 1979  
A

DDC FILE COPY

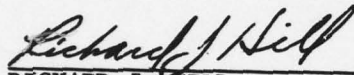


NOTICE

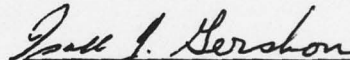
When Government drawings, specifications, or other data are used for any purpose other than in connection with a definitely related Government procurement operation, the United States Government thereby incurs no responsibility nor any obligation whatsoever; and the fact that the government may have formulated, furnished, or in any way supplied the said drawings, specifications, or other data, is not to be regarded by implication or otherwise as in any manner licensing the holder or any other person or corporation, or conveying any rights or permission to manufacture, use, or sell any patented invention that may in any way be related thereto.

This report has been reviewed by the Information Office (OI) and is releasable to the National Technical Information Service (NTIS). At NTIS, it will be available to the general public, including foreign nations.

This technical report has been reviewed and is approved for publication.

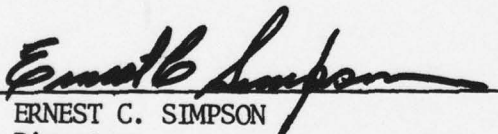


RICHARD J. HILL  
Project Engineer  
Propulsion Branch  
Turbine Engine Division



ISAK J. GERSHON  
Acting Branch Chief  
Propulsion Branch  
Turbine Engine Division

FOR THE COMMANDER



ERNEST C. SIMPSON  
Director  
Turbine Engine Division

"If your address has changed, if you wish to be removed from our mailing list, or if the addressee is no longer employed by your organization please notify AFAPL/TBP, W-PAFB, OH 45433 to help us maintain a current mailing list".

Copies of this report should not be returned unless return is required by security considerations, contractual obligations, or notice on a specific document.

UNCLASSIFIED

SECURITY CLASSIFICATION OF THIS PAGE (When Data Entered)

REPORT DOCUMENTATION PAGE		READ INSTRUCTIONS BEFORE COMPLETING FORM
1. REPORT NUMBER (18) AFAPL-TR-78-106	2. GOVT ACCESSION NO.	3. RECIPIENT'S CATALOG NUMBER
4. TITLE (and Subtitle) (6) STRUCTURAL LIFE PREDICTION AND ANALYSIS TECHNOLOGY	5. TYPE OF REPORT & PERIOD COVERED (9) Final Report Oct 1975 - Nov 1978	
7. AUTHOR(s) (10) T. A. Cruse T. G. Meyer	6. PERFORMING ORG. REPORT NUMBER FR-10896	
9. PERFORMING ORGANIZATION NAME AND ADDRESS Pratt & Whitney Aircraft Group United Technologies Corp. P.O. Box 2691 West Palm Beach, Florida 33402	8. CONTRACT OR GRANT NUMBER(s) (15) F33615-75-C-2063	
11. CONTROLLING OFFICE NAME AND ADDRESS AFAPL/TBP W-PAFB, Ohio 45433	10. PROGRAM ELEMENT, PROJECT, TASK AREA & WORK UNIT NUMBERS PE-62203F 30661229 (12) 123A	
14. MONITORING AGENCY NAME & ADDRESS (if different from Controlling Office) (16) 3066 (17) 12	12. REPORT DATE (11) December 1978	
	13. NUMBER OF PAGES 109 Pages	
	15. SECURITY CLASS. (of this report) Unclassified	
16. DISTRIBUTION STATEMENT (of this Report) Approved for public release; distribution unlimited (14) PWA-FR-10896		
17. DISTRIBUTION STATEMENT (of the abstract entered in Block 20, if different from Report)		
18. SUPPLEMENTARY NOTES		
19. KEY WORDS (Continue on reverse side if necessary and identify by block number) LCF in Disks Low Cycle Fatigue Bolt Hole Life in Disks Mission Effect on Life		
20. ABSTRACT (Continue on reverse side if necessary and identify by block number) An improved low cycle fatigue (LCF) life exhaustion method has been developed for gas turbine engine disks subjected to complex mission history loading. The method has been incorporated into a computer program for LCF life exhaustion prediction as a function of component, material, mission history, and mission ordering. → next page (CONTINUED ON REVERSE SIDE)		

DD FORM 1 JAN 73 1473 EDITION OF 1 NOV 65 IS OBSOLETE

UNCLASSIFIED

SECURITY CLASSIFICATION OF THIS PAGE (When Data Entered)

392 887

JOB

UNCLASSIFIED

SECURITY CLASSIFICATION OF THIS PAGE(When Data Entered)

20. ABSTRACT (Cont'd)

Principal advances in LCF life modeling include a simple strain range-mean stress correlation model, a predictive model for the effects of strain-hardened surface layers due to machining and the effects of dwell (creep) due to elevated temperature exposure time, a fracture mechanics-based nonlinear, cumulative damage model, a statistical basis for minimum part life prediction, and full-scale component verification. Simplified procedures for nonlinear stress (strain) analysis of notches were developed and calibrated with finite element results.

Recommendations for further research emphasize the need for improved constitutive models of cyclic creep/plasticity, a better definition of the effects of various machining operations on material work hardening, as well as residual stresses. Calibrated models for small flaw fracture mechanics would benefit the definition of the cumulative damage algorithm. Finally, the need to control process variability in order to improve part life is emphasized.

UNCLASSIFIED

SECURITY CLASSIFICATION OF THIS PAGE(When Data Entered)

## FOREWORD

The research and development effort reported herein was conducted under Air Force Contract F33615-75-C-2063, "Structural Life Prediction and Analysis Technology." The effort was sponsored by the Air Force Aero Propulsion Laboratory, Air Force Systems Command, United States Air Force, Wright-Patterson AFB, Ohio, under the direction of Mr. R. J. Hill, Project Engineer, AFAPL/TBP. The work was performed by Pratt & Whitney Aircraft Group, Government Products Division, West Palm Beach, Florida. Principal contributor to the research and development effort was Mr. T. G. Meyer, under the direction of Dr. T. A. Cruse; both authors are from the Commercial Products Division in East Hartford, Connecticut.

The authors of this report gratefully acknowledge the substantial technical contributions of the numerous individuals in both the Commercial Products Division and Government Products Division whose support made this program a success.

This report was submitted by the authors on 3 November 1978.

This technical report has been reviewed and is approved.

Accession For	
NTIS GRA&I	<input checked="checked" type="checkbox"/>
DDC TAB	<input type="checkbox"/>
Unannounced	<input type="checkbox"/>
Justification	
By _____	
Distribution/ _____	
Availability Codes	
Dist.	Avail and/or special
A	



## TABLE OF CONTENTS

Section		Page
I	INTRODUCTION	1
	1.1 Program Description	1
	1.2 Program Relevance	2
	1.3 Major Program Accomplishments	4
II	MISSION SURVEYS AND GENERIC MISSIONS	5
	2.1 Phase I – Fan Disk Missions	5
	2.2 Phase II – Turbine Disk Missions	9
III	TEST PROGRAM OVERVIEW	13
	3.1 Simple Cycle Fatigue Tests	13
	3.2 Cumulative Damage Tests	16
	3.3 Ferris Wheel Disk Tests	18
IV	CHARACTERIZATION OF LOCAL NOTCH BEHAVIOR	19
	4.1 Elastoplastic Analysis	19
	4.2 Bolt-Hole Surface Layer Response	22
	4.3 Stress Relaxation	23
V	SIMPLE CYCLE LIFE MODEL	25
	5.1 Phase I – Simple Cycle Life Correlation	25
	5.2 Phase II – Simple Cycle Life Correlation	32
VI	CUMULATIVE DAMAGE LIFE MODEL	41
	6.1 The Double-Damage Model	41
	6.2 Phase I – Cumulative Damage Tests	44
	6.2.1 TFR Specimen Testing	44
	6.2.2 Cumulative Damage Specimen Tests	45
	6.2.3 Ferris Wheel Tests	48
	6.3 Phase II – Cumulative Damage Tests	53
	6.3.1 Cumulative Damage Specimen Tests	53
	6.3.2 Ferris Wheel Tests	55
	6.4 Cumulative Damage Prediction Computer Program	61
VII	CONCLUSIONS AND RECOMMENDATIONS	63
	7.1 LCF Life Exhaustion Models	63
	7.2 Surface Layer Models and Machining Effects	64
	7.3 Dwell (Creep) Effects	64
	7.4 Cumulative Damage Model	64
	7.5 Design Models For LCF Life Exhaustion	65

## TABLE OF CONTENTS (Cont'd)

Section	Page
<b>Appendix A MATERIAL CHARACTERIZATION</b>	<b>67</b>
<b>Appendix B SURFACE LAYER ALGORITHM</b>	<b>73</b>
<b>Appendix C MEAN STRESS RELAXATION MODEL</b>	<b>75</b>
<b>Appendix D STATISTICAL CONSIDERATIONS</b>	<b>81</b>
<b>Appendix E COMPUTER PROGRAM</b>	<b>87</b>
<b>References</b>	<b>109</b>

## LIST OF ILLUSTRATIONS

Figure	Page
1 Elements of Life Prediction	1
2 Increased Replacement Costs of Compressor and Turbine Disks are Due Largely to Requirements for Higher Stressed, Lighter, More Complex Disks	3
3 Typical Fighter Aircraft Training Mission Profile	6
4 Subcycles Which Include Over 90 Percent of Speed Excursion Define an "Operating Live"	8
5 Generic Mission Loading Spectra for Test Definition	8
6 Comparison of Generic Missions and Simulated Usage in Terms of Accumulated Subcycles Versus Number of Flights	9
7 TF30-P-100 Low-Pressure Turbine Disk Stress History During a Training Mission	10
8 Turbine Disk Generic Missions	12
9 Strain Controlled (SC) Specimen (77-551-9091)	13
10 Phase I Bolt Hole (BH) Specimen, $K_T = 2.55$ (77-551-9898-5)	14
11 Phase II Bolt Hole (BH) Specimen, $K_T = 2.34$ (XPN-15021)	15
12 Simple Cycle Bolt Hole Tests	16
13 Notched Round Bar (NRB) Specimen	17
14 Cumulative Damage Bolt Hole Tests	17
15 Determination of Local Cyclic Conditions by the Neuber Calculation	19
16 Finite Element Results versus Neuber Calculation for PWA 1216 Material	20
17 Finite Element Results versus Neuber Calculation for PWA 1057 Material	21
18 Strain Calibration Curves for Neuber Calculation	21
19 Surface Layer Plastic Response	22
20 Constant Life Curves	25

## LIST OF ILLUSTRATIONS (Cont'd)

Figure		Page
21	Phase I Strain Controlled (SC) Data Correlation	27
22	Phase I SC Correlation Weibull Plots	29
23	Surface Layer and Subsurface Response for Phase I Simple Cycle Bolt Hole (BH) Tests	30
24	Correlation of Phase I SC and BH Data Using the Surface Layer Mean Stress Algorithm	30
25	Phase I Combined Data Set Weibull Plots	31
26	Prediction of Phase I BH Data Without Consideration of Surface Layer	32
27	Phase II SC Data Correlation	34
28	Phase II SC Correlation Weibull Plots	35
29	Surface Layer and Subsurface Response for Phase II Simple Cycle BH Tests	37
30	Prediction of Phase II BH Data Without Consideration of Surface Layer and Relaxation	37
31	Mean Stress Relaxation	39
32	Correlation of Phase II SC and BH Data	39
33	Phase II Combined Data Set Weibull Plots	40
34	Terrain Following Radar (TFR) Simulation	44
35	Bolt Hole Specimens Tested at $50 \pm 50$ Ksi Nominal Stress	45
36	Nonlinear Cumulative Damage Effects	47
37	Correlation of Phase I Simple Cycle and Cumulative Damage Specimen Testing	48
38	Phase I Ferris Wheel Disk	49
39	Dimension of Phase I Ferris Wheel Disk	49



## LIST OF ILLUSTRATIONS (Cont'd)

Figure		Page
40	Specimen and Ferris Wheel Surface Layer and Subsurface Response	51
41	Surface Residual Stress for the Second and Third Disks Shows the Effect of Partial Surface Layer Removal	52
42	Correlation of Phase I Specimen and Ferris Wheel Data	52
43	Phase I Overall Correlation	53
44	Subsurface Mean Stress Relaxation	54
45	Correlation of Phase II Simple Cycle and Cumulative Damage Specimen Testing	57
46	Phase II Ferris Wheel Rig	57
47	Phase II Ferris Wheel Disk in Test Rig	58
48	Dimensions of Phase II Ferris Wheel Disk	58
49	Local $\sigma$ , $\epsilon$ Response to Room Temperature Loading	60
50	Correlation of Phase II Specimen and Ferris Wheel Data	61
51	Phase II Overall Correlation	62
A-1	Strain Controlled Constitutive Test Specimen	67
A-2	Creep Specimen	67
A-3	PWA 1216 Room Temperature Monotonic Stress-Strain Curve	68
A-4	PWA 1057 Monotonic Stress-Strain Curve	68
A-5	Load-Deflection Tracing Showing Discontinuous Yielding of PWA 1057 at 900°F	69
A-6	Incremental Step Tests Used to Establish Hysteresis Curve	70

# LIST OF ILLUSTRATIONS (Cont'd)

Figure	Page
A-7 PWA 1216 Hysteresis Curve Shape	70
A-8 PWA 1057 Hysteresis Curves Show Dependence Upon Strain Range	71
A-9 PWA 1057 Hysteresis Curve Shapes	71
A-10 PWA 1057 900°F Creep Data Using Standard Creep Specimen	72
A-11 Results of PWA 1057 Cyclic Relaxation Test	72
B-1 Cyclic Loading of a Bolt Hole Specimen	74
C-1 The Component Activities in a Typical Mission	75
C-2 Simplified History of the i <sup>TH</sup> Mission Activity	76
C-3 Cyclic Test Characterization	79
D-1 Sample Weibull Distribution	83
D-2 Weibull Plot Used to Determine Life Debit Factor	84

## LIST OF TABLES

Table		Page
1	Subcycle Activity Characterization	1
2	Principal Stress Events of Turbine Disks and Generic Missions	11
3	Surface and Subsurface Stresses and Strains for Illustrative Example	23
4	Phase I Strain Controlled Specimen Simple Cycle LCF Data	26
5	Phase I Bolt Hole Specimen Single Cycle LCF Data	29
6	Phase II Strain Controlled Specimen Simple Cycle LCF Data	33
7	Phase II Bolt Hole Specimen Simple Cycle LCF Data	36
8	Phase I Cumulative Damage Specimen Test Conditions and Results	46
9	Phase I Ferris Wheel Test Conditions and Results	50
10	Phase II Cumulative Damage Specimen Test Conditions and Results	56
11	Phase II Ferris Wheel Test Conditions and Results	59

## SECTION I

### INTRODUCTION

#### 1.1 PROGRAM DESCRIPTION

The purpose of the Structural Life Prediction and Analysis Technology research and development program was to develop and verify a systematic method for predicting fatigue life exhaustion of military gas turbine engine disks on a mission utilization basis. Major emphasis was given to the evaluation of procedures for modeling structural response to mission loading, the development of a systematic fatigue life exhaustion specimen test program and improved fatigue life prediction model, and verification of the life prediction methodology with full-scale component tests. The major elements of a structural life prediction methodology are shown in Figure 1.

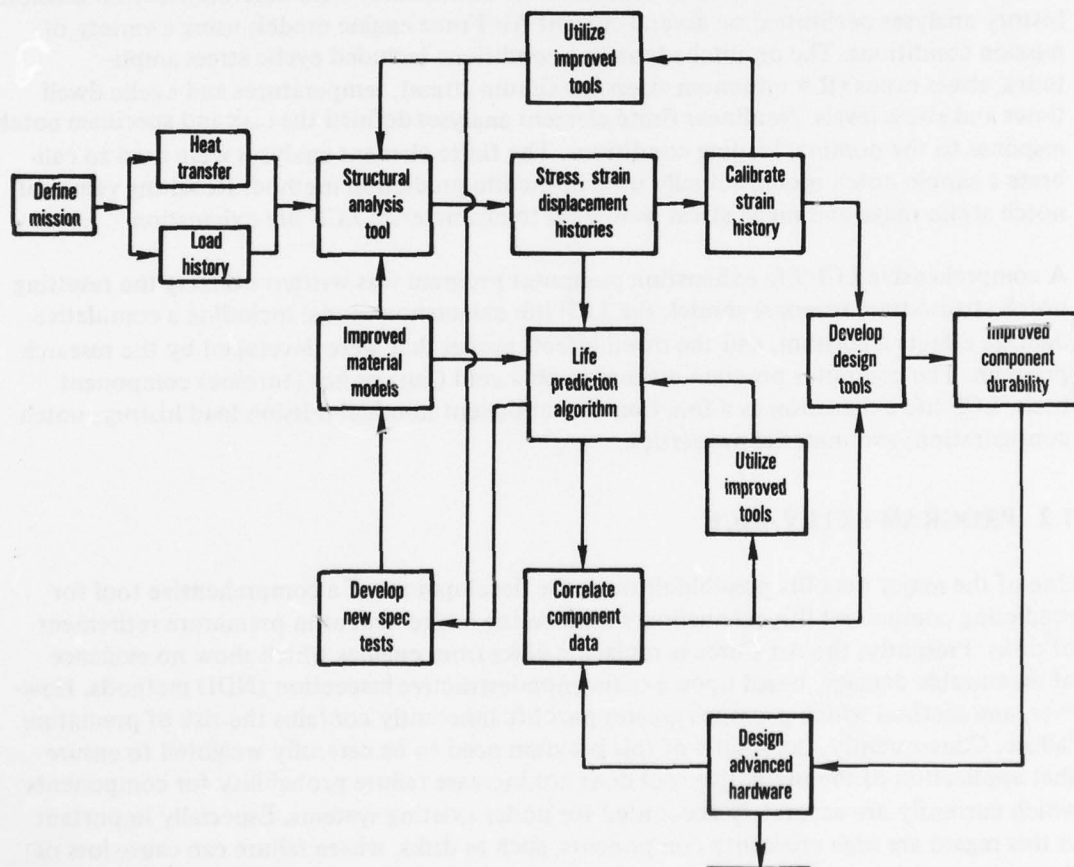


Figure 1 Elements of Life Prediction



The program was divided into two phases. The first phase concerned fan and low-pressure compressor disk environments where dwell (creep) response is minimal; the second phase concerned high-pressure compressor and turbine environments including dwell effects. Full-scale component testing for each phase utilized engine disk designs which contained low cycle fatigue (LCF) life limited bolt-holes and were tested to representative, complex cycle, mission histories. The first phase utilized a prototypical F100 fan disk geometry and titanium alloy (Ti-6Al-2Sn-4Zr-6Mo) tested in a servo-hydraulic Ferris Wheel to simulate flight loading conditions at the bolt-holes. The second phase utilized a prototypical advanced transport high-pressure turbine disk made of Waspaloy<sup>®</sup>, a nickel base superalloy.

LCF specimen testing was performed on unnotched, strain-controlled (SC) specimens, notched, load-controlled specimens including notched round bars (NRB) and the bolt-hole (BH) subcomponent specimen. All specimens were machined from the same heats of material used to obtain the full-scale disks, with one heat for each alloy.

The nominal (unnotched) loading conditions for both phases were determined from mission history analyses performed on several current Air Force engine models using a variety of mission conditions. The unnotched loading conditions included cyclic stress amplitudes, stress ratios ( $R$  = minimum stress/maximum stress), temperatures and cyclic dwell times and stress levels. Nonlinear finite element analyses defined the disk and specimen notch response to the nominal loading conditions. The finite element analyses were used to calibrate a simple notch model actually used in the life prediction method. Resulting values of notch strain range and mean stress were used to characterize LCF life exhaustion.

A comprehensive LCF life exhaustion computer program was written utilizing the resulting notch stress/strain response model, the LCF life exhaustion model including a cumulative damage effects algorithm, and the dwell effects model that were developed by the research program. The computer program estimates, on a cold (fan) or hot (turbine) component basis, LCF life exhaustion as a function of component nominal mission load history, notch configuration, and material properties.

## 1.2 PROGRAM RELEVANCE

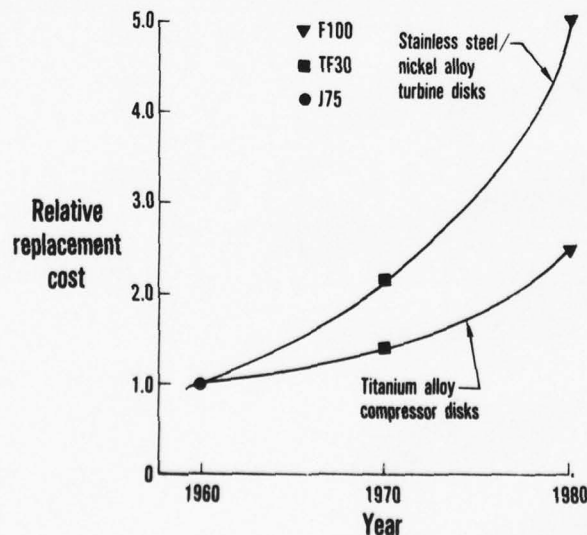
One of the major benefits possible through the development of a comprehensive tool for predicting component life exhaustion would be the improvement in premature retirement of disks. Presently, the Air Force is replacing disks from engines which show no evidence of measurable damage, based upon existing nondestructive inspection (NDI) methods. However, any method which promises greater part life inherently contains the risk of premature failure. Consequently, the results of this program need to be carefully weighted to ensure that application of the predictive tool does not increase failure probability for components which currently are accurately accounted for under existing systems. Especially important in this regard are high criticality components, such as disks, where failure can cause loss of the entire engine.

Application of the prediction tool promises a better understanding of the application of testing procedures to verify accumulated damage in real hardware. Accelerated test procedures which incorporate component normal operational fleet life exhaustion events on a one-to-one basis are impossible to design. A realistic test which verifies design goals requires a knowledge of how accelerated endurance damage accumulation is related to real time fleet damage accumulation. Procedures developed within this program could result in significant cost savings in designing endurance life verification tests. Development of these test procedures promises savings in the elimination of redesigns during the development phase of engine programs, as well as savings in avoidance of costly redesigns.

Recent occurrences of component failures resulting from fatigue related damage have had an impact on engine development programs and fleet deployment. An example is the disk lug ruptures which occurred during MQT endurance testing of the F100 engine. The MQT testing was subsequently judged to be very severe when compared to actual field usage. In other instances, cracking of engine components has occurred within a few hundred hours of operational use, even though thousands of hours of test stand running were accumulated on the engine model. The cost of retrofit of component hardware following service introduction and the attendant delays in full deployment are major concerns to both the services and the manufacturer.

No less important is the long range impact of replacement of life exhausted components. In the last 20 years, the cost of military fighter engines has multiplied by a factor of three to five, based on adjustment to 1978 dollars.

Costs of replacing disks have risen accordingly, especially for complex turbine disks. These increases are dictated largely by the requirement for higher stresses and lighter weight; this requirement necessitates use of advanced alloys and machining of complex shapes. It can be extrapolated from Figure 2 that replacement costs of future engines could reach five to ten times today's fleet replacement costs. This program provides the essential effort to obtain a comprehensive life exhaustion diagnostic tool to minimize the impact of the escalating costs of component replacements.



**Figure 2** Increased Replacement Costs of Compressor and Turbine Disks Are Due Largely to Requirements for Higher Stressed, Lighter, More Complex Disks

### 1.3 MAJOR PROGRAM ACCOMPLISHMENTS

The Structural Life Prediction and Analysis Technology research program has successfully established a basis for LCF life exhaustion modeling relevant to Air Force needs. It was established that unnotched SC specimens, together with a model for a workhardened surface layer in a machined component, can be used to predict the LCF life of machined BH specimens. Further, nonlinear cumulative damage effects were clearly established for mission-relevant load histories, and these effects have been successfully modeled using a fracture mechanics based methodology. The effects of dwell (creep) on LCF life were predicted using a simple mean cyclic stress relaxation model. These accomplishments form the basis of the cyclic life prediction algorithm.

Cost-effective numerical modeling of the bolt-hole notch was developed by calibration of a simple notch model with detailed, nonlinear finite element results. The notch model algorithm defines the cyclic stress (strain) conditions in terms of the strain range and mean stress for the material adjacent to the notch. The research program clearly established the validity of these variables for predicting LCF life exhaustion.

Finally, the resulting LCF life exhaustion model, incorporating all of these advanced features, successfully correlated the full scale component test results. Mission simulation testing of both sets of engine disks included important variations of load level, mission complexity, and mission ordering. The resulting model has been converted to a computer program for Air Force use.

The following report summarizes these accomplishments and describes the analytical and empirical models in detail. The computer program is described in separate documents<sup>1,2\*</sup>.

---

\*Superscript numbers are references (see page 109).



## SECTION II

### MISSION SURVEYS AND GENERIC MISSIONS

In order to define specimen and component test parameters appropriate to the investigation of bolt-hole fatigue behavior as experienced by service components, an extensive survey of missions typically flown by F111 and F15 aircraft was undertaken. The results of these surveys and the selection of the relevant loading cycles for each phase of the effort are discussed in this section.

#### 2.1 PHASE I – FAN DISK MISSIONS

Phase I of the contract effort is restricted to the fan disk bolt-hole region. This restriction permits us to neglect thermally induced stresses and relate bolt-hole loading and engine operating conditions solely in terms of low rotor speed,  $N_1$ . On this basis, a typical mission can be readily divided into distinct, activity associated blocks of subcycle activity, e.g., the "Touch and Go" activity of Figure 3.

Table 1 lists specific subcycle activities identified and characterizes each in terms of subcycle speed excursion and frequency of occurrence for each aircraft. The data are derived from a number of usage surveys performed by the Air Force and by Pratt & Whitney Aircraft and is judged to reflect the mix of subcycle activity in the overall Air Force Fleet. Subcycle amplitudes and levels are identified as percentage of take-off maximum low-pressure rotor speed ( $N_1$ ). The representation permits consistent comparison of subcycles experienced by different disks from different engines. The objective was to set ranges of stress variation (proportional to  $N_1^2$ ) which, when applied to the test specimens and disks, reflect the range of subcycle bolt-hole loading activity experienced in the Air Force Fleet.

Those subcycles which occur at least 100 times during 100 typical fleet missions are shown in Figure 4. From this figure it is seen that the great majority (over 90 percent) of speed excursions have a maximum speed very nearly equal to the maximum take-off speed. Thus, an "operating line" is defined along which nearly all significant subcycle activities lie.

Three generic mission profiles, Figure 5, have been defined utilizing the subcycle definition data discussed above. These profiles do not represent usage of a specific aircraft performing identified activities but are instead a composite usage profile which reflects the range of subcycle level and frequency in the Air Force Fleet. This connectivity is made evident in Figure 4 where the generic mission subcycles can be compared to the activities experienced in actual operation. In Figure 6, the missions are also compared to an operating band developed by a Monte Carlo simulation of Air Force F15 activity. The Monte Carlo simulation considers only major subcycle activity and corresponds very nearly with our Mission B. Generic Mission A shows a higher subcycle density since it includes a large number of smaller excursions which the simulation neglects.



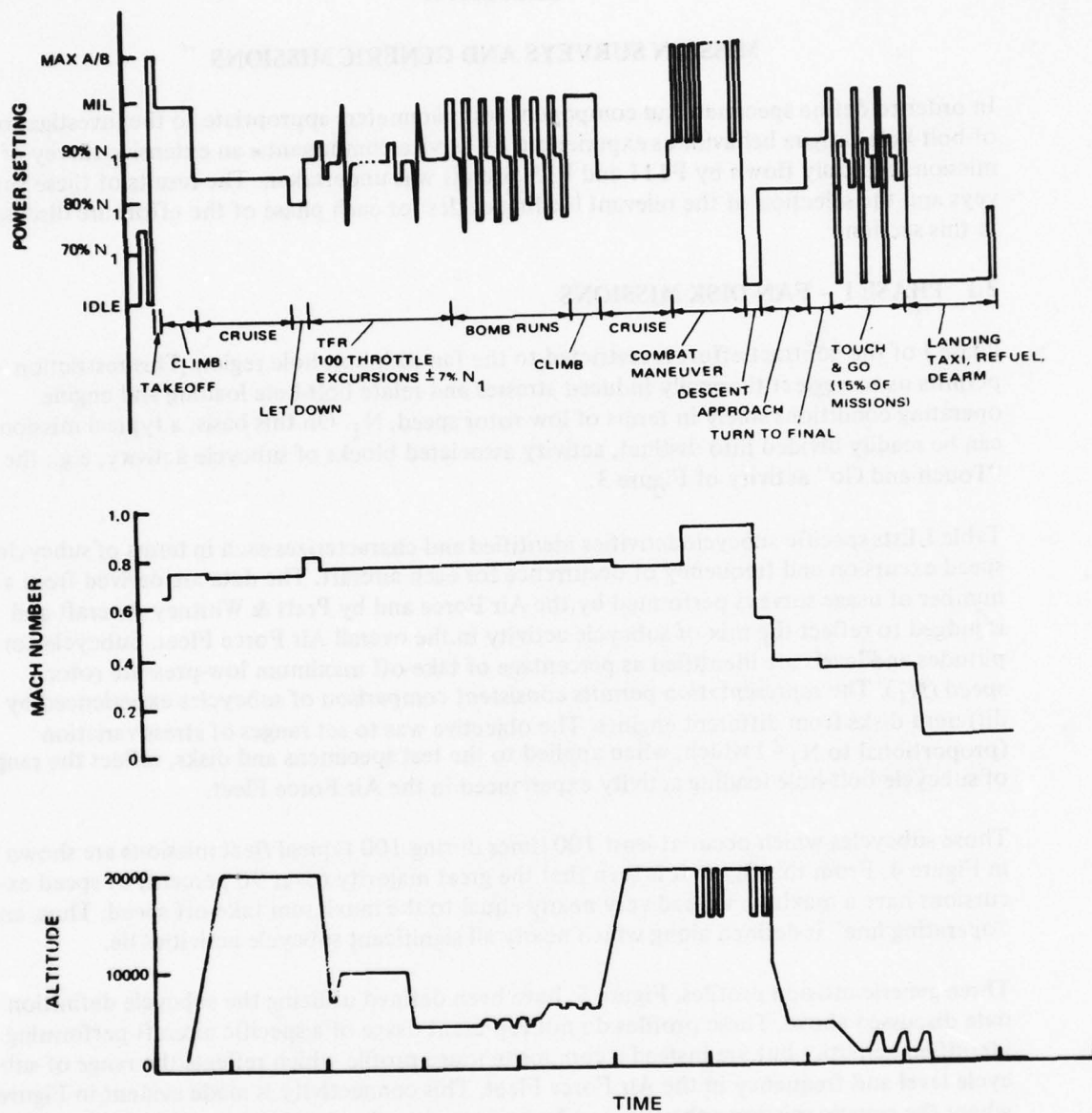


Figure 3 Typical Fighter Aircraft Training Mission Profile

TABLE 1

## SUBCYCLE ACTIVITY CHARACTERIZATION

Aircraft	Engine	Excursion Max $N_1$ (% of T/O $N_1$ )	Excursion Min $N_1$ (% of T/O $N_1$ )	Number of Excursions per 100 Flights
F111	TF30-P-7	100	0	167
		98	58	100
		98	43	466
		85	60	100
		85	55	133
	TF30-P-3	100	0	100
		100	74	2825
		98	45	475
		97	53	100
		97	74	100
	TF30-P-9	100	0	100
		97	62	2825
		95	44	475
		98	53	100
		91	65	100
	TF30-P-100	100	0	100
		96	52	63
		88	52	63
		96	88	450
		95	86	450
		98	59	360
		75-90	75-90 Random	*
		97	67	62
		93	82	16
		97	89	10
		78	62	10
		100	78	15
		97	62	360
	F100	100	0	100
		100	49	100
		99	41	200
		100	50	700
F-15	F100	100	0	100
		100	49	100
		99	41	200
		100	50	700

\*This is the random portion of TFR Activity, and therefore it is difficult to assign a number of significant excursions to the significant  $N_1$  variations.

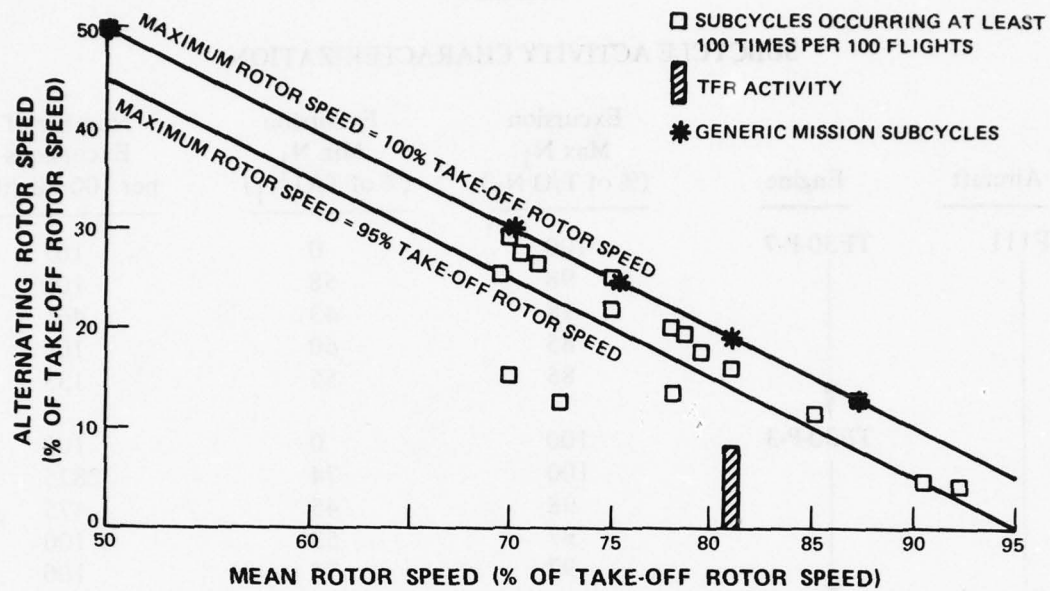


Figure 4 Subcycles Which Include Over 90 Percent of Speed Excursion Define an "Operating Life"

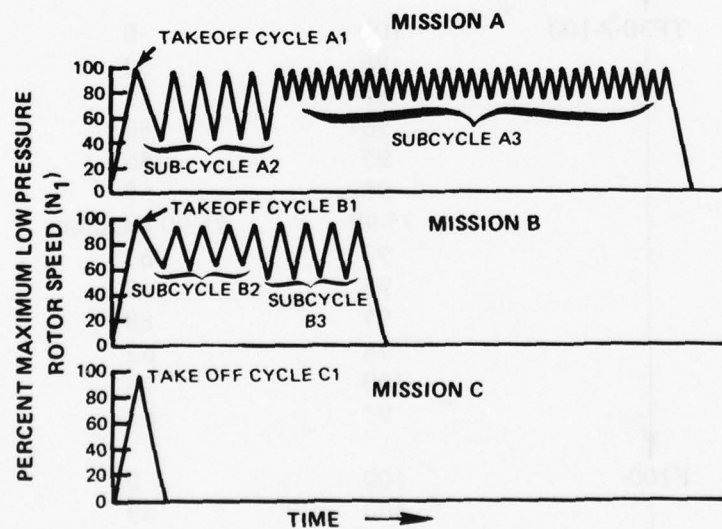


Figure 5 Generic Mission Loading Spectra for Test Definition

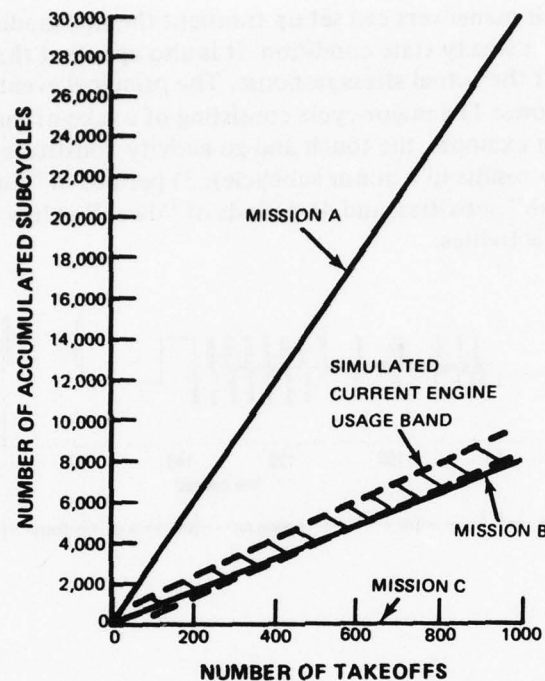


Figure 6 Comparison of Generic Missions and Simulated Usage in Terms of Accumulated Subcycles Versus Number of Flights

The loading spectra of Figure 5 have been used as the basis for the test program including both specimens and components. In addition a computer generated random loading sequence corresponding to a  $\pm 7$  percent power lever angle (PLA) excursion was used to investigate damage accumulation during a terrain following radar (TFR) activity. Specific operating line levels were chosen to provide for loading levels and test durations of interest and will be detailed in subsequent sections of this report.

## 2.2 PHASE II – TURBINE DISK MISSIONS

Turbine disk bolt-hole stresses respond to both mechanical loading (high-pressure rotor speed,  $N_2$ ) and local temperature gradients. Unlike the fan disk bolt-hole response discussed in the previous section, turbine disk stress excursions during a mission are not generally proportional to  $N_2^2$ . In order to properly evaluate the mission usage of turbine disk bolt holes, a complete flight analysis, including the effects of changing rotor speed and temperature gradients, is essential. Such analyses have been performed for four turbine disks and serve as the basis for selection of relevant test loadings in this program.

Figure 7 shows the stress response of the TF30-P-100 third-stage turbine disk bolt hole as used in the Training Mission shown in Figure 3. Also noted in Figure 7 are the approximate bolt-hole operating temperatures during the various mission activities. The effect of changing disk thermal gradients during an activity are apparent in the “bomb-run” and “touch and



go" activities. Rapid air maneuvers can set up transient thermal gradients which may require several cycles to reach a steady state condition. It is also apparent that simple scaling by  $N_2^2$  would not predict the actual stress response. The principal events in the stress history can be grouped as follows: 1) a major cycle consisting of a take-off and landing; 2) subcycles, of varying severity (for example, the touch and go activity constitutes a major subcycle while the TFR activity results in a minor subcycle); 3) periods of "dwell" at high stress occurring during "climb" activities; and 4) periods of "dwell" at low stress occurring during "approach" or "taxi" activities.

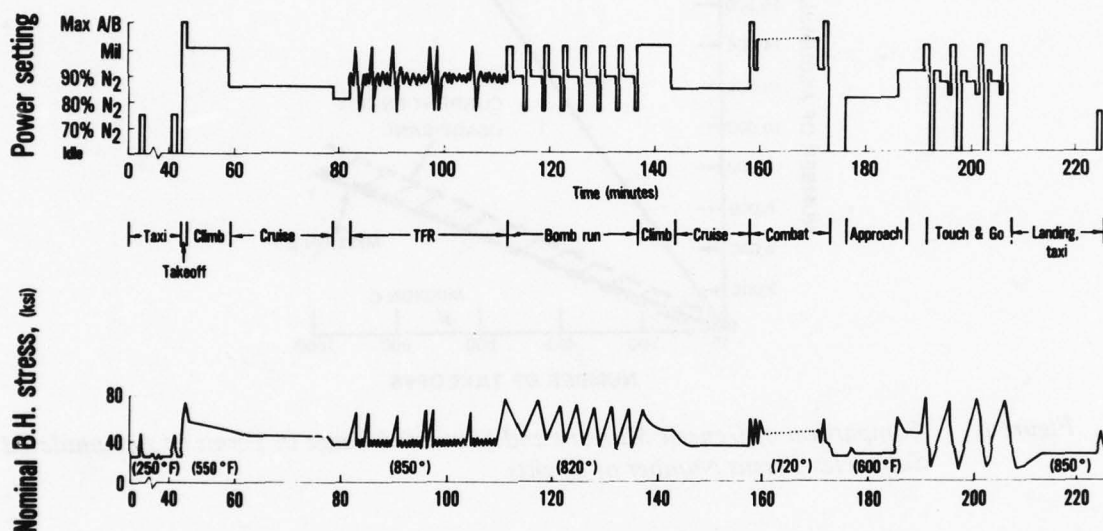


Figure 7 TF30-P-100 Low-Pressure Turbine Disk Stress History During a Training Mission

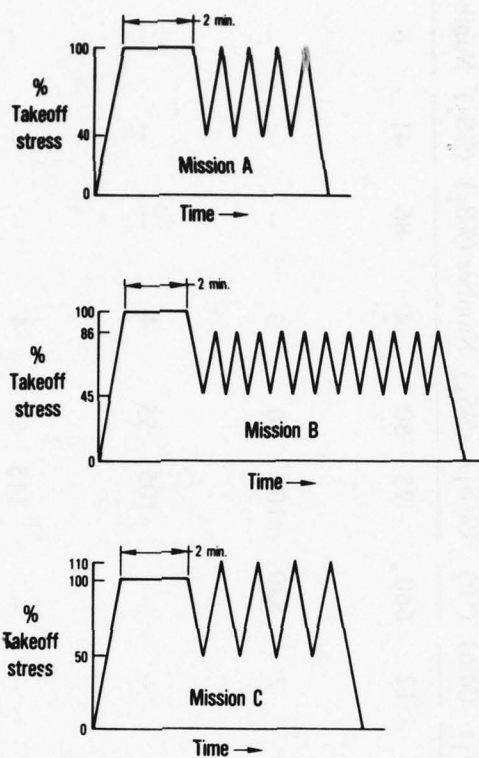
Principal stress events for the four disks analyzed are shown in Table 2. The TFR activity is listed as the minor subcycle for the TF30-P-100 low-pressure turbine (LPT) disk because its amplitude is comparable to both TFR and bomb-run activities, thus representing a significant damage event which is substantially different from the major subcycle. It should also be noted that since actual TF30-P-9 and TF30-P-100 high-pressure turbine (HPT) disks do not have bolt holes, the nominal stresses and temperatures listed in Table 2 were computed at a typical bolt circle radius.

Three generic missions were chosen to represent the principal stress events listed in Table 2. These missions are shown in Figure 8, and their principal events for the Ferris Wheel (F/W) disk used in this program are also listed in Table 2. Absolute levels of stress will be discussed in subsequent sections of this report. Low stress dwell is not included in these missions because the low stress and temperature levels were judged insufficient to produce significant time dependent material response. The generic missions serve to investigate the interaction of dwell periods and subcycles and the effect of stress "overloads" on the dwell effect.

TABLE 2

## PRINCIPAL STRESS EVENTS OF TURBINE DISKS AND GENERIC MISSIONS

Disk	Take-Off		High Stress Dwell			Low Stress Dwell			Major Subcycle		Minor Subcycle			
	Max. Nominal Stress ~ S <sub>1</sub> (ksi)	Temp. (°F)	Stress (% S <sub>1</sub> )	Time (Min)	Temp. (°F)	Stress (% S <sub>1</sub> )	Time (Min)	Temp. (°F)	Max. Stress (% S <sub>1</sub> )	Stress Range (% S <sub>1</sub> )	Number	Max. Stress (% S <sub>1</sub> )	Stress Range (% S <sub>1</sub> )	Number
TF30-P-100 LPT	78	550	66	5	680	35	12	660	95	80	4	86	41	6
F100 2T HPT	90	970	97	2	1100	50	2	530	108	50	3	—	—	—
TF30-P-9 HPT Mock B/H	66	960	—	—	—	—	—	—	105	55	4	—	—	—
TF30-P-100 HPT Mock B/H	71	950	—	—	—	—	—	—	115	68	4	—	—	—
Mission A	—	900	100	2	900	Not Used			100	60	4	Not Used		
Mission B	—	900	100	2	900	Not Used			Not Used			86	41	11
Mission C	—	900	100	2	900	Not Used			110	60	4	Not Used		



**Figure 8** Turbine Disk Generic Missions

### SECTION III

#### TEST PROGRAM OVERVIEW

The development of the cumulative damage models in the contract involved three major areas of fatigue testing and prediction. First, basic material fatigue data were obtained for simple cycle loading. Cumulative damage specimen tests were conducted next to identify the cumulative damage mechanisms. Finally, the cumulative damage models were substantiated with complex mission testing of component-like disks.

#### 3.1 SIMPLE CYCLE FATIGUE TESTS

The Strain Controlled (SC) specimen shown in Figure 9 was used to develop a basic simple cycle fatigue life prediction equation. This specimen was used because gage section stresses and strains are known explicitly for each test and thus allow the development of a fatigue system which is independent of notch geometry and notch stress/strain estimation. The SC specimens were electrochemically machined to achieve a stress free surface.

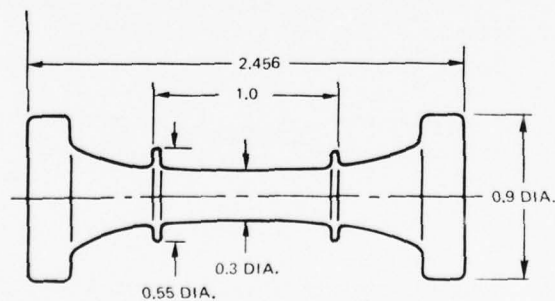
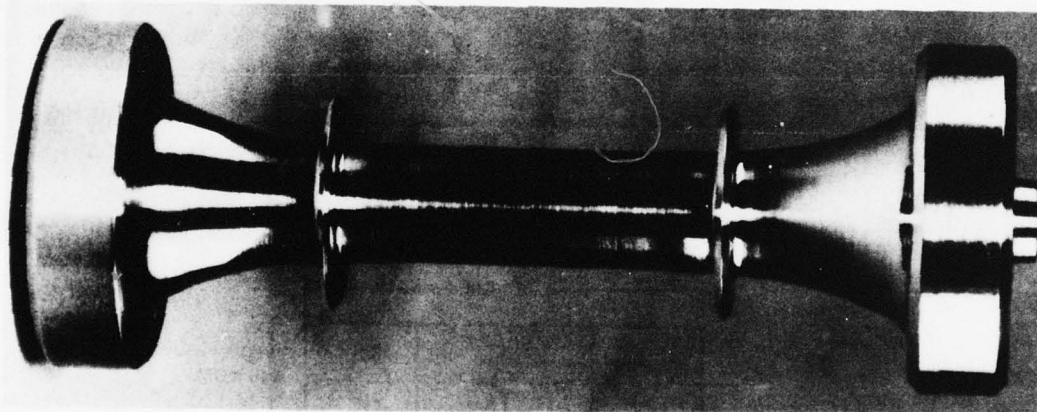


Figure 9 Strain Controlled (SC) Specimen (77-551-9091)



The Bolt Hole (BH) specimens shown in Figures 10 and 11 were used to find the relation between the simple cycle LCF behavior of bolt holes and the smooth SC specimens. From these back-to-back tests, the presence of a bolt-hole surface residual stresses was inferred in both the PWA 1216 and PWA 1057 bolt holes. A surface residual stress algorithm which accounts for the effect of the residual stress and the cyclic hardened condition of the surface layer was developed and is described in Appendix B. The use of this algorithm showed that the basic fatigue behavior equation developed with the SC specimen was applicable to the BH specimens as well. This merging of the SC and BH fatigue data confirmed the expectation that fatigue behavior prediction can effectively be transferred from specimens to components if the local notch mechanical conditions are accurately known.

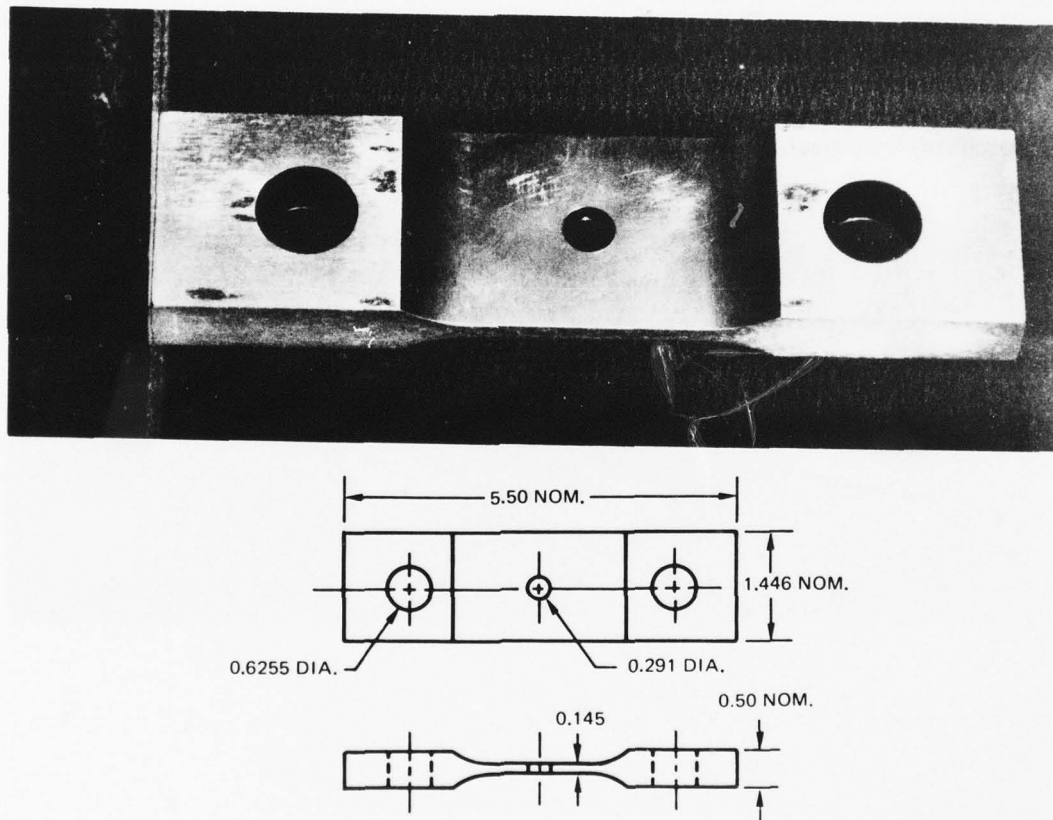


Figure 10 Phase I Bolt Hole (BH) Specimen,  $K_T = 2.55$  (77-551-9898-5)

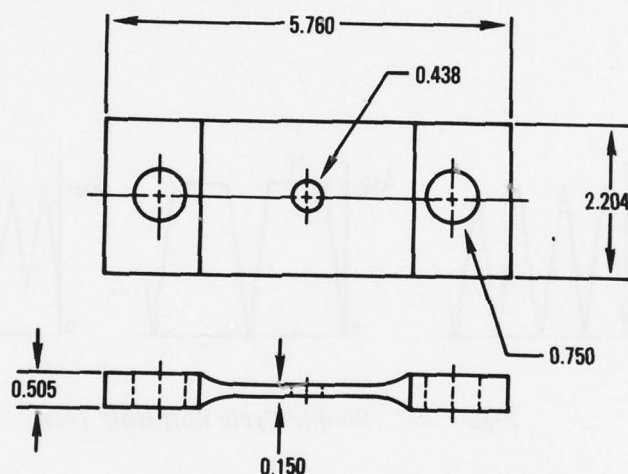
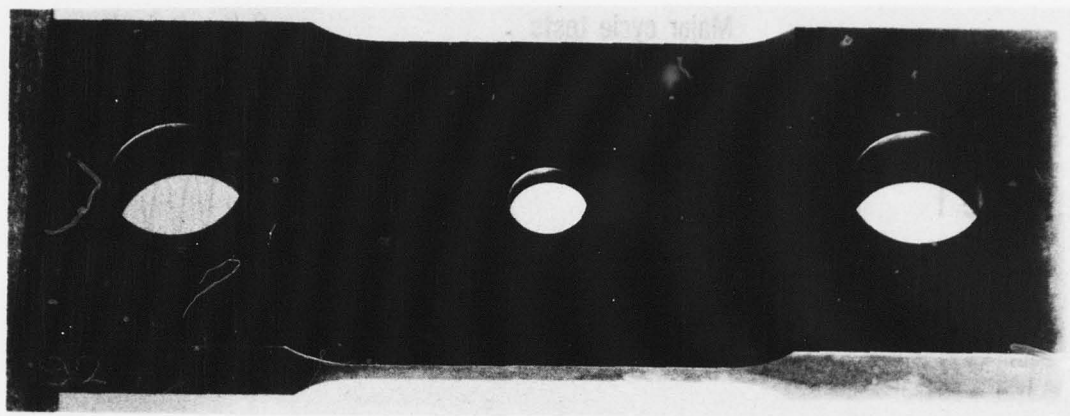


Figure 11 Phase II Bolt Hole (BH) Specimen,  $K_T = 2.34$  (XPN-15021)

The simple cycle bolt-hole test conditions were chosen to simulate principal component usage identified in the mission surveys discussed in Section II. Bolt-hole specimen loading cycles are shown schematically in Figure 12.

In Phase I testing, the principal features were major cycle tests corresponding to take-off and landing and various amplitudes of subcycle testing corresponding to in-flight activities. Two levels of maximum nominal stress ( $S_{max}$ ) were evaluated in the major cycle tests, and two levels of nominal stress range,  $\Delta S$ , were tested in the subcycle tests. All tests were conducted at room temperature.

In Phase II, major cycle tests with and without the effect of high stress dwell, and subcycle tests without dwell were conducted. Three levels of  $S_{max}$  and three levels of  $\Delta S$  were evaluated. All tests were conducted isothermally at 900°F to simulate engine environment.

Details of the testing and fatigue model are discussed in Section V.

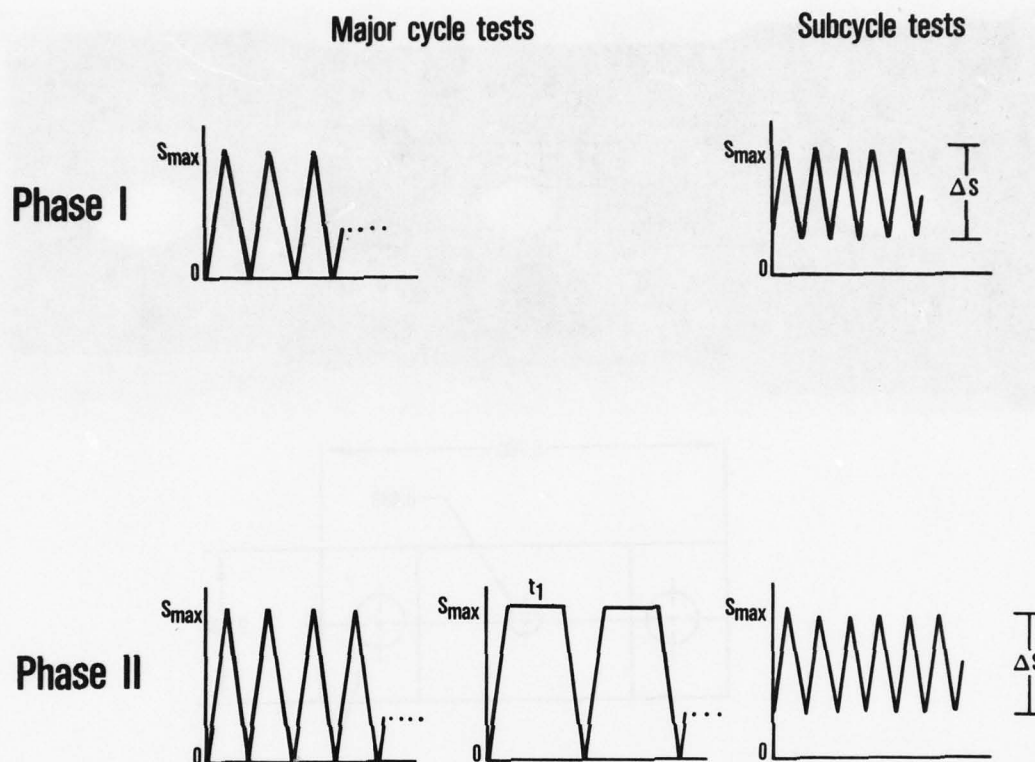


Figure 12 Simple Cycle Bolt Hole Tests

During Phase I, a limited number of simple cycle LCF tests were conducted using the notched round bar (NRB) specimen shown in Figure 13. However, elastoplastic finite element analysis of this specimen showed that the stress-strain response of the notch was significantly different in character from the response of either the SC or BH specimens due to a very high degree of biaxiality in the notch. These results were previously reported<sup>3</sup>. The incorporation of the data was therefore inappropriate for the development of a bolt-hole life prediction model. Consequently, no NRB tests were conducted during Phase II of this contract, and NRB behavior will not be considered in this report.

### 3.2 CUMULATIVE DAMAGE TESTS

Cumulative damage investigations were conducted using various combinations of test conditions already characterized in the simple cycle testing program. Only two sorts of cumulative damage tests are possible; block loading or sequenced tests as shown schematically in Figure 14. Nearly all testing was of the block loading type in which load ordering effects can easily be observed. The sequenced test does not evaluate the effect of ordering.

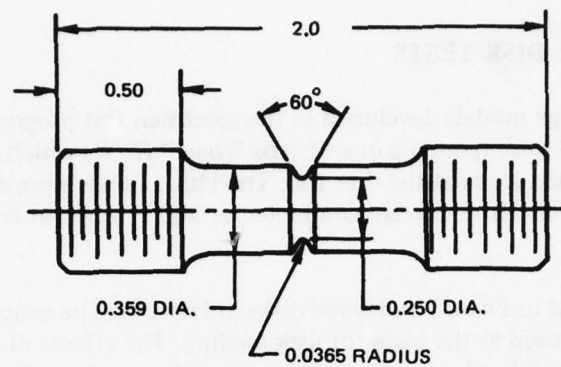


Figure 13 Notched Round Bar (NRB) Specimen

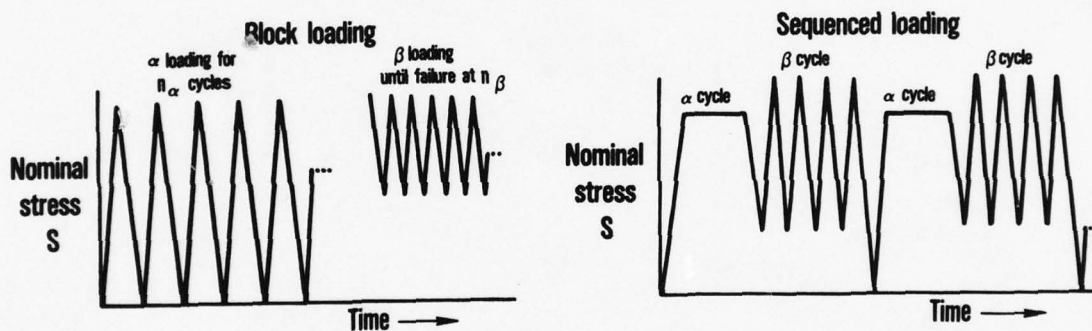


Figure 14 Cumulative Damage Bolt Hole Tests

In both Phase I and Phase II, the block loading tests revealed a strong influence due to ordering which was modeled successfully by double-damage concepts. In Phase II, the effect of the dwell cycle was also found to be modeled properly by double-damage concepts.

The test conditions were chosen to reflect the ordering effects of interest identified by the mission surveys. For example, the effect of a stress overload following a dwell cycle was investigated in both block loading and sequenced tests during Phase II.

Details of the cumulative damage specimen testing are discussed in Section VI.



### 3.3 FERRIS WHEEL DISK TESTS

The cumulative damage models developed in the specimen test program were verified by testing of full-size disk-like components in a "Ferris Wheel" (F/W) which simulates engine loading through radially applied loads at the disk rim. The Phase I tests were conducted at room temperature, while the Phase II tests were conducted at 900°F without temperature gradients at the bolt circle.

Four disks were tested in Phase I and three disks in Phase II. The generic missions shown in Figures 5 and 8 were used as the basis for disk loading. The effects of mission mixture and different maximum load levels were included to provide a reasonably comprehensive test of the cumulative damage prediction model.

The F/W tests are discussed in detail in Section VI.

## SECTION IV

### CHARACTERIZATION OF LOCAL NOTCH BEHAVIOR

Accurate characterization of local bolt-hole mechanical conditions such as strain range and mean stress is fundamental to accurate LCF life prediction of the hole. Because the operating load levels for engine disks often result in local plastic deformation at the bolt hole, elastoplastic stress analyses are essential. In addition, the operating temperatures and stresses in turbine disk bolt holes are often sufficiently high to cause time dependent material nonlinear behavior. Calculation of local notch stresses and strains in the presence of these two nonlinear effects are described below.

#### 4.1 ELASTOPLASTIC ANALYSIS

Two nonlinear models were used in this contract to predict local mechanical variables for both monotonic and cyclic plastic response. The first model is the well-known Neuber model<sup>4</sup>. The stress concentration and strain concentration factors, given by

$$K_{\sigma} = \sigma/S,$$

$$K_{\epsilon} = \epsilon E/S$$

are related by the elastic value of the stress concentration factor,  $K_t$

$$K_{\sigma} K_{\epsilon} = K_t^2 \quad (1)$$

Equation (1) defines a Neuber hyperbola for a given applied nominal stress ( $S$ ). The intersection of the Neuber hyperbola and the stress-strain curve defines the local notch stress and strain values as shown in Figure 15.

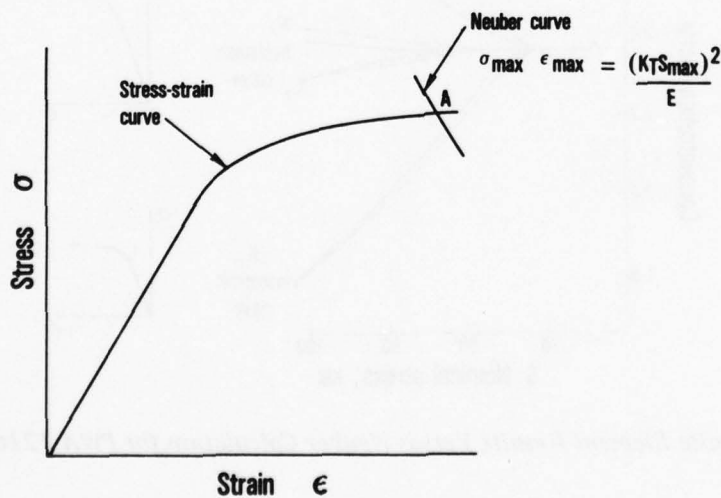


Figure 15 Determination of Local Cyclic Conditions by the Neuber Calculation

The second model is an elastoplastic finite element analysis using the MARC\* computer program. The finite element analysis was judged to be the most accurate characterization method, but was too cumbersome for routine calculations. The Neuber notch model was judged to be extremely efficient, but had to be modified by the finite element results to obtain necessary levels of modeling accuracy.

Comparison of the two models for the BH specimens is shown in Figures 16 and 17 in terms of the local strain concentration ( $K_\epsilon$ ) and stress concentration ( $K_\sigma$ ) factors. The comparison is made at a material location just below the bolt-hole surface which corresponds to the location of the nearest finite element stress solution point. The comparison is judged to be valid also for the bolt-hole surface itself. The comparison is given for both the monotonic stress-strain curve and the hysteresis curve for the material tested in Phase I and for the monotonic curve used in Phase II. Details of the stress-strain curves are given in Appendix A. It is properly concluded that the Neuber model gives good results for local stress and strain values so long as the stress-strain curve exhibits a high degree of strain hardening (i.e., the stress-strain curve is relatively "steep") and can, therefore be used with the hysteresis curves. However, use of the Neuber model with the monotonic curves (low strain hardening) is seen to lead to significant over-estimation of strains. Figures 16 and 17 can be used to modify or correct the Neuber calculation. The Neuber correction curves for the bolt-hole specimens responding to the monotonic stress-strain curves are given in Figure 18. The Neuber approach, properly corrected for use with the monotonic stress-strain curves, was used in both Phase I and Phase II of the contract.

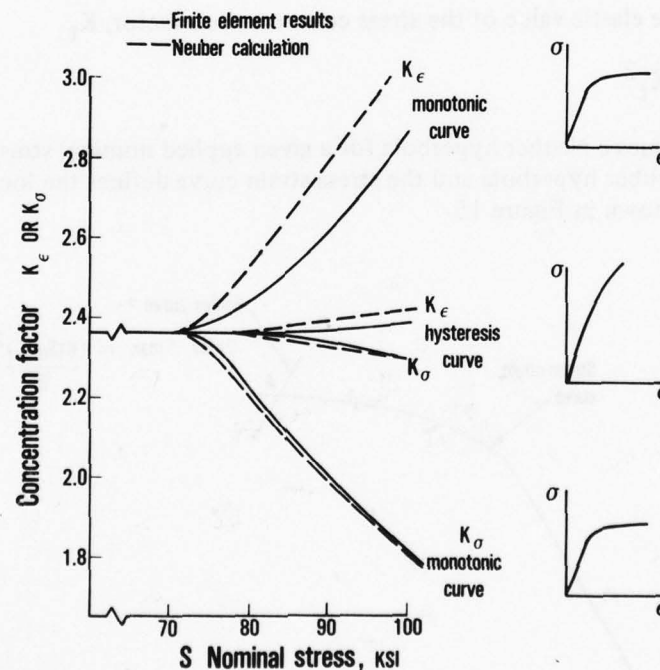


Figure 16 Finite Element Results Versus Neuber Calculation for PWA 1216 Material

\*The MARC general purpose, nonlinear finite element code, MARC Analysis Corporation, Providence, R. I.

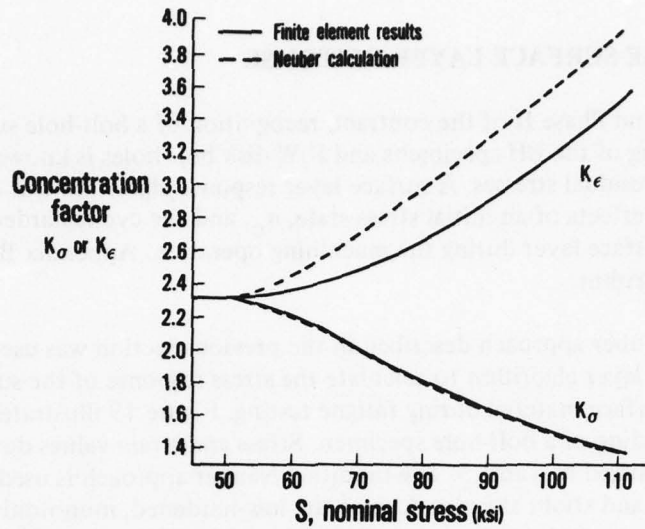


Figure 17 Finite Element Results Versus Neuber Calculation for PWA 1057 Material

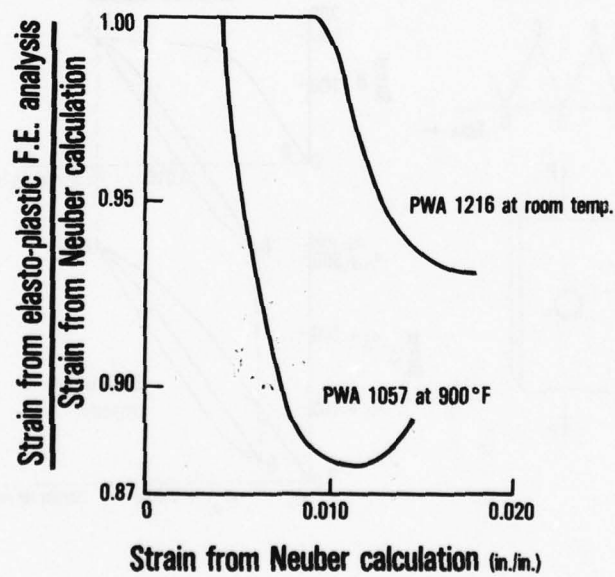


Figure 18 Strain Calibration Curves for Neuber Calculation



## 4.2 BOLT-HOLE SURFACE LAYER RESPONSE

In both Phase I and Phase II of the contract, recognition of a bolt-hole surface layer was crucial. Machining of the BH specimens and F/W disk bolt holes is known to introduce compressive surface residual stresses. A surface layer response algorithm was developed which accounts for the effects of an initial stress state,  $\sigma_0$ , and the cyclic hardened condition developed in the surface layer during the machining operation. Appendix B provides an explanation of this algorithm.

The modified Neuber approach described in the previous section was used in conjunction with this surface layer algorithm to calculate the stress response of the surface layer and the underlying subsurface material during fatigue testing. Figure 19 illustrates the method for two cycles of loading of a bolt-hole specimen. Stress and strain values during the cycle for this example are listed in Table 3. The modified Neuber approach is used to calculate the subsurface stress and strain at point A since the low-hardened, monotonic curve is involved. Subsequent stress excursions, from A to B and from B to C for both surface and subsurface, follow the high-hardened, hysteresis curve, so the Neuber calculation need not be modified.

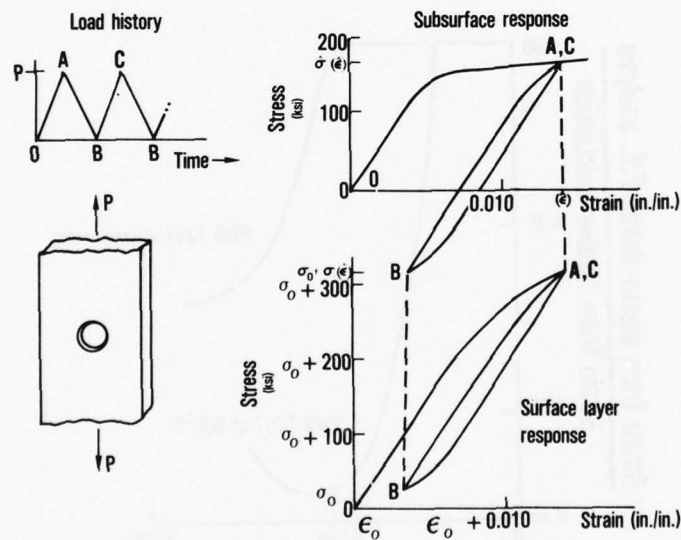


Figure 19 Surface Layer Plastic Response

TABLE 3  
SURFACE AND SUBSURFACE STRESSES AND STRAINS  
FOR ILLUSTRATIVE EXAMPLE

Reference Point in Load History	Surface Layer		Subsurface Layer	
	Stress	Strain	Stress	Strain
O	$\sigma_o$	$\epsilon_o$	O	O
A	$\sigma_o + \sigma(\hat{\epsilon})$	$\hat{\epsilon} + \epsilon_o$	$\hat{\sigma}(\hat{\epsilon})$	$\hat{\epsilon}$
B	$\sigma_o + \sigma(\hat{\epsilon}) - \sigma(\Delta\epsilon)$	$\hat{\epsilon} - \Delta\epsilon + \epsilon_o$	$\hat{\sigma}(\hat{\epsilon}) - \sigma(\Delta\epsilon)$	$\hat{\epsilon} - \Delta\epsilon$
C	$\sigma_o + \sigma(\hat{\epsilon})$	$\hat{\epsilon} + \epsilon_o$	$\hat{\sigma}(\hat{\epsilon})$	$\hat{\epsilon}$

#### 4.3 STRESS RELAXATION

The temperatures and stress levels experienced in turbine disks and in the test conditions of Phase II were sufficiently severe to cause noticeable creep in a standard creep specimen as reported in Appendix A. In a strain controlled environment, the material's nonlinear behavior will be exhibited as a stress relaxation. Two cyclic relaxation tests of the Phase II material, PWA 1057, were conducted using the SC specimen shown in Figure 9. These data, reported in Appendix A, showed that the mean stress during cycling decayed exponentially and the relaxation of the mean stress,  $\bar{\sigma}_R$ , could be written as

$$\bar{\sigma}_R = \sigma_m^o (e^{-0.002T} - 1) \quad (2)$$

where:  $\sigma_m^o$  is the time averaged mean stress in the first cycle and T is the total time spent at the maximum strain limit during cycling.

Since all testing under Phase II was isothermal, the assumption is made that the exponential decay rate is the same for all stress levels and the relaxation is given by (2). A complete derivation of  $\bar{\sigma}_R$  for complex missions and simple cycle tests is provided in Appendix C. The relaxation of both surface and subsurface stresses is recognized fully in the simple cycle and complex cycle LCF life predictions in the Phase II effort.

## SECTION V

### SIMPLE CYCLE LIFE MODEL

A mathematically simple model has been used to correlate the simple cycle LCF data. The model recognizes that LCF life is dependent upon the severity of the hysteresis activity experienced locally, measured in terms of the local strain range,  $\Delta\epsilon$ , and the mean stress value,  $\sigma_m$ , at which this activity occurs. The life correlating model is given by

$$N = A \Delta\epsilon^B 10^{C\sigma_m} \quad (3)$$

where  $N$  is the LCF life, and  $A$ ,  $B$ , and  $C$  are material dependent constants. Constant life curves from (3) are shown in Figure 20.

This section discusses the specific use of (3) in correlating the simple cycle LCF data in Phase I and Phase II.

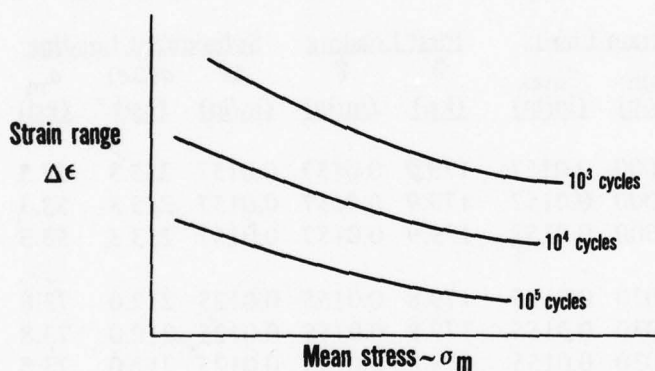


Figure 20 Constant Life Curves

#### 5.1 PHASE I – SIMPLE CYCLE LIFE CORRELATION

During Phase I PWA 1216 strain controlled specimens (Figure 9) of a single heat code (CAAZ) were cycled between fixed strain limits and periodically inspected to establish the number of cycles,  $N$ , needed to initiate a 1/32 inch surface length crack. Table 4 provides a list of test conditions and resulting LCF lives for each specimen. Also included in Table 4 are the corresponding values of stress and strain occurring during the first loading and during subsequent cycling between the strain limits. The values of stress listed here were obtained directly from the monotonic and hysteresis curves given in Appendix A and do not involve any nonlinear analysis. The mean stress level,  $\sigma_m$ , is given by

$$\sigma_m = \hat{\sigma} - \frac{1}{2} \sigma(\Delta\epsilon) \quad (4)$$

where  $\hat{\sigma}$  is the maximum stress occurring during the first loading cycle obtained from the monotonic stress strain curve, and  $\sigma(\Delta\epsilon)$  is the cyclic stress resulting from the strain excursion  $\Delta\epsilon$  obtained from the hysteresis stress strain curve.

The logarithmic form of (3),

$$\log N = \log A + B \log \Delta\epsilon + C\sigma_m \quad (5)$$

lends itself to standard multivariate linear regression techniques in which  $\log \Delta\epsilon$  and  $\sigma_m$  are treated as the independent variables. Appendix D contains a discussion of multivariate regression analyses. The constants  $\log A$ ,  $B$ , and  $C$  determined by such an analysis can be identified in the following equation.

$$\log N = -8.0979 - 6.7319 \log \Delta\epsilon - 0.020306 \sigma_m \quad (6)$$

TABLE 4

PHASE I STRAIN CONTROLLED SPECIMEN  
SIMPLE CYCLE LCF DATA

Test Condition	Strain Limits		First Loading		Subsequent Loading			Actual Life (cycles)	Predicted Life* (cycles)
	$\epsilon_{\min}$ (in/in)	$\epsilon_{\max}$ (in/in)	$\hat{\sigma}$ (ksi)	$\hat{\epsilon}$ (in/in)	$\Delta\epsilon$ (in/in)	$\sigma(\Delta\epsilon)$ (ksi)	$\sigma_m$ (ksi)		
SC1	0.0000	0.0157	179.9	0.0157	0.0157	253.3	53.3	740	960
	0.0000	0.0157	179.9	0.0157	0.0157	253.3	53.3	750	960
	0.0000	0.0157	179.9	0.0157	0.0157	253.3	53.3	850	960
SC2	0.0030	0.0155	179.8	0.0155	0.0125	212.0	73.8	1,800	1,700
	0.0030	0.0155	179.8	0.0155	0.0125	212.0	73.8	2,000	1,700
	0.0030	0.0155	179.8	0.0155	0.0125	212.0	73.8	2,400	1,700
SC3	0.0062	0.0155	179.8	0.0155	0.0093	162.8	98.4	2,800	3,800
	0.0062	0.0155	179.8	0.0155	0.0093	162.8	98.4	2,800	3,800
	0.0062	0.0155	179.8	0.0155	0.0093	162.8	98.4	3,400	3,800
	0.0062	0.0155	179.8	0.0155	0.0093	162.8	98.4	3,600	3,800
SC4	0.0010	0.0103	173.3	0.0103	0.0093	162.8	91.9	5,700	5,200
	0.0010	0.0103	173.3	0.0103	0.0093	162.8	91.9	8,700	5,200
	0.0010	0.0103	173.3	0.0103	0.0093	162.8	91.9	9,400	5,200
SC5	0.0000	0.0093	162.8	0.0093	0.0093	162.8	81.4	6,600	8,600
	0.0000	0.0093	162.8	0.0093	0.0093	162.8	81.4	8,000	8,600
	0.0000	0.0093	162.8	0.0093	0.0093	162.8	81.4	11,000	8,600
	0.0000	0.0093	162.8	0.0093	0.0093	162.8	81.4	11,500	8,600
SC6	0.0002	0.0093	162.8	0.0093	0.0073	127.8	98.9	12,500	19,100
	0.0002	0.0093	162.8	0.0093	0.0073	127.8	98.9	18,100	19,100

\* using equation (5) with fatigue constants (10)



The SC data correlation and the 95 percent confidence band is shown in Figure 21. The confidence band shows the limits of lives within which a data point would be expected to fall 95 percent of the time based on the accuracy of the prediction model (6). Figure 21 shows that the good correlation has been achieved for the data set taken as a whole and that the correlation of individual groups of data is quite consistent.

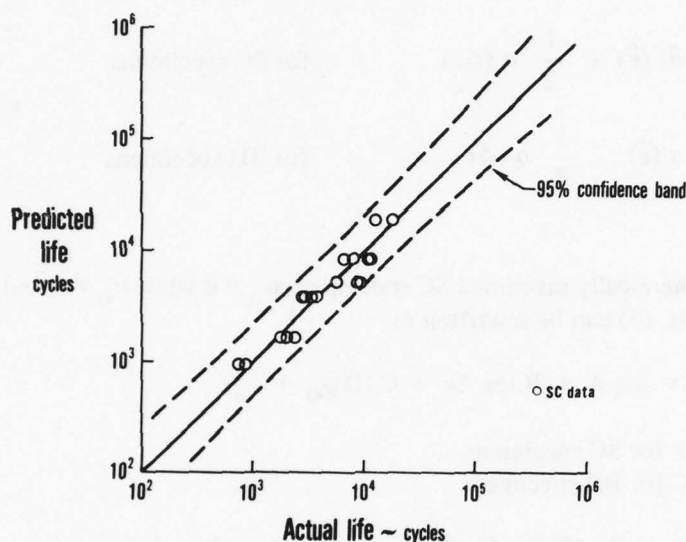


Figure 21 Phase I Strain Controlled (SC) Data Correlation

Figure 22 compares the Weibull distributions for the data as correlated with (6) and for a "perfect" correlation model. (See Appendix D for further discussions of the Weibull distribution.) The additional scatter introduced by the correlation model (indicated by the decrease in slope  $\beta$ ) is not judged to be excessive, especially in view of the relative simplicity of the correlation model. Furthermore, the Weibull distribution is continuous, and Table 4 reveals no patterns of consistently poor correlation for any particular subset of the data. The overall correlation is judged to be very good.

Bolt-hole specimens, as shown in Figure 10, were loaded cyclicly between fixed nominal stress levels and periodically inspected to establish the 1/32 inch crack life. Table 5 lists the test conditions and actual lives. Included in Table 5 are the stresses and strains used to characterize the local notch behavior. The values are calculated using the appropriate modified Neuber calculation and the surface residual stress algorithms discussed in Section IV and Appendix B. Figure 23 illustrates the hysteresis activities for each test condition in  $\sigma$ - $\epsilon$  space. The mean stress of the surface layer is given by

$$\sigma_m = \sigma_o + \sigma(\bar{\epsilon}) - \frac{1}{2} \sigma(\Delta\epsilon) \quad (7)$$

The value of  $\sigma_o$  is not known explicitly but was found through regression techniques as follows.

The mean stress for both SC and BH specimens is composed of two parts:  $\sigma_o$ , an initial stress state, and  $\sigma_a$ , the stress excursions from the initial stress state to the mean stress level. That is

$$\sigma_m = \sigma_o + \sigma_a \quad (8)$$

$$\text{where } \sigma_a = \hat{\sigma}(\hat{\epsilon}) - \frac{1}{2} \sigma(\Delta\epsilon) \quad \text{for SC specimens}$$

$$\sigma_a = \sigma(\hat{\epsilon}) - \frac{1}{2} \sigma(\Delta\epsilon) \quad \text{for BH specimens}$$

For the electrochemically machined SC specimens,  $\sigma_o = 0$  while  $\sigma_o \neq 0$  but is unknown for the BH specimens. (5) can be rewritten as

$$\log N = \log A + B \log \Delta\epsilon + C(D\sigma_o + \sigma_a) \quad (9)$$

$$\begin{aligned} \text{where } D &= 0 \text{ for SC specimens} \\ D &= 1 \text{ for BH specimens} \end{aligned}$$

This equation reduces to (3) for the SC specimens. A multivariate regression analysis with three independent variables, ( $\log \Delta\epsilon$ ,  $\sigma_a$ , and  $D$ ) for each data point, will yield the constants  $\log A$ ,  $B$ ,  $C$  and  $C\sigma_o$  for the combined BH plus SC data set. The value of  $\sigma_o$  can then be easily calculated. The values for such a regression analysis are as follows:

$$\begin{aligned} \log A &= -8.0508 \\ B &= -6.7195 \\ C &= -0.020476 \\ \sigma_o &= -136.1 \end{aligned} \quad (10)$$

It is clear that the material fatigue constants,  $\log A$ ,  $B$ , and  $C$ , agree very closely with those obtained from considering the SC data only, (6). Predicted values of life using constants from the combined data set, are shown in Tables 4 and 5. Figure 24 shows that the overall correlation of the combined data set is excellent; all data points lie well within the 95 percent confidence band expected for SC data only, and the mean lives of each data set are correlated very well. The Weibull plot of Figure 25 shows that the scatter in the overall correlation is not significantly larger than the inherent scatter in the data. It is, in fact, closer to the scatter in a perfect correlation than was achieved by the SC data alone, see Figure 22. This is due to a better definition of the scatter resulting from a larger population and the obvious success of the merger of the BH and SC data sets. Thus, the correlation is judged to be very good, and it is clear that the correlation model adequately accounts for the major fatigue influencing parameters.

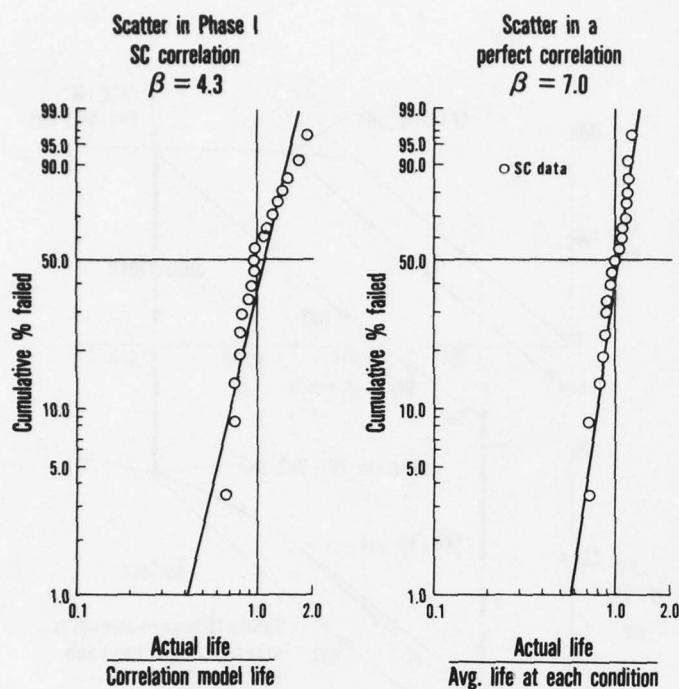


Figure 22 Phase I SC Correlation Weibull Plots

TABLE 5

PHASE I BOLT-HOLE SPECIMEN  
SIMPLE CYCLE LCF DATA

Test Condition	Nominal Stress Limits (ksi)	First Loading			Subsequent Loading			Actual Life (cycles)	Predicted Life* (cycles)
		Subsurface $\hat{\sigma}$ (ksi)	Surface $\hat{\epsilon}$ (in/in)	$\sigma(\hat{\epsilon})$ (ksi)	$\Delta\epsilon$ (in/in)	$\sigma(\Delta\epsilon)$ (ksi)	$\sigma_m - \sigma_o$ (ksi)		
BH1	50 ± 50	181.5	0.0191	279.0	0.0151	246.1	156.0	4,500	6,000
	50 ± 50	181.5	0.0191	279.0	0.0151	246.1	156.0	5,300	6,000
	50 ± 50	181.5	0.0191	279.0	0.0151	246.1	156.0	5,600	6,000
	50 ± 50	181.5	0.0191	279.0	0.0151	246.1	156.0	5,800	6,000
	50 ± 50	181.5	0.0191	279.0	0.0151	246.1	156.0	6,000	6,000
	50 ± 50	181.5	0.0191	279.0	0.0151	246.1	156.0	6,500	6,000
	50 ± 50	181.5	0.0191	279.0	0.0151	246.1	156.0	7,200	6,000
	50 ± 50	181.5	0.0191	279.0	0.0151	246.1	156.0	7,400	6,000
	50 ± 50	181.5	0.0191	279.0	0.0151	246.1	156.0	7,600	6,000
BH2	60 ± 40	181.5	0.0191	279.0	0.0119	203.0	177.5	10,000	10,800
	60 ± 40	181.5	0.0191	279.0	0.0119	203.0	177.5	13,900	10,800
BH3	70 ± 30	181.5	0.0191	279.0	0.0088	157.6	200.2	23,500	28,100
	70 ± 30	181.5	0.0191	279.0	0.0088	157.6	200.2	31,000	28,100
BH4	40 ± 40	179.1	0.0127	214.8	0.0119	203.0	113.3	157,000	223,000

\* using equation (5) with fatigue constants (10)

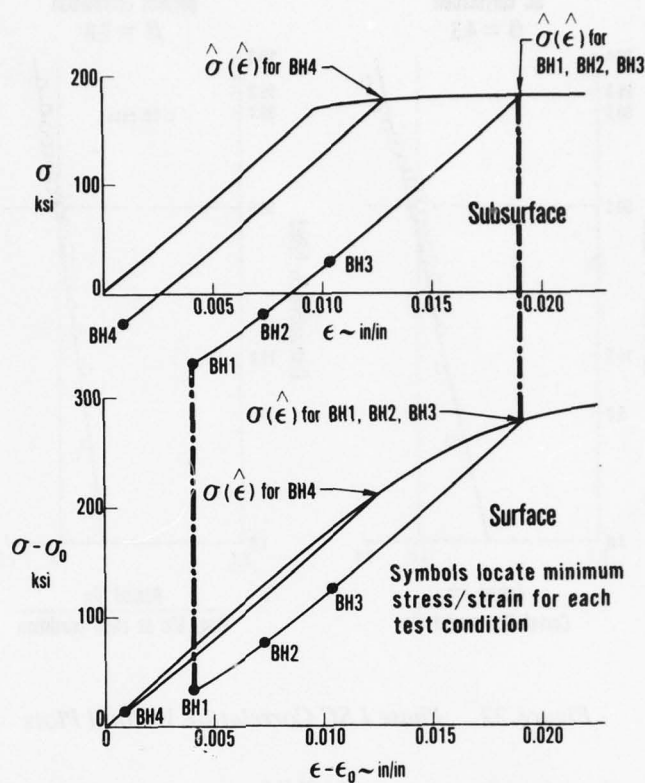


Figure 23 Surface Layer and Subsurface Response for Phase I Simple Cycle Bolt Hole (BH) Tests

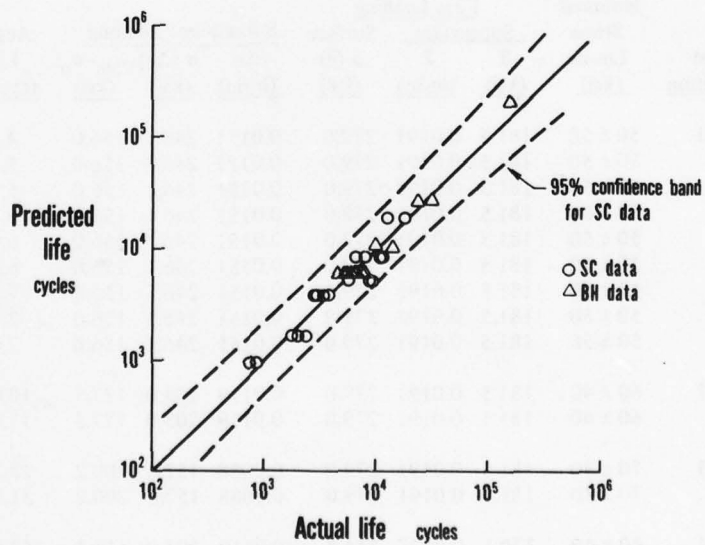


Figure 24 Correlation of Phase I SC and BH Data Using the Surface Layer Mean Stress Algorithm



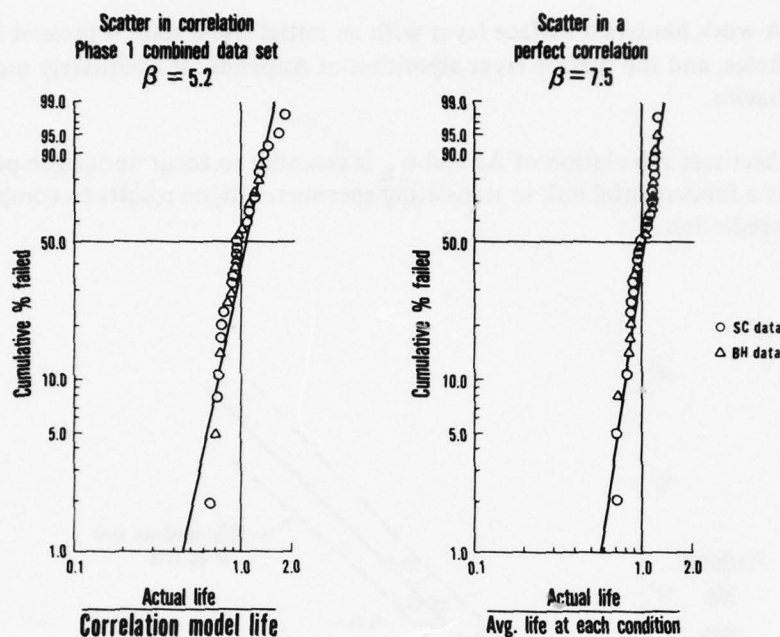


Figure 25 Phase I Combined Data Set Weibull Plots

The value of  $\sigma_0$  resulting from the regression must be evaluated in terms of its physical interpretation in the surface layer algorithm; the value of  $-136.1$  ksi is certainly a reasonable value for a residual surface stress.

The close agreement of the fatigue constants and the reasonable value of  $\sigma_0$  indicate that the surface layer algorithm is reasonable. In order to further evaluate the algorithm, an attempt was made to predict the BH data using mean stress values given by (4) (i.e., the value of  $\sigma_m$  as if no surface layer were present) and (6) developed for the SC data alone. The results of this attempt are shown in Figure 26. It is obvious that a very significant improvement is achieved by the use of the surface layer residual stress algorithm.

Several important conclusions were made from the above analyses:

- 1) The local mechanical parameters, strain range,  $\Delta\epsilon$ , and mean stress,  $\sigma_m$ , as used in the life model (3) are the principal variables affecting the fatigue life in bolt-hole-like regions.
- 2) The constants A, B and C are basic material fatigue constants that can be determined from well controlled SC testing. This suggests an alternate approach to finding the value of  $\sigma_0$  for a notch; with material constants A, B, and C known from SC tests, the value of  $\sigma_0$  can be evaluated by using (9). This approach was used in Phase II.

- 3) A work hardened surface layer with an initial stress state is present in the bolt holes, and the surface layer algorithm of Appendix B adequately models its behavior.
- 4) Accurate calculation of  $\Delta\epsilon$  and  $\sigma_m$  is essential to accurate fatigue prediction and is a fundamental link in translating specimen fatigue results to component life prediction.

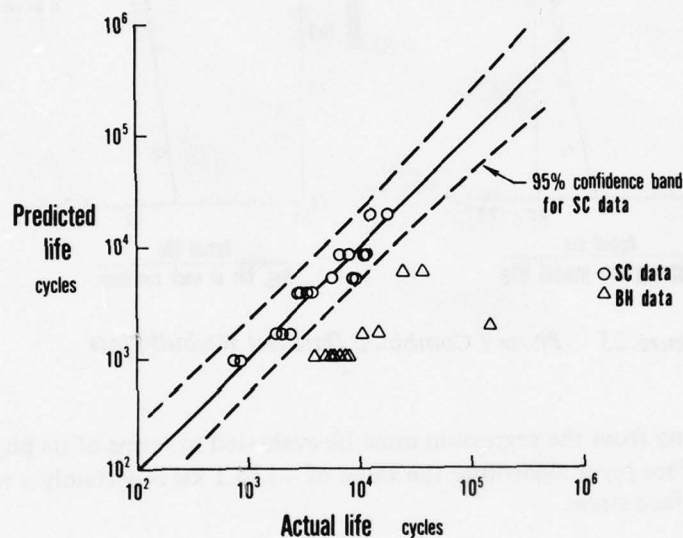


Figure 26 Prediction of Phase I BH Data Without Consideration of Surface Layer

## 5.2 PHASE II – SIMPLE CYCLE LIFE CORRELATION

During Phase II testing, the element of elevated temperature effects was added to the investigation of fatigue behavior. All tests were conducted isothermally at 900°F using a single heat code (XNNZ) of PWA 1057. The basic approach in the investigation remained essentially the same as that followed in the Phase I room temperature testing. That is, the same life correlating model (3) was employed, and SC tests were used to establish the material's fatigue constants A, B, and C. Next, bolt-hole testing, with appropriate accounting of surface layer and stress relaxation, was evaluated against the fatigue model.

Table 6 lists the individual SC test conditions and resulting 1/32 inch crack lives. As noted in Appendix A, the PWA 1057 material hysteresis curves were dependent upon strain range and, in general, showed more variability than the PWA 1216 room temperature behavior, thus making calculation of mean stress levels from standard material curves more difficult than in Phase I. In addition, even small temperature fluctuations while testing in a strain controlled mode caused noticeable variations in recorded specimen load levels. Consequently, the average mean stress values for each test condition were obtained from the load records of each test and used in the data reduction. The regression analysis of these data, using the logarithmic form of (3), yielded the material fatigue constants as follows:

$$\begin{aligned}\log A &= -6.0796 \\ B &= -4.8057 \\ C &= -0.013647\end{aligned}\tag{11}$$

TABLE 6  
PHASE II STRAIN CONTROLLED SPECIMEN  
SIMPLE CYCLE LCF DATA

Test Condition	Specimen Number	$\epsilon_{\min}$ (in/in)	$\epsilon_{\max}$ (in/in)	$\Delta\epsilon$ (in/in)	$\sigma_m$ (ksi)	Actual Life (cycles)	Predicted Life (cycles)
SC1	1057-9	0.0000	0.0140	0.0140	2.0	900	600
SC2	1057-12	0.0050	0.0140	0.0090	27.0	2300	2400
	1057-18	0.0050	0.0140	0.0090	41.5	1000	1500
SC3	1057-20	0.0042	0.0118	0.0076	34.5	3000	4300
	1057-21	0.0041	0.0119	0.0078	39.0	1600	3300
	1057-23	0.0042	0.0118	0.0076	42.5	2600	3400
	1057-25	0.0043	0.0121	0.0077	56.0	2000	2100
SC4	1057-22	0.0000	0.0098	0.0098	26.5	2000	1600
	1057-24	0.0005	0.0098	0.0093	42.0	2000	2600
SC5	1057-27	0.0022	0.0098	0.0086	44.0	1000	1800
	1057-28	0.0022	0.0099	0.0087	48.5	2300	1500
SC6	1057-36	0.0025	0.0090	0.0065	40.0	7000	7700
SC7	1057-30	0.0003	0.0079	0.0076	40.5	6000	3600
	1057-31	0.0002	0.0079	0.0077	32.5	6000	4300
SC8	1057-32	0.0015	0.0078	0.0063	57.0	9000	5200
	1057-37	0.0015	0.0080	0.0065	46.0	8500	6400

The overall correlation is shown in Figure 27. The Weibull curves in Figure 28 compare the degree of scatter in the correlation to the best estimate of perfect correlation. It is seen that the increase in scatter introduced by the correlation model is comparable to that observed in Phase I. And again, no patterns of overprediction or underprediction are apparent from Table 6. As expected, the higher degree of variability associated with high temperature testing and material behavior is reflected in a larger degree of scatter in both the material's inherent scatter and in overall data correlation.

As concluded in the Phase I testing, the constants (11) were viewed as material constants and were used directly in the correlation of the BH data. However, there is a significant difference in the nature of the BH tests between Phase I and Phase II which must be recognized.

The high temperature environment caused relaxation of the mean stress in the bolt-hole region. Since the mean stress has been identified as a primary fatigue correlating variable, relaxation models had to be incorporated in the characterization of the mean stress. Of the several models investigated, the model discussed in Appendix C and in Section IV was judged to be the most straight-forward and reasonable. This model was developed from direct observation of cyclic relaxation tests, and employs a single decay rate,  $\alpha$  ( $= 0.002 \text{ hr}^{-1}$ ), which is viewed as characteristic of the material's behavior at  $900^\circ\text{F}$ .

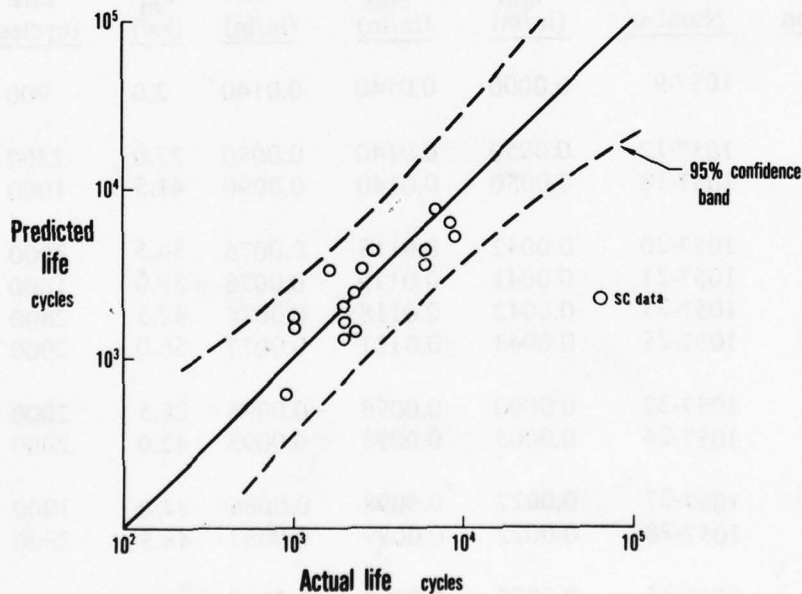


Figure 27 Phase II SC Data Correlation



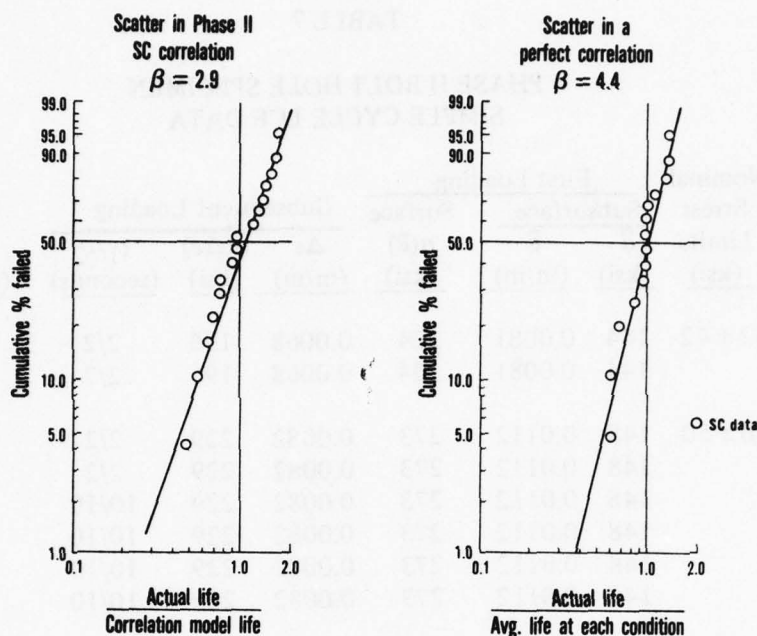


Figure 28 Phase II SC Correlation Weibull Plots

The BH test conditions were selected to span the range of load levels and nominal stress ratios,  $R_s$ , pertinent to actual component usage as described in the mission surveys (Section II). The test conditions and actual lives are given in Table 7, and the surface and subsurface stress conditions are shown in Figure 29.

Prior to incorporating either the mean stress relaxation model or the surface layer algorithm into the calculation of BH mean stresses, an attempt was made to predict the BH data using the fatigue constants (11) and mean stress values given by

$$\sigma_m = \hat{\sigma} - \frac{1}{2} \sigma (\Delta\epsilon) \quad (12)$$

that is, as if neither a surface layer nor stress relaxation were present in the BH specimens. Figure 30 shows the results of this prediction. It is clear that (12) does not adequately describe the mean stress.

Incorporating the surface layer mean stress algorithm in the life equation for the BH specimens

TABLE 7

PHASE II BOLT HOLE SPECIMEN  
SIMPLE CYCLE LCF DATA

Test Condition	Nominal Stress Limits (ksi)	First Loading		Surface $\sigma(\hat{\epsilon})$ (ksi)	Subsequent Loading			Actual Life (cycles)	Predicted Life Eq. (16) (cycles)
		Subsurface $\hat{\sigma}$ (ksi)	$\hat{\epsilon}$ (in/in)		$\Delta\epsilon$ (in/in)	$\sigma(\Delta\epsilon)$ (ksi)	$t_1/t_2$ (seconds)		
BH1	42 ± 42	144	0.0081	224	0.0068	196	2/2	15,700	55,800
		144	0.0081	224	0.0068	196	2/2	49,000	55,800
BH2	50 ± 50	148	0.0112	273	0.0082	229	2/2	7,000	9,300
		148	0.0112	273	0.0082	229	2/2	8,000	9,300
		148	0.0112	273	0.0082	229	10/10	6,000	9,300
		148	0.0112	273	0.0082	229	10/10	8,000	9,300
		148	0.0112	273	0.0082	229	10/10	8,500	9,300
		148	0.0112	273	0.0082	229	10/10	9,000	9,300
BH3	55 ± 55	150	0.0136	294	0.0092	246	2/2	5,000	3,600
		150	0.0136	294	0.0092	246	2/2	6,000	3,600
BH4	80 ± 30	150	0.0136	294	0.0048	140	2/2	> 64,000	16,700
		150	0.0136	294	0.0048	140	2/2	> 64,000	16,700
BH5	70 ± 30	148	0.0112	273	0.0048	140	2/2	185,000	32,900
		148	0.0112	273	0.0048	140	2/2	> 185,000	32,900
BH9	72.5±37.5	150	0.0136	294	0.0061	175	2/2	72,400	8,700
		150	0.0136	294	0.0061	175	2/2	96,000	8,700
BH7	50 ± 50	148	0.0112	273	0.0082	229	105/2	30,000	36,900
		148	0.0112	273	0.0082	229	105/2	55,000	36,900
BH6	55 ± 55	150	0.0136	294	0.0092	246	105/2	8,000	16,300
		150	0.0136	294	0.0092	246	105/2	9,000	16,300

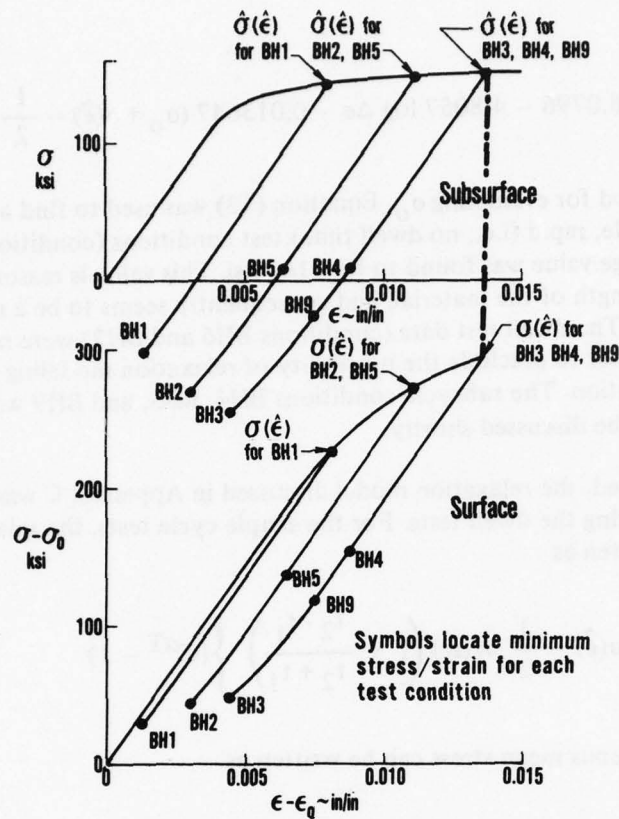


Figure 29 Surface Layer and Subsurface Response for Phase II Simple Cycle BH Tests

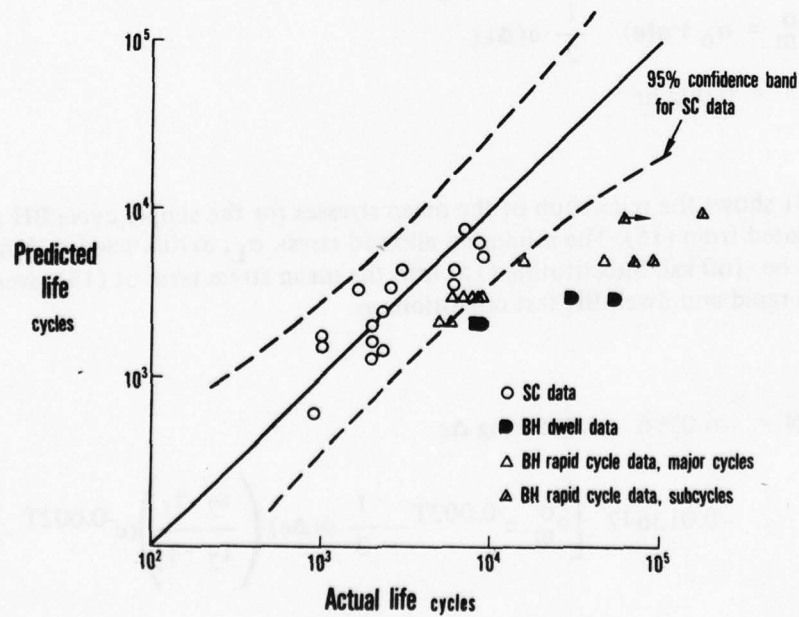


Figure 30 Prediction of Phase II BH Data Without Consideration of Surface Layer and Relaxation

$$\log N = -6.0796 - 4.8057 \log \Delta\epsilon - 0.013647 (\sigma_0 + \sigma(\hat{\epsilon}) - \frac{1}{2} \sigma(\Delta\epsilon)) \quad (13)$$

provides a method for evaluating  $\sigma_0$ . Equation (13) was used to find a value of  $\sigma_0$  for each of the major cycle, rapid (i.e., no dwell time) test conditions (conditions BH1, BH2, and BH3). The average value was found to be -160 ksi. This value is reasonably close to the compressive strength of the material, and consequently seems to be a reasonable value for a residual stress. The dwell test data (conditions BH6 and BH7) were not included for calculating  $\sigma_0$  in order to preclude the possibility of relaxation modeling inaccuracies affecting the  $\sigma_0$  determination. The subcycle conditions BH4, BH5, and BH9 were not included for reasons that will be discussed shortly.

With  $\sigma_0$  established, the relaxation model discussed in Appendix C was used to calculate the mean stresses during the dwell tests. For the simple cycle tests, the relaxation of the mean stress can be written as

$$\sigma_R = \left\{ \sigma_0 + \sigma(\hat{\epsilon}) - \frac{1}{2} \sigma(\Delta\epsilon) \left( 1 + \frac{t_2 - t_1}{t_2 + t_1} \right) \right\} (e^{-\alpha T} - 1) \quad (14)$$

and the instantaneous mean stress can be written as

$$\sigma_m = \sigma_m^0 e^{-\alpha T} - \frac{1}{2} \sigma(\Delta\epsilon) \left( \frac{t_2 - t_1}{t_2 + t_1} \right) (e^{-\alpha T} - 1) \quad (15)$$

$$\text{where } \sigma_m^0 = \sigma_0 + \sigma(\hat{\epsilon}) - \frac{1}{2} \sigma(\Delta\epsilon)$$

$$\alpha = 0.002 \text{ hr}^{-1}$$

Figure 31 shows the relaxation of the mean stresses for the simple cycle BH test conditions as calculated from (15). The minimum allowed stress,  $\sigma_L$ , as discussed in Appendix C was taken to be -160 ksi. Substituting (15) into the mean stress term of (13) gives a life equation for both rapid and dwell BH test conditions as:

$$\log N = -6.0796 - 4.8057 \log \Delta\epsilon$$

$$-0.013647 \left[ \sigma_m^0 e^{-0.002T} - \frac{1}{2} \sigma(\Delta\epsilon) \left( \frac{t_2 - t_1}{t_2 + t_1} \right) (e^{-0.002T} - 1) \right] \quad (16)$$



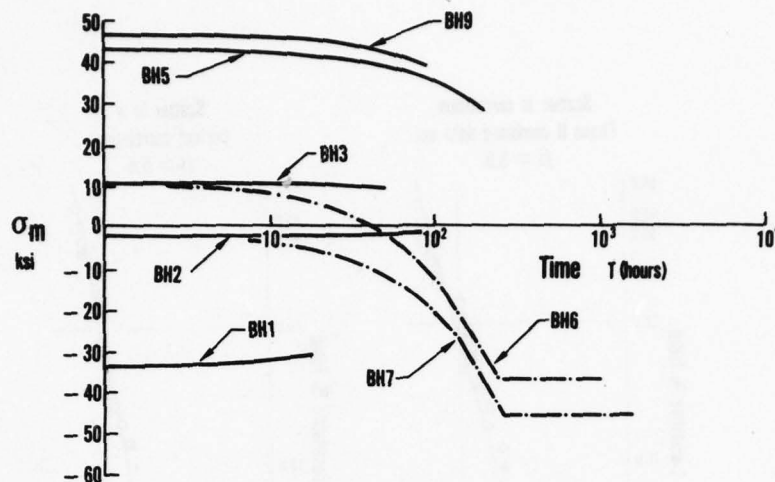


Figure 31 Mean Stress Relaxation

Since  $T$  is a function of  $N$ , an iterative procedure was used to find the predicted life. Resulting predicted fatigue lives are listed in Table 7, and the resulting correlation is shown in Figure 32. The correlation of both rapid and dwell major cycle data is good with the single exception of one specimen tested at condition BH1. This specimen failed much sooner than expected and lies outside of the 95 percent confidence band established by the SC data; all other major cycle data lies well within the confidence band. This single data point is suspected as a statistical "outlier". Figure 33 compares the Weibull distributions resulting from the correlation model to the hypothetical "perfect" model for the SC and the major cycle BH data. The single data point suspected as an outlier is indicated in the plot but was not included in determining the slope of the distribution. Its position suggests even more strongly that it is an outlier. Once again, the quality of the correlation model is judged to be good for the major cycle data based on the results shown in Figures 32 and 33.

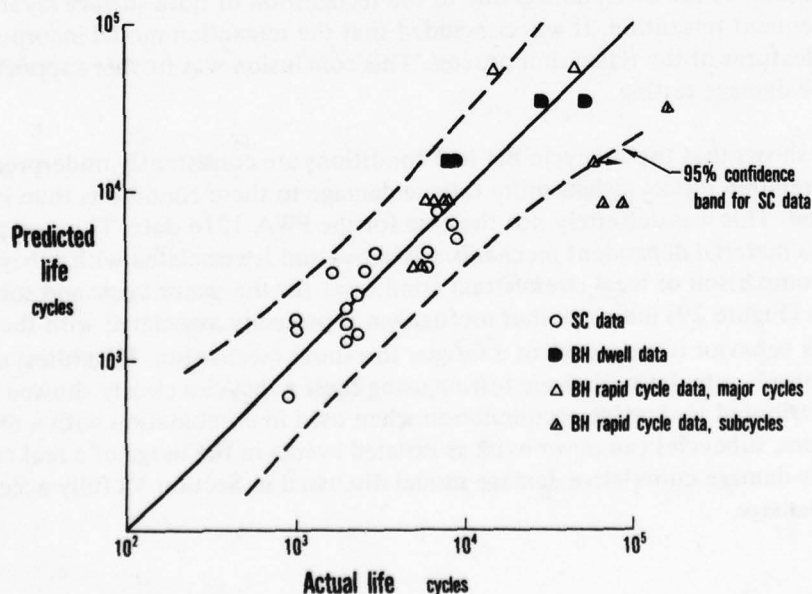


Figure 32 Correlation of Phase II SC and BH Data

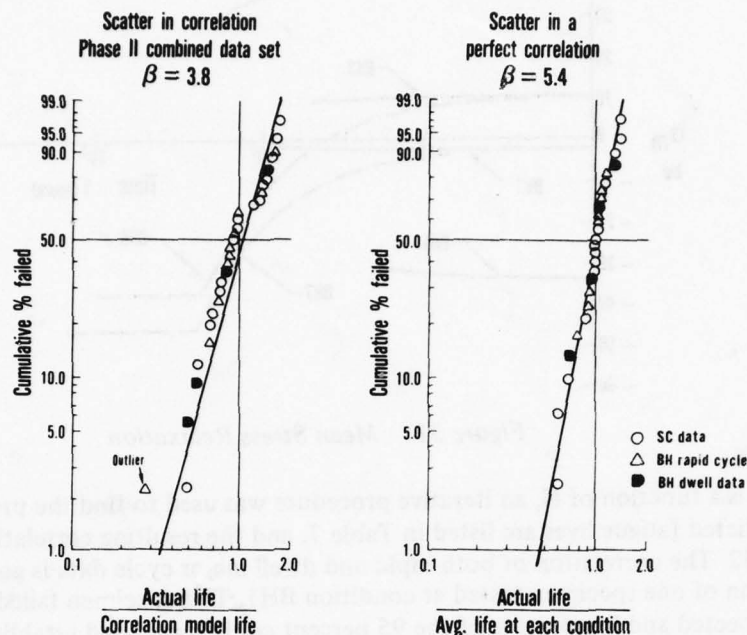


Figure 33 Phase II Combined Data Set Weibull Plots

The principal influence in correlating the rapid cycle test points is the recognition of the surface layer since very little relaxation takes place for those data points (see Figure 31). It is clear that a surface layer does exist in the bolt-hole specimens and that its behavior is modeled accurately by the same algorithm as employed for the PWA 1216 bolt-hole specimens. The correlation of the dwell data is due to the recognition of both surface layer stresses and their subsequent relaxation. It was concluded that the relaxation model incorporated the principal features of the relaxation process. This conclusion was further supported with the cumulative damage testing.

Figure 32 shows that the subcycle BH test conditions are consistently underpredicted. That is, the correlation model assigns more fatigue damage to these conditions than is actually experienced. This was definitely not the case for the PWA 1216 data. This comparison suggests that a material dependent mechanism is active and is associated with subcycle activity. Further, comparison of local stress/strain conditions for the major cycle and subcycle test conditions (Figure 29) indicates that mechanism is probably associated with the strain range. This behavior is suggestive of a fatigue threshold mechanism. Regardless of the mechanism involved, cumulative damage testing using these subcycles clearly showed that subcycles contributed to damage accumulation when used in combination with a major cycle. Furthermore, subcycles can never exist as isolated events in the usage of a real component. The double-damage cumulative damage model discussed in Section VI fully accounts for the subcycle damage.

## SECTION VI

### CUMULATIVE DAMAGE LIFE MODEL

#### 6.1 THE DOUBLE-DAMAGE MODEL

A cumulative fatigue damage model was developed using the double-damage effect described by Manson<sup>5</sup>. This model is most easily illustrated for a block-loading test such as shown in Figure 14. For such a test, the familiar linear Miner's<sup>6</sup> rule assesses the damage done during each block of loading to be

$$D_i = n_i/N_i \quad (16)$$

where  $D_i$  is the relative damage due to  $n_i$  cycles at a load condition which has a simple cycle life of  $N_i$ .

The double-damage effect recognizes that the entire life of the part is composed of a crack initiation phase and a crack propagation phase. For a given value of  $D_i$ , the crack size (following initiation) developed during high stress amplitude loading such as the  $\alpha$  - loading in Figure 14 is larger than the crack that would have been developed during low stress amplitude loading. Thus, a low amplitude loading block following a high amplitude loading block, during which initiation has occurred, will result in failure sooner than would be predicted by the linear Miner's rule damage model.

Linear damage modeling predicts (for the block loading test shown in Figure 14) that the cycles to failure in the  $\beta$ -loading block,  $n_\beta$ , following  $n_\alpha$  cycles at the  $\alpha$  - loading block is found from the Miner's rule equation

$$1 = \frac{n_\alpha}{N_\alpha} + \frac{n_\beta}{N_\beta} \quad (17)$$

If, however, a crack,  $\hat{a}$ , has been initiated at the end of the  $\alpha$  - loading block, then the double-damage model implies that  $n_\beta$  is governed by fracture mechanics.

The crack growth law is needed to derive an expression for  $n_\beta^*$ , the cyclic life remaining under  $\beta$  - loading as predicted by fracture mechanics. The crack growth law is given by

$$\frac{da}{dN} = C \Delta K^n \quad (18)$$

where  $\frac{da}{dN}$  = crack growth rate  
 $\Delta K$  = alternating stress intensity factor  
 $n$  = crack growth exponent  
 $C$  = crack growth constant

The alternating stress intensity factor  $\Delta K$  must include the effects of local stress ratio,  $R$  ( $= \sigma_{\min}/\sigma_{\max}$ ). For the materials considered in this contract, the R-ratio model can be incorporated in the equation for  $\Delta K$  as

$$\Delta K = \Delta \sigma \left( \frac{b}{d - R} \right) \sqrt{\pi a} Y \quad (19)$$

where  $a$  = crack size  
 $Y$  = crack shape function  
 $\Delta \sigma$  = local stress range [ $= \sigma(\Delta \epsilon)$ ]  
 $b, d$  = material constants derived from R-ratio crack growth tests

Integration of the crack growth law (18) gives an expression for  $n_{\beta}^*$ , the number of cycles required to grow the crack,  $\hat{a}$  to a final length of 1/32 inch length under  $\beta$  - loading.

$$n_{\beta}^* = \frac{1}{C \left[ \sqrt{\pi} Y \frac{b}{d - R_{\beta}} \Delta \sigma_{\beta} \right]^n (n/2 - 1)} \left\{ \hat{a}^{1 - n/2} - \left( \frac{1}{32} \right)^{1 - n/2} \right\} \quad (20)$$

If, instead, the crack  $\hat{a}$  had been propagated under  $\alpha$  - loading conditions, the remaining life would simply have been equal to  $N_{\alpha} - n_{\alpha}$ . And integration of (18) would now result in the expression

$$N_{\alpha} - n_{\alpha} = \frac{1}{C \left[ \sqrt{\pi} Y \frac{b}{d - R_{\alpha}} \Delta \sigma_{\alpha} \right]^n (n/2 - 1)} \left\{ \hat{a}^{1 - n/2} - \left( \frac{1}{32} \right)^{1 - n/2} \right\} \quad (21)$$

Combining (20) and (21),

$$n_{\beta}^* = \left[ \frac{(d - R_{\beta}) \Delta \sigma_{\alpha}}{(d - R_{\alpha}) \Delta \sigma_{\beta}} \right]^n (N_{\alpha} - n_{\alpha}) \quad (22)$$



Manipulating (22), the following modified Miner's rule is obtained:

$$1 = \frac{n_\alpha}{N_\alpha} + \frac{n_\beta^*}{D_{\alpha\beta} N_\beta} \quad (23)$$

$$\text{where} \quad D_{\alpha\beta} = \left( \frac{d - R_\beta}{d - R_\alpha} \right)^n \left( \frac{\Delta\sigma_\alpha}{\Delta\sigma_\beta} \right)^n \left( \frac{N_\alpha}{N_\beta} \right)$$

Thus, double-damage effects have the influence of modifying the Miner's linear damage rule. It can be shown that the double-damage debit factor,  $D_{\alpha\beta}$ , is less than one for low amplitude loading following high amplitude loading (a "High-Low" test) and is greater than one for high amplitude loading following low amplitude loading (a "Low-High" test). For (23) to apply, it is only necessary that a coherent crack be initiated at some time during  $\alpha$  - loading.

While the double-damage model can be written in the form of a modified Miner equation, (23), it should be remembered that it is actually a fracture mechanics approach which recognizes the exhaustion of the initiation life during the first loading block. This fact is further illustrated by writing (23) in an expanded form and noting that the simple cycle life of the second loading block,  $N_\beta$ , does not enter into the calculation of  $n_\beta^*$ :

$$1 = \frac{n_\alpha}{N_\alpha} + \frac{n_\beta^*}{\left( \frac{d - R_\beta}{d - R_\alpha} \right)^n \left( \frac{\Delta\sigma_\alpha}{\Delta\sigma_\beta} \right)^n \left( \frac{N_\alpha}{N_\beta} \right) N_\beta} \quad (24)$$

Stated yet another way, the double-damage equation (24) simply evaluates the crack growth during the second loading by evaluating the severity of crack growth conditions in the second loading block relative to the loading which exhausted the initiation life.

After a crack has been initiated, it propagates both along the surface of the bolt hole as well as into the subsurface region. It is reasonable to assume that the propagation of the crack is governed essentially by the more positive R-ratio subsurface region. For this reason, subsurface stress ranges and R-ratios are used in the double-damage equation (24).

As stated above, for (24) to apply, it is only necessary that a crack,  $\hat{a}$ , exist at the end of the  $\alpha$  - loading block in a block - loading type of test. If  $\hat{a}$  does not exist at that time, Miner's rule initiation life exhaustion damage (16) continues to accumulate. In such a case, for a two-block loading test, the double-damage rule would reduce to the simple Miner's Rule.

For more complicated mission type loading such as the sequenced test shown in Figure 14, it is clear that the initiation life is not exhausted by just one of the various type of cycles but is instead exhausted by major and minor cycles acting together. As such,  $\hat{a}$  does not

exist until after some unknown number of missions. As stated previously, prior to the existence of  $\hat{a}$ , the initiation life exhaustion is given by (16) and not until after  $\hat{a}$  exists is it appropriate to apply the double-damage rule. The assumption is made in this program that all minor cycles contribute to the propagation life exhaustion. Thus, some flight-by-flight subcycles experienced early in the component life will not see the small crack initiated by the major cycles and the assumption will be conservative. For very long lived components, this assumption becomes increasingly more conservative.

## 6.2 PHASE I – CUMULATIVE DAMAGE TESTS

### 6.2.1 TFR Specimen Testing

One gang of four bolt-hole specimens was used to determine the fatigue damage done during the terrain following radar (TFR) portion of an actual mission. The specimen nominal stress spectrum shown in Figure 34 was developed by considering a random sequence of  $\pm 7$  percent (maximum) PLA excursions for the F100 second-stage fan bolt-hole location. The loading was repeated continuously until 390,000 subcycles were imposed, corresponding to roughly 6,500 fleet-typical flights of the TF30 engine in the F-111. Testing was terminated at this point and subsequent testing of one of the TFR specimens at test condition BH1 ( $50 \pm 50$  ksi nominal stress) showed that the 1/32 inch crack life was no different from virgin specimens tested under the same loading (see Figure 35). It was therefore concluded that the TFR specimens could be considered to be virgin specimens. One of these specimens was subsequently tested at simple cycle condition BH4. The results of that test were reported in Section V. The remaining two specimens were subsequently tested at nominal stresses of  $33 \pm 33$  ksi for 155,000 cycles and then at  $40 \pm 40$  ksi until failure. A discussion of this test (labeled BH54) is included in the next section (6.2.2).



Figure 34 Terrain Following Radar (TFR) Simulation

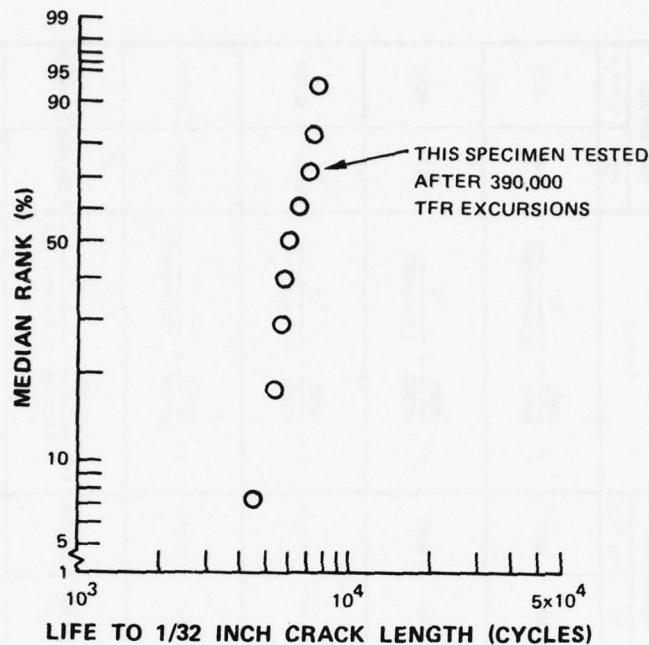


Figure 35 Bolt Hole Specimens Tested at  $50 \pm 50$  Ksi Nominal Stress

#### 6.2.2 Cumulative Damage Specimen Tests



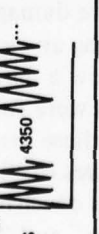
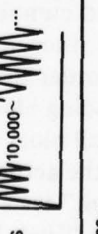
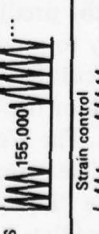
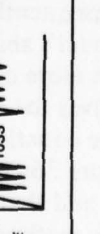
Phase I BH and SC cumulative damage test conditions and resulting lives are shown in Table 8, along with corresponding Miner's Rule (17) and double-damage (24) life predictions. The double-damage debit factor,  $D_{\alpha\beta}$ , used in these predictions is

$$D_{\alpha\beta} = \left( \frac{1.64 - R_{\beta}}{1.64 - R_{\alpha}} \right)^{4.84} \left( \frac{\Delta\sigma_{\alpha}}{\Delta\sigma_{\beta}} \right)^{4.84} \left( \frac{N_{\alpha}}{N_{\beta}} \right) \quad (25)$$

The PWA 1216 room temperature crack propagation rate exponent ( $n = 4.84$ ) and the R-ratio model were established from independent testing.

Tests BH12 and BH23 can be considered "High-Low" tests (i.e., high amplitude loading preceeding low amplitude loading) and, as noted previously, the double-damage debit factors for these tests are less than one. Conversely, tests BH21 and BH 32 are "Low-High" tests and have  $D_{\alpha\beta}$ 's greater than one. Predicted simple cycle lives (as discussed in Section V) were used in both the Miner's Rule and Double-Damage calculations shown in Table 8. Consequently the predicted cumulative damage lives are influenced by the simple cycle life model's ability to predict, thus making an evaluation of the two cumulative damage models more difficult. So, in order to allow a more accurate evaluation, the average simple cycle lives for each of the loading blocks were first used in the Miner's Rule and double-damage equations. The Weibull plots of these results are shown in Figures 36a and 36b. In Figure 36a it is clear that the actual lives of "High-Low" tests are consistently over-predicted and that the "Low-High" tests are consistently under predicted. However, the double-damage method predicts both "High-Low" and "Low-High" tests uniformly as shown in Figure 36b. Thus, double-damage effects are clearly displayed and are predicted by the double-damage equation (24). Figure 36c shows the effect of using predicted simple cycle lives in (24); again, the tests appear to be uniformly predicted.

TABLE 8  
PHASE I CUMULATIVE DAMAGE SPECIMEN TEST CONDITIONS AND RESULTS

Test Conditions				Actual Lives		Miner's Rule		Double damage	
Schematic	$\alpha$ - Loading		$\beta$ - Loading	$n_\beta$	$n_\alpha + n_\beta$	Formula	$n_\beta$	Formula	Predicted lives
	Nom. stress	$n_\alpha$	Nom. stress						$n_\beta^*$
BH12 S 	50±50 (ksi)	2000	60±40 (ksi)	3000 5000 5200 7200 8000	5000 7000 7200 10,000	$1 = \frac{2000}{6000} + \frac{n_\beta}{10,800}$	7200	$1 = \frac{2000}{6000} + \frac{n_\beta^*}{0.767(10,800)}$	5520 7520
BH21 S 	60±40 (ksi)	6500	50±50 (ksi)	2200 4300 5000 5500	8700 10,800 11,500 12,000	$1 = \frac{6500}{10,800} + \frac{n_\beta}{6000}$	2390	$1 = \frac{6500}{10,800} + \frac{n_\beta^*}{1,304(6000)}$	3110 9610
3H23 S 	60±40 (ksi)	4350	70±30 (ksi)	12,650 15,150	17,000 19,500	$1 = \frac{4350}{10,800} + \frac{n_\beta}{28,100}$	16,780	$1 = \frac{4350}{10,800} + \frac{n_\beta^*}{0.621(28,100)}$	10,420 14,780
BH32 S 	70±30 (ksi)	10,000	60±40 (ksi)	8000 9600	18,000 19,600	$1 = \frac{10,000}{28,100} + \frac{n_\beta}{10,800}$	6960	$1 = \frac{10,000}{28,100} + \frac{n_\beta^*}{1.611(10,800)}$	11,210 21,210
BH54 S 	33±33 (ksi)	155,000	40±40 (ksi)	23,000 31,000	178,000 186,000	$1 = \frac{155,000}{3,400,000} + \frac{n_\beta}{227,700}$	212,550	$1 = \frac{155,000}{3,400,000} + \frac{n_\beta^*}{9.226(227,700)}$	1,960,000 2,116,000
SC23 ε 	Strain control 0.0093 ± 0.0062 (in/in)	1033	Strain control 0.0109 ± 0.0046 (in/in)	1470	2500	$1 = \frac{1033}{1700} + \frac{n_\beta}{3800}$	1490	$1 = \frac{1033}{1700} + \frac{n_\beta^*}{0.716(3800)}$	1060 2090



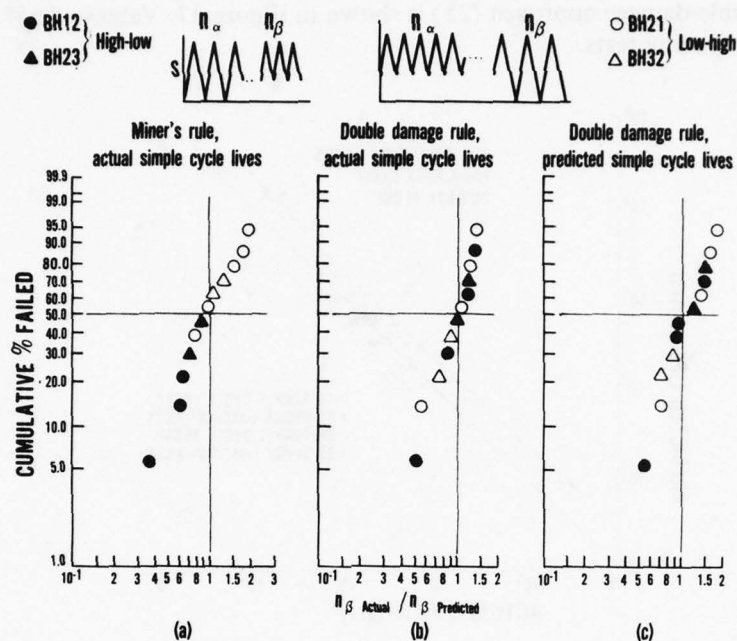


Figure 36 Nonlinear Cumulative Damage Effects

The clear existence of the double-damage effect implies that a crack,  $\hat{a}$ , existed at the end of the first loading block in these tests. In each of the tests, the number of cycles applied in the first loading block was approximately 50 percent of the number of cycles needed to initiate a small (approximately 0.008 inch) crack at that loading condition as established from simple cycle testing. Thus, it seems reasonable that a small sub-detectable crack,  $\hat{a}$ , could indeed have existed at the end of the first loading block.

The test labeled BH54 is included in Table 8 for completeness even though it is judged not to be directly applicable for the purposes of this contract. As shown in Table 8, BH54 is correlated by neither the Miner's Rule nor the double-damage equation, but examination of the calculations shown in the table indicate some obvious limits in the prediction systems. First, the calculated simple cycle life (3,400,000 cycles) for the first loading block is obviously much too optimistic since the specimens failed shortly after the first 155,000 cycles had been applied. This over prediction is not surprising since the data base is limited to much lower lives. Secondly, the double-damage calculation predicts that the effect of  $D_{\alpha\beta}$  is to enhance the life of the second loading block. That is, the prior loading is predicted to have caused  $n_{\beta}^*$  to be larger than the simple cycle life of the second block,  $N_{\beta}$ . Clearly, this implies a limit on  $D_{\alpha\beta}$  for "Low-High" tests. This limit has been exceeded somewhat in condition BH32 as well, although it has not been exceeded as substantially as exhibited in the calculation for BH54. Lastly, such a limitation of the double-damage calculation occurs only in the "Low-High" type of loading (where  $D_{\alpha\beta} > 1.0$ ). This type of loading never occurs in component usage. For this reason, the implied limit in the double-damage calculation does not have to be considered further for the cumulative damage predictions considered in this program.

The correlation of the cumulative damage specimen tests (including the single SC test) using the double-damage approach (25) is shown in Figure 37. Values of  $n\beta^*$  are plotted for the block loading tests.

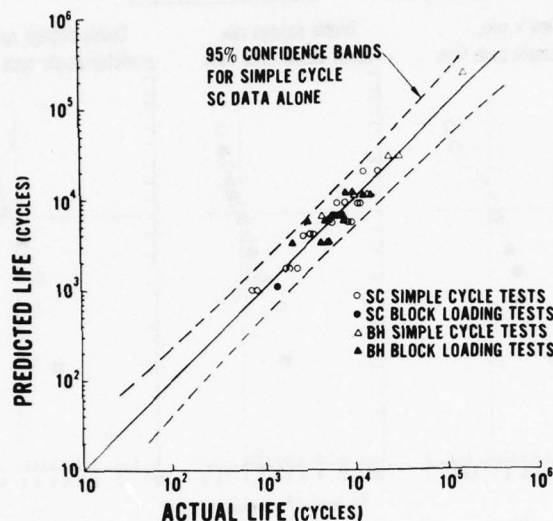


Figure 37 Correlation of Phase I Simple Cycle and Cumulative Damage Specimen Testing

### 6.2.3 Ferris Wheel Tests

Verification of the fatigue life prediction models described in previous sections was achieved by tests of four fan test disks. The disk, shown in Figures 38 and 39 was designed to be LCF life limited in the bolt hole. The elastic stress concentration factor ( $K_T = 2.427$ ) was determined from extensive finite element and finite difference analyses and verified with strain gage surveys. Disk testing was performed in a "Ferris Wheel" (F/W) which simulates engine operating stresses through radial loading applied at the disk rim.

The generic missions established from the mission surveys reported in Section II were used as the basis for the disk testing. Actual disk nominal stress levels and the resulting lives are shown in Table 9. The major cycle local stresses and strains of each Ferris Wheel disk test are shown in relation to the BH specimen test condition in Figure 40. Three of the disk tests were run to final failure but F/W4 test was suspended with no bolt holes cracked. All three disks tested to completion failed from a single bolt hole; postfailure examinations revealed no crack indications in any of the remaining holes.

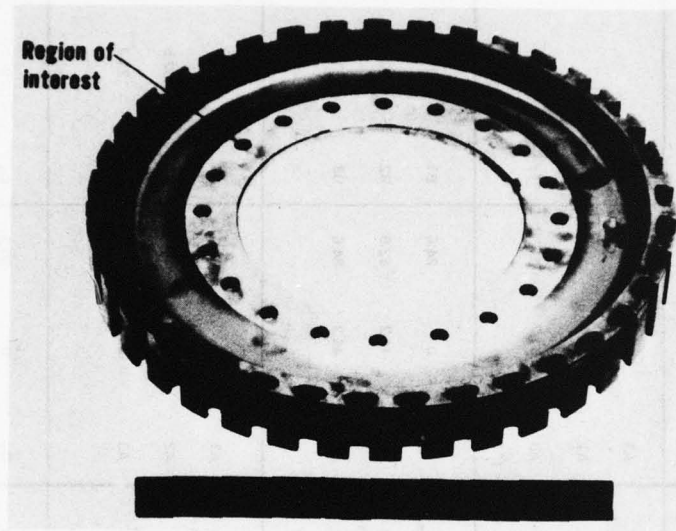


Figure 38 Phase I Ferris Wheel Disk (J16937-1)

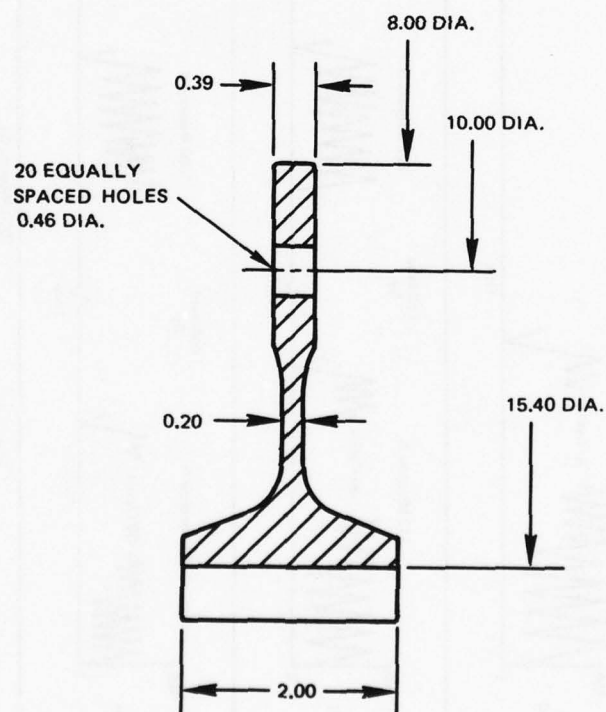


Figure 39 Dimension of Phase I Ferris Wheel Disk

TABLE 9

## PHASE I FERRIS WHEEL TEST CONDITIONS AND RESULTS

	Order of Missions	Predicted life	Nominal stress levels			
			Subcycle	First mission Smin (ksi)	Smax (ksi)	Second mission Subcycle Smin (ksi) Smax (ksi)
F/W <sub>1</sub>	<p>169 Missions A 30 Cycles</p>	189 Missions A	A1	0	112.7	
			A2	18.9	110.4	
			A3	61.7	112.7	
F/W <sub>2</sub>	<p>312 Missions A 672 Missions B</p>	312 Missions A + 840 Missions B	A1	0	84.6	B1 0 84.6
			A2	14.2	82.9	B2 32.5 79.6
			A3	46.3	84.6	B3 21.2 84.6
F/W <sub>3</sub>	<p>641 Missions A 1880 Missions B</p>	641 Missions A + 1500 missions B	A1	0	68.0	B1 0 84.6
			A2	14.8	66.6	B2 32.5 79.6
			A3	40.5	68.0	B3 21.2 84.6
F/W <sub>4</sub>	<p>37,000 Missions C<sub>1</sub> 7000 Missions C<sub>2</sub> test suspended with No Cracks</p>	37,000 Missions C <sub>1</sub> + 53,800 missions C <sub>2</sub>	C <sub>1</sub>	0	80.3	C <sub>2</sub> 0 88.9



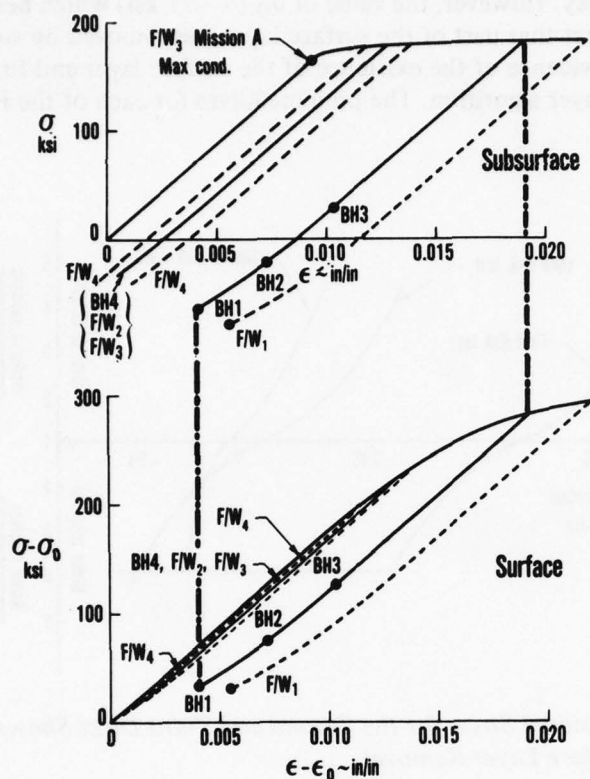


Figure 40 Specimen and Ferris Wheel Surface Layer and Subsurface Response

The life prediction methods described in previous sections have been developed for predicting typical or mean LCF life behavior, but because each test disk could have failed from any one of twenty bolt holes, life predictions for the test disks were made for the appropriate probability of failure rate. Based on the probability distribution of actual versus average lives for the BH specimens, the lowest lived of twenty holes would fail at 65 percent of the mean predicted LCF life.

The disk bolt holes were manufactured using machining parameters which duplicated those used in the BH specimen machining. However, the bolt holes in the second and third disks were found to have machining marks atypical of the BH specimens and were subsequently reoperated by honing to a maximum diametral increase of 0.008 inch. Thus, the surface layer of the second and third disks were not the same as for the first and fourth disks. The double-damage model discussed in previous sections was used to predict the number of missions required to fail the first hole in each disk. Due to the very low amplitude of loading in Mission A of  $F/W_3$ , this mission was assumed to contribute only to the exhaustion of initiation life; no double-damage effects are assumed to be present in Mission A. Figure 41 shows how the correlation of actual and predicted missions varies with the assumed values of surface layer machining stress,  $\sigma_0$ . It is clear that  $F/W_2$  and  $F/W_3$  behave differently than  $F/W_1$ . Furthermore, the value of  $\sigma_0$  ( $= -133$  ksi) which correlates  $F/W_1$  is nearly identical

to  $\sigma_0$  determined for the BH specimens. This correlation is expected since these parts were machined in the same way. However, the value of  $\sigma_0$  ( $= -71$  ksi) which best correlates F/W<sub>2</sub> and F/W<sub>3</sub> reflects the fact that part of the surface layer was removed by subsequent honing. This is viewed as clear evidence of the existence of the surface layer and firmly establishes validity of the surface layer algorithm. The predicted lives for each of the F/W tests is shown in Table 9.

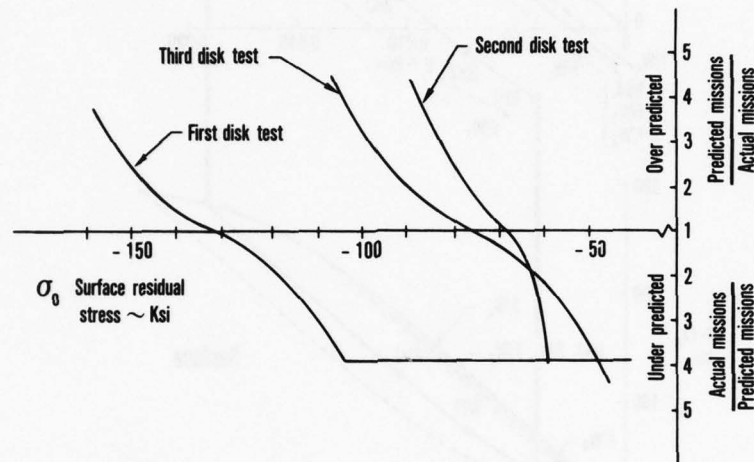


Figure 41 Surface Residual Stress for the Second and Third Disks Shows the Effect of Partial Surface Layer Removal

Overall correlation of all specimen and Ferris Wheel test data is shown in Figures 42 and 43. This correlation is judged to be extremely good considering the wide variety of specimens, components, and loading conditions considered.

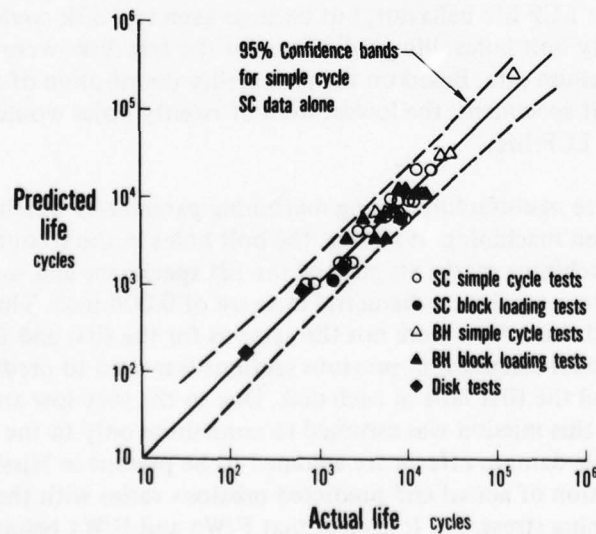


Figure 42 Correlation of Phase I Specimen and Ferris Wheel Data

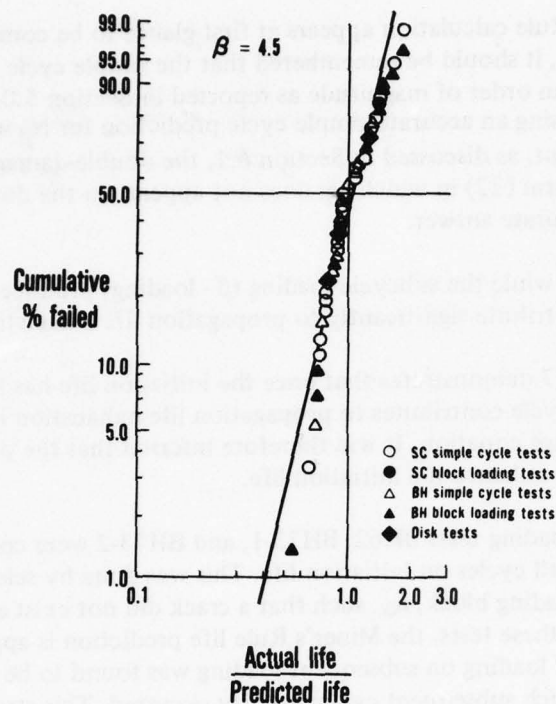


Figure 43 Phase I Overall Correlation

## 6.3 PHASE II – CUMULATIVE DAMAGE TESTS

### 6.3.1 Cumulative Damage Specimen Tests

The PWA 1057 cumulative damage investigation involved several block loading tests and one sequenced test. The actual test conditions and resulting lives are shown in Table 10. The Miner's Rule and double-damage life calculations for each test condition are also shown in the table. The double-damage debit factor  $D_{\alpha\beta}$  used in these predictions is

$$D_{\alpha\beta} = \left( \frac{1.077 - R_{\beta}}{1.077 - R_{\alpha}} \right)^2 \left( \frac{\Delta\sigma_{\alpha}}{\Delta\sigma_{\beta}} \right)^2 \left( \frac{N_{\alpha}}{N_{\beta}} \right) \quad (26)$$

The PWA 1057 900°F crack propagation rate exponent ( $n = 2.0$ ) and the R-ratio model were established from independent testing.

Consider first those tests involving only rapid cycle testing: BH32-2, BH29-1, and BH29-2. In test BH32-2 the Miner's Rule life calculation is the better of the two methods for correlating the life. This is reasonable since it is relatively certain that a crack,  $\hat{a}$ , was not initiated during the first loading block ( $\alpha$  - loading). It required approximately 2000 cycles at  $\alpha$  - loading level to initiate a "pin-point" crack (approximately 0.008 inch) in the simple cycle testing. As stated in Section 6.1, the double-damage concept reduces to Miner's Rule for such cases. Tests BH29-1 and 29-2 illustrate again that the double-damage model is appropriate.

While the Miner's Rule calculation appears at first glance to be comparable to the double-damage calculation, it should be remembered that the simple cycle life prediction for  $n_{\beta}^*$  can be too low by nearly an order of magnitude as reported in Section 5.0. Thus, a Miner's Rule prediction for  $n_{\beta}$  using an accurate simple cycle prediction for  $N_{\beta}$  would be much higher than the observed  $n_{\beta}$ . But, as discussed in Section 6.1, the double-damage equation for  $n_{\beta}^*$  can be written in the form (22) in which  $N_{\beta}$  does not appear. So the double-damage calculation leads to a more accurate answer.

It is clear then that while the subcycle loading ( $\beta$  - loading) produces essentially no damage in itself, it does contribute significantly to propagation life exhaustion.

Test condition BH27 demonstrates that once the initiation life has been exhausted by prior loading, the dwell cycle contributes to propagation life exhaustion in the manner described by the double-damage equation. It was therefore inferred that the principal influence of the dwell cycle is to enhance the initiation life.

Subsequent block loading tests BH62, BH73-1, and BH73-2 were conducted to investigate the influence of dwell cycles on initiation life. This was done by selecting the number of cycles in the first loading block,  $n_{\alpha}$ , such that a crack did not exist at the end of the  $\alpha$  - loading block. Thus for these tests, the Miner's Rule life prediction is appropriate. The principal effect of prior dwell loading on subsequent loading was found to be a reduction of the mean stress levels over which subsequent cyclic activity occurred. This stress condition is reflected in the simple cycle lives,  $N_{\beta}$ , for the  $\beta$  - loading condition. For the double-damage calculation, the relaxation of both surface layer (affecting  $N_{\beta}$  values) and the subsurface region (affecting the crack growth calculation) was recognized. The relaxation of the mean stress of the subsurface region is shown in Figure 44.

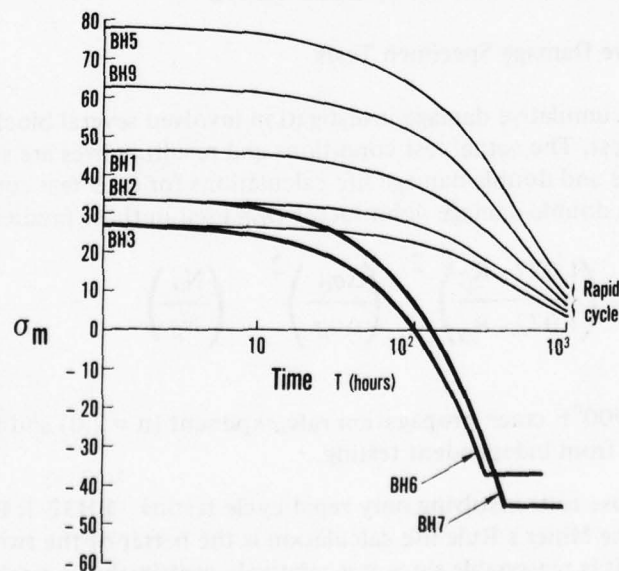


Figure 44 Subsurface Mean Stress Relaxation



In a similar manner, for the sequenced test, BH73S, the effect of the dwell period was taken to be the relaxation of the mean stress level of the rapid cycles. In the double-damage calculation, the propagation behavior of the dwell subcycle was debited relative to the principal life exhausting cycle (the  $50 \pm 50$  ksi rapid cycle). The relaxation, both surface and sub-surface occurs over a period of several hours and eventually reaches a fully relaxed condition as discussed in Appendix C. The simple cycle lives and double-damage debit,  $D_{\alpha\beta}$ , shown in Table 10 were calculated for the fully relaxed condition, but it was calculated that nearly 10000 missions would be required to achieve the fully relaxed condition. It is apparent that if a partially relaxed condition were to be used as the basis for calculation, lower lives would be predicted. This result suggests an iterative process for determining the  $N_i$  and  $D_{ij}$  for sequenced tests. From Table 10, it appears, once again, that the double-damage method provides the better correlation.

Figure 45 shows the overall correlation of the cumulative damage tests. Total lives ( $n_\alpha + n_\beta$ ) are plotted here. The correlation is well within the 95 percent confidence band established by the SC data alone.

### 6.3.2 Ferris Wheel Tests

Verification tests were performed on Ferris Wheel disks at a constant temperature of 900°F. Figures 46 and 47 show the actual disks mounted in the test rig with the heating mechanisms in place. Figure 48 shows the dimensions of the test disk. This shape contains the major features of a typical turbine disk. The elastic stress concentrations factor for the disk was determined to be 2.33.

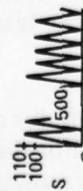



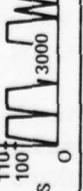
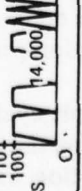
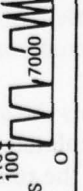

Actual test loading, based on the generic missions of Section II, is shown in Table 11. Each disk was subjected to a room temperature calibration run prior to testing to ensure that proper loading conditions were being achieved. For tests F/W<sub>1</sub> and F/W<sub>3</sub>, the room temperature calibrations were made using a maximum nominal stress equal to that experienced during 900°F testing. However, in the room temperature calibration of F/W<sub>2</sub>, the maximum stress was 16 percent higher than the maximum stress experienced during subsequent cycling. The effects of these room temperature cycles were accounted for in the prediction of the F/W test results. Figure 49 shows schematically how the effect of the room temperature loading was calculated. Simply stated, the room temperature monotonic and hysteresis curves are used to calculate an initial stress and strain state (point B in Figure 49) for subsequent high temperature loading. The high temperature loading continues from point B along the 900°F hysteresis curve for both the surface layer and surface region.

The surface layer algorithm, using  $\sigma_0 = -160$  ksi as determined from BH tests, and the relaxation algorithm (Appendix C) were used to calculate the local bolt-hole stresses and strains. The double-damage equation was used in the life prediction. None of the tests reached a fully relaxed condition prior to the end of testing.

In all cases the simple cycle lives,  $N_i$ , and the double-damage debits,  $D_{ij}$ , for a given mission were calculated using the stresses occurring at the end of that mission. For the final mission in a test, the relaxation was calculated at the number of missions corresponding to first cracking. All life predictions were made for typical bolt-hole behavior, i.e., half of the holes in the disk showing 1/32 inch cracks. In all three tests, a sufficient portion of the bolt holes were cracked to establish the actual typical lives. Typical lives are shown in Table 11.

TABLE 10

## PHASE II CUMULATIVE DAMAGE SPECIMEN TEST CONDITIONS AND RESULTS

Test conditions				Actual lives		Miner's rule		Double damage	
Schematic	$\alpha$ -Loading		$\beta$ -Loading	$n_\beta$	$n_\alpha + n_\beta$	Formula	$n_\beta$	$n_\alpha + n_\beta$	Formula
	S	$n_\alpha$							
BH32-2 	55-55 (ksi)	500	50-50 (ksi)	3000 8500	8500 9000	$1 = \frac{500}{3600} + \frac{n_\beta}{9250}$	7970	8470	$1 = \frac{500}{3600} + \frac{n_\beta}{0.494(9250)}$
BH29-1 	50-50 (ksi)	3000	73-37 (ksi)	8000 8000	11,000 11,000	$1 = \frac{3000}{9250} + \frac{n_\beta}{8730}$	>5900	>8900	$1 = \frac{3000}{9250} + \frac{n_\beta}{1.064(8730)}$
BH29-2 	50-50 (ksi)	1500	73-37 (ksi)	8000 8000	9500 9500	$1 = \frac{1500}{9250} + \frac{n_\beta}{8730}$	>7300	>8800	$1 = \frac{1500}{9250} + \frac{n_\beta}{1.064(8730)}$
BH27 	50-50 (ksi)	3000	50-50 (ksi) Dwell	4000 4000	7000 7000	$1 = \frac{3000}{9250} + \frac{n_\beta}{36,900}$	24,930	27,930	$1 = \frac{3000}{9250} + \frac{n_\beta}{0.252(36,900)}$
BH62 	55-55 (ksi) Dwell	3000	50-50 (ksi)	22,000 38,000	25,000 41,000	$1 = \frac{3000}{16,250} + \frac{n_\beta}{16,000}$	13,050	16,050	$1 = \frac{3000}{16,250} + \frac{n_\beta}{1.350(16,000)}$
BH73-1 	50-50 (ksi) Dwell	14,000	55-55 (ksi)	3500 5000	17,500 19,000	$1 = \frac{14,000}{36,900} + \frac{n_\beta}{15,600}$	9680	23,680	$1 = \frac{14,000}{36,900} + \frac{n_\beta}{1.532(15,600)}$
BH73-2 	50-50 (ksi) Dwell	7000	55-55 (ksi)	4000 11,000	11,000 18,000	$1 = \frac{7000}{36,900} + \frac{n_\beta}{12,900}$	10,450	17,450	$1 = \frac{7000}{36,900} + \frac{n_\beta}{2.098(12,900)}$
BH73S 	50-50 (ksi) Dwell	-	55-55 (ksi)	-	1608 1808	$1 = \frac{1}{36,900} + \frac{4}{14,300}$	-	3260	$1 = \frac{4}{14,300} + \frac{1}{0.400(36,900)}$

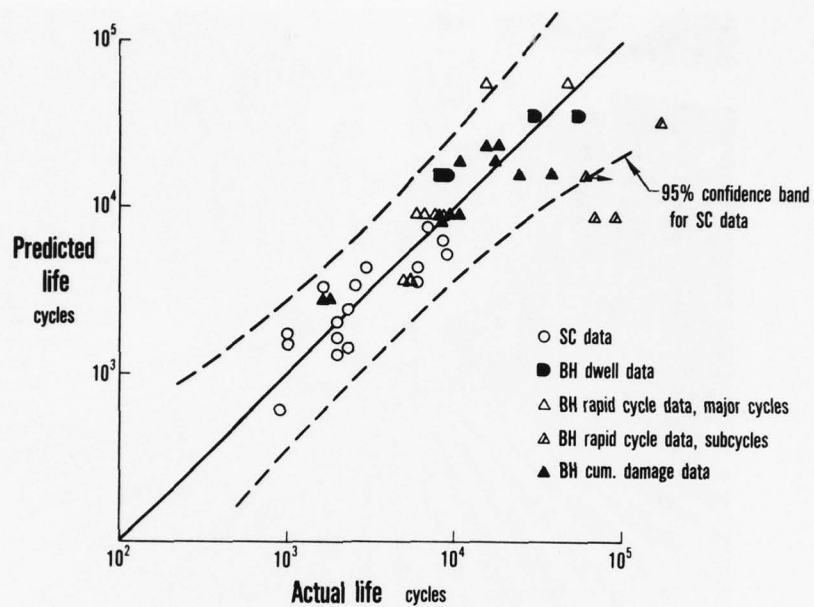


Figure 45 Correlation of Phase II Simple Cycle and Cumulative Damage Specimen Testing

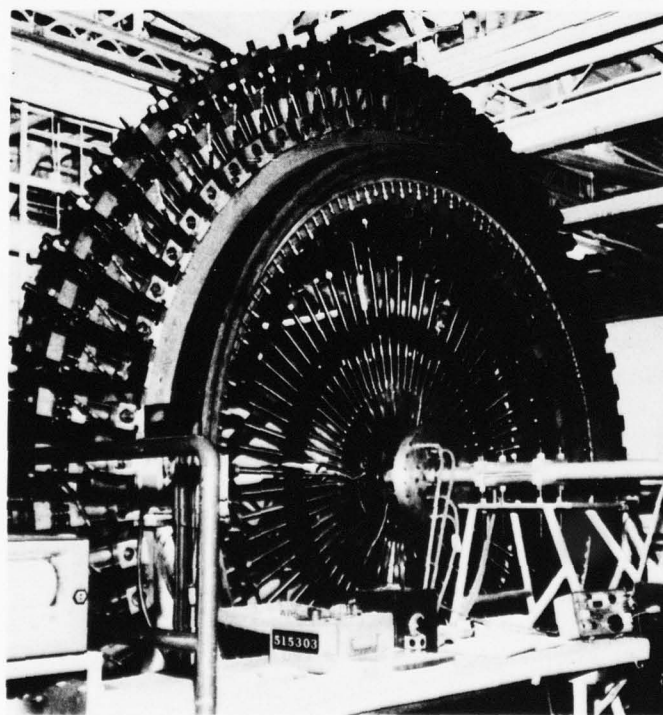


Figure 46 Phase II Ferris Wheel Rig (77-441-4008-A)

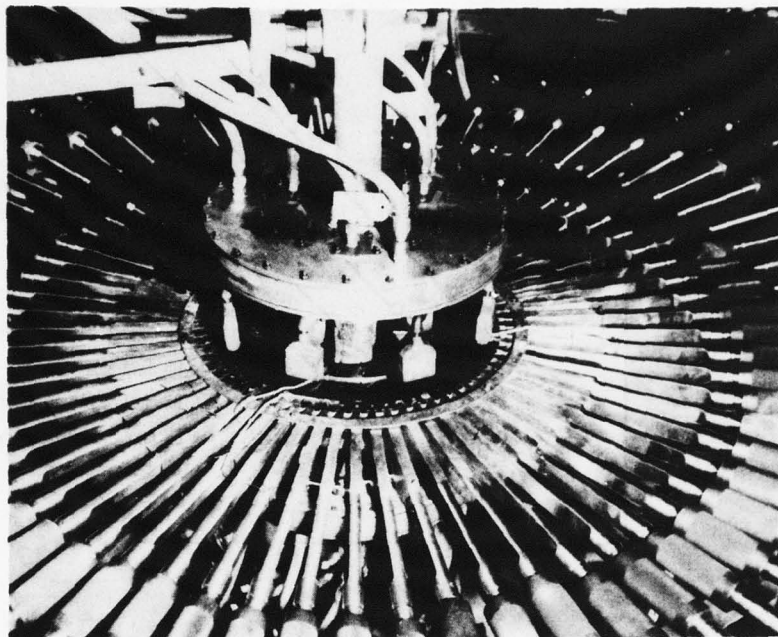


Figure 47 Phase II Ferris Wheel Disk in Test Rig (77-441-4008-B)

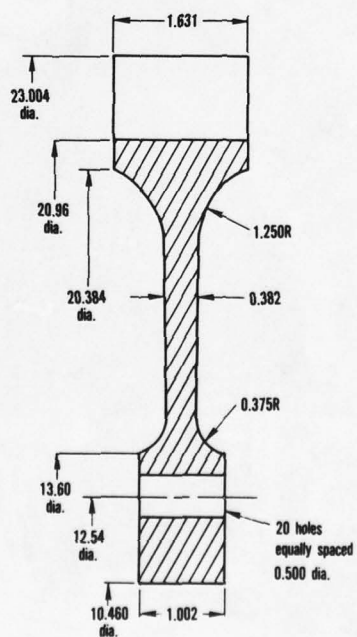


Figure 48 Dimensions of Phase II Ferris Wheel Disk



TABLE 11

## PHASE II FERRIS WHEEL TEST CONDITIONS AND RESULTS

	Order of loading	Nominal stress levels						
		Predicted life of last type	First Mission			Second Mission		Third Mission
			Event	Smin and (t <sub>2</sub> )	Smax (t <sub>1</sub> )	Smin (t <sub>2</sub> )	Smax (t <sub>1</sub> )	Smin and (t <sub>2</sub> ) Smax and (t <sub>1</sub> )
F/W <sub>1</sub>		440	Dwell	-	115.9 ksi (106 sec)	-	-	-
			Subcycle	47.5 ksi (12 sec)	115.9 ksi (4 sec)	-	-	-
F/W <sub>2</sub>		4430	Dwell	-	90.1 ksi (105 sec)	-	90.1 ksi (105 sec)	-
			Subcycle	36.9 ksi (5 sec)	90.1 ksi (5 sec)	46.9 ksi (5 sec)	100.0 ksi (6 sec)	-
F/W <sub>3</sub>		3250	Dwell	-	90.1 ksi (105 sec)	-	90.1 ksi (114 sec)	90.1 ksi (105 sec)
			Subcycle	46.9 ksi (5 sec)	100.0 ksi (5 sec)	36.9 ksi (3 sec)	77.5 ksi (4 sec)	46.9 ksi (5 sec) 100.0 ksi (5 sec)

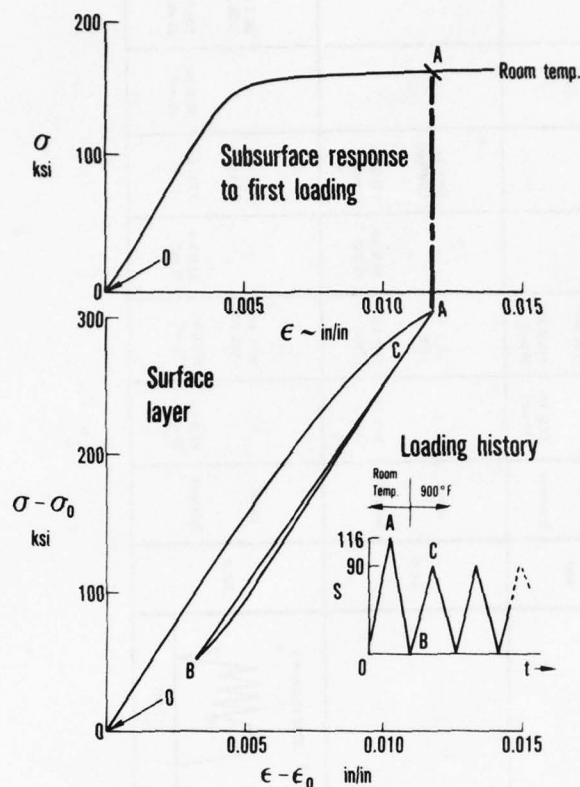


Figure 49 Local  $\sigma$ ,  $\epsilon$  Response to Room Temperature Loading

In disk tests F/W<sub>2</sub> and F/W<sub>3</sub>, the loading was changed from one type of mission to another relatively early in the life of the disk, thus creating the possibility that the initiation life was not exhausted prior to the change in mission type. As stated previously, the double-damage debit,  $D_{ij}$ , is properly applied only to those cycles occurring after the initiation life has been exhausted. In the case of disk test F/W<sub>3</sub>, the assumption that the initiation life was exhausted (i.e.,  $\hat{a}$  existed) during the first applications of Mission C leads to a double-damage prediction that the disk would have failed during Mission B loading. This assumption obviously was not the case. On the other hand, if the 1300 Mission C and the 2500 Missions B contributed only to initiation damage, the double-damage model would predict an additional 3250 Missions C until failure of half of the bolt holes which agrees very well with actual life.

It is clear that if 1300 Missions C were insufficient to exhaust the initiation life in F/W<sub>3</sub>, then certainly only 850 Missions A would also not exhaust the initiation life in F/W<sub>2</sub>. The double-damage life model then predicts that an additional 4430 Missions C would be needed to fail 50 percent of the bolt holes. This prediction also agrees very well with the actual typical life as shown in Table 11.

Since only one type of mission was used in disk test F/W<sub>1</sub>, all subcycles were assumed to contribute to the propagation of the crack,  $\hat{a}$ . Consequently, the predicted life is conservative. But again, the agreement between actual and predicted lives is good.

Figure 50 shows the overall correlation of all Phase II specimen and Ferris Wheel tests. The correlation of all the cumulative damage tests is within the 95 percent confidence band determined from the SC data alone. The Weibull distribution of the data (subcycle data not included as discussed previously) is shown in Figure 51. This overall correlation is judged to be very good indicating that the various components of the prediction model accurately describe the damage processes that occurred.

#### 6.4 CUMULATIVE DAMAGE PREDICTION COMPUTER PROGRAM

A computer program was written for the prediction of disk cumulative damage life exhaustion using the methods discussed in this report. The program recognizes the existence of a surface layer and the relaxation of stresses caused by dwell periods. The cumulative damage effects are modeled by the double-damage method described above. The assumption is made that all minor cycles contribute to propagation life exhaustion. The computer program is discussed further in Appendix E. Computer program documentation is contained in References 1 and 2.

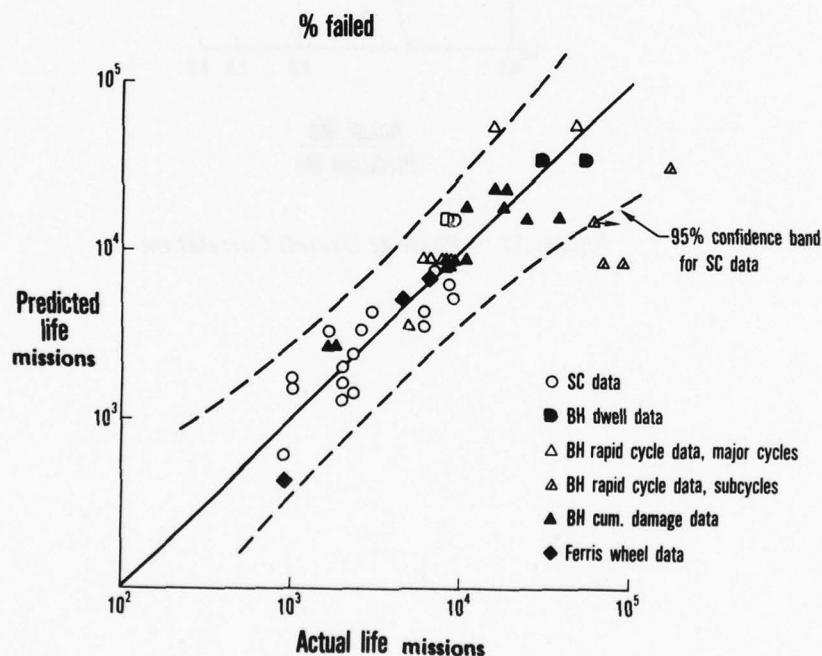


Figure 50 Correlation of Phase II Specimen and Ferris Wheel Data

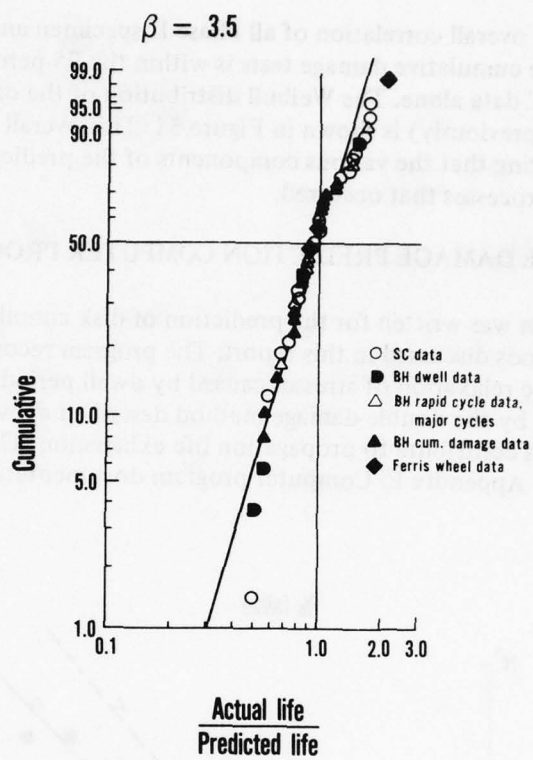


Figure 51 Phase II Overall Correlation



## SECTION VII

### CONCLUSIONS AND RECOMMENDATIONS

#### 7.1 LCF LIFE EXHAUSTION MODELS

Prediction of low cycle fatigue (LCF) damage due to complex load history is an active area of research<sup>7,8</sup> and is not limited to aerospace applications<sup>9</sup>. A major conclusion of the current work is that most of the published fatigue results (such as those presented in Dowling et al<sup>10</sup>) are inappropriate for the current research effort due to the use of balanced strain testing which neglects mean stress effects. Further, it is concluded that no acceptable design model can be generated that does not reflect differences due to specimen type and machining effects.

The approach used in the reported research and development program was the local strain approach, as discussed by Dowling et al; that is, unnotched, strain controlled specimens are tested at conditions of strain range and mean stress that represent those of the loaded notch. The notch conditions were necessarily modeled in a manner that accounted as fully as possible for nonlinear response, in a cost-effective manner. However, it was clearly concluded that notched specimens, representative of the actual component notch including all machining operations, must be tested in order to predict component life. Further conclusions on machining effects are discussed in Section 7.2.

Simple correlation models such as used in the current effort can successfully fit LCF data taken over a wide range of loading and specimen conditions if proper care is taken to define the local strain and mean stress conditions. The approach used emphasizes automated correlation methods, as opposed to engineer-interpreted design curves. With care, some of the "scatter" between actual lives and the simple correlation model can be reduced by local adjustments in the life curves. However, the risk that the adjustment could be in error for other load conditions is perhaps as great as the original error. It is concluded that the simple correlation model is as good an approach for design as hand drawn life curves, for the data obtained in the current program.

The life prediction model is based on correlating the number of LCF cycles to initiate a 1/32 inch surface length crack in the specimens and components. It was concluded that while some propagation of a coherent crack was involved in the LCF initiation life, the effects of different stress (strain) gradients was not important. Further, it was concluded that all lives (with a possible exception for very short LCF life data) included demonstrable initiation and propagation behavior. While further research into microcrack growth modeling is recommended, the use of a fracture mechanics model for the LCF life data obtained is not recommended<sup>11</sup>.

## 7.2 SURFACE LAYER MODELS AND MACHINING EFFECTS

Clearly, one of the most important conclusions from the current research and development effort was the need to systematically account for a surface layer of previously worked material in the tested notches. While it is generally accepted that both residual stress and surface cyclic work hardening are important effects<sup>12</sup>, the authors are not aware of a simple model for these effects, comparable to the one successfully adopted in the current effort.

Scatter in LCF life data is a major influence on minimum design life calculations for a safe-life design methodology. Control of scatter to increase the minimum cyclic life is a critical area for future research. The simple surface layer model developed in the current effort is based only on bolt holes, machined under carefully controlled conditions. Further research is required to establish better models for the nature of the surface layer work hardening, the level of the imposed residual stresses, and the effects of different machining operations. While such an effort is a major undertaking, the potential pay-off appears to be quite attractive in terms of increased performance and reduced cost for critical rotating structure components.

## 7.3 DWELL (CREEP) EFFECTS

The presence of time dependent behavior in turbine disks was clearly established in the current effort. All of the elevated temperature testing emphasized dwell events at high stress levels which generally benefit life. However, the analytical model adopted for dwell effects on mean cyclic stress includes the potential for life debits due to dwell at low stress levels. Further testing to verify the potential life debit is recommended.

It was generally concluded that no acceptable material behavior analytical model exists for predicting the time-dependent creep effect which can account for cyclic loading at locally high stress levels. Thus, cyclic test data had to be obtained which could be used to develop a simple exponential decay model for cyclic dwell stresses. The model used was based on data at one stress level and one temperature. Further work is required to develop a calibrated model of dwell stress relaxation for different stresses and temperatures.

Finally, the current effort did not involve creep-fatigue interaction effects. While such problems also involve time-dependent plasticity, the temperature levels of the current effort are not judged to be sufficient to contribute creep damage to the material microstructure. Major new research efforts are required to model creep-fatigue damage at a level of confidence comparable to that achieved in the current effort.

## 7.4 CUMULATIVE DAMAGE MODEL

An early conclusion in the research and development effort was that the nature of LCF cycles in military gas turbine engine disks contained one critical simplification. Essentially all important cyclic stress excursions at the disk bolt-holes shared a common maximum stress. Thus, nonlinear overload damage retardation modeling was not required. This conclusion will generally apply to all disk notch locations with the exception of those seeing major transient, thermally driven excursions.

The only nonlinear damage effect that remained was named by Manson<sup>13</sup> as the "double-damage" effect. Simply stated, a stress (strain) cycle does damage at a different rate on cracked material than on uncracked material. The data generated in the current program clearly supported this hypothesis. A fracture mechanics based model was developed which accounts for this effect by debiting the cyclic initiation life of low amplitude cycles to account for the cracking damage done by the major cycles. While somewhat conservative, the adopted algorithm was found to give good nonlinear damage estimates for military mission modeling.

## 7.5 DESIGN MODELS FOR LCF LIFE EXHAUSTION

The model developed by the current effort is judged to be suitable for design purposes under a few stipulated limitations. The current effort was calibrated only for disk bolt-holes, although the procedures are felt to be generally applicable. Single heats of the two materials and single machining operations were included in the current statistical base. Actual design implementation of the current model must include the greater statistical scatter associated with heat-to-heat and processing variables. Application of the current model to hot section components is limited to zero creep-fatigue interaction and to mission cycles represented by nearly constant values of peak tensile cyclic stresses. Also, calibration of the dwell model used is limited, as discussed in Section 7.3, to a single temperature and dwell stress level.

Use of the developed LCF life exhaustion model for engine disk design is possible for new alloy systems where data generation can be obtained along lines similar to those used in the reported program. Application of the developed model to old materials is not recommended without the development of the necessary new data base. In both cases, it should be clearly recognized that the development of a data base for LCF life exhaustion modeling for design purposes is a major undertaking.

## APPENDIX A

## MATERIAL CHARACTERIZATION

Basic material characterization tests were conducted for a single heat code of each of two disk alloys: Ti (6Al-2Sn-4Zr-6Mo), (PWA 1216), heat code CAAZ and WASPALOY<sup>®</sup> (PWA 1057), heat code XNNZ. Monotonic and cyclic uniaxial stress-strain tests were performed for both materials using the close-loop, servo-controlled MTS testing machine. The specimen used is the strain controlled specimen shown in Figure A-1. Gage section strains were controlled within  $\pm 0.001$  in/in; loads were measured with an accuracy of  $\pm 30$  lb. In addition cyclic relaxation and standard creep tests were performed for PWA 1057 using the specimens shown in Figures A-1 and A-2 respectively.

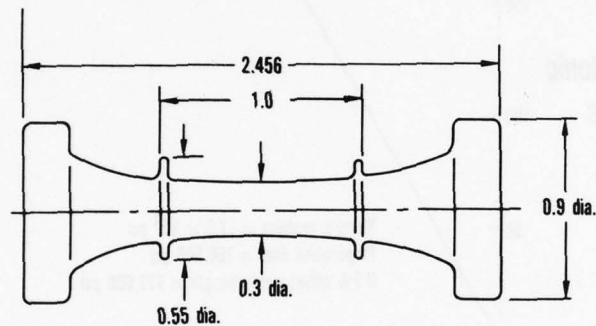


Figure A-1 Strain Controlled Constitutive Test Specimen

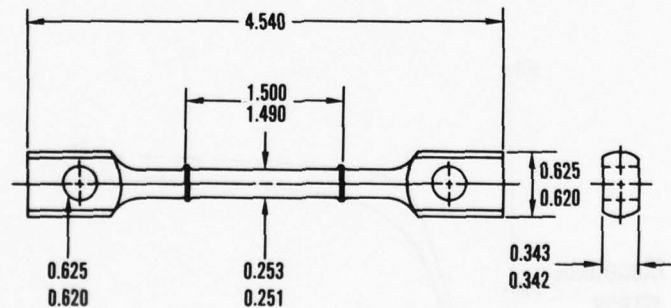


Figure A-2 Creep Specimen



The monotonic stress-strain curves are shown in Figures A-3 and A-4. No strain rate sensitivity was observed over the range of strain rates of interest; 0.01 in/in/min to 0.10 in/in/min. Yield behavior of the PWA 1057 was discontinuous at 900°F. Figure A-5 is a tracing of an actual load-deflection plot showing this discontinuous behavior. These slip bursts were accompanied by acoustical emissions and were observed only during monotonic straining greater than approximately 0.007 in/in. The load drop during these slip bursts were within the variation of the monotonic strengths from repeated tests and were therefore not modeled explicitly by the monotonic curve adopted for use in this program.

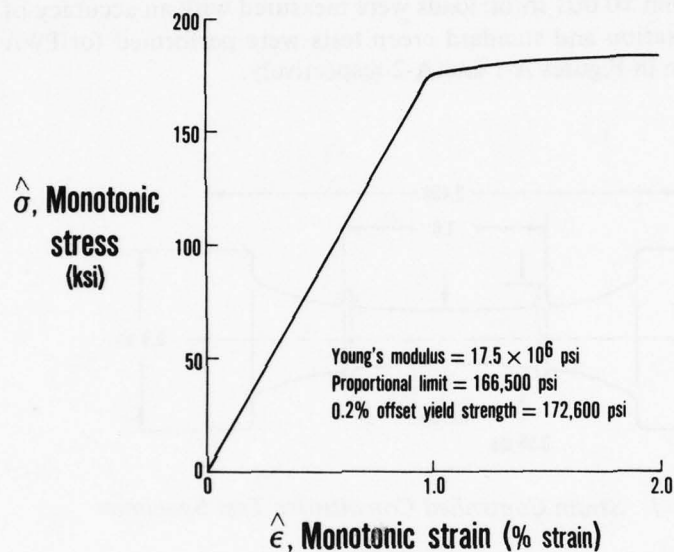


Figure A-3 PWA 1216 Room Temperature Monotonic Stress-Strain Curve

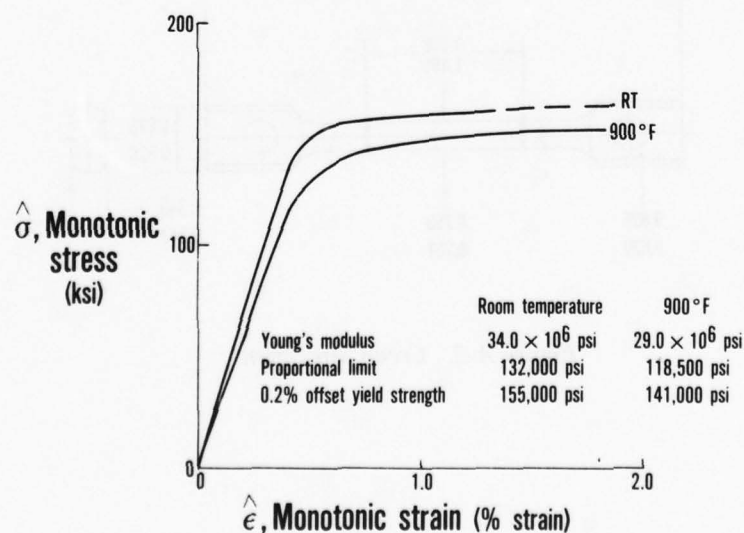


Figure A-4 PWA 1057 Monotonic Stress-Strain Curve

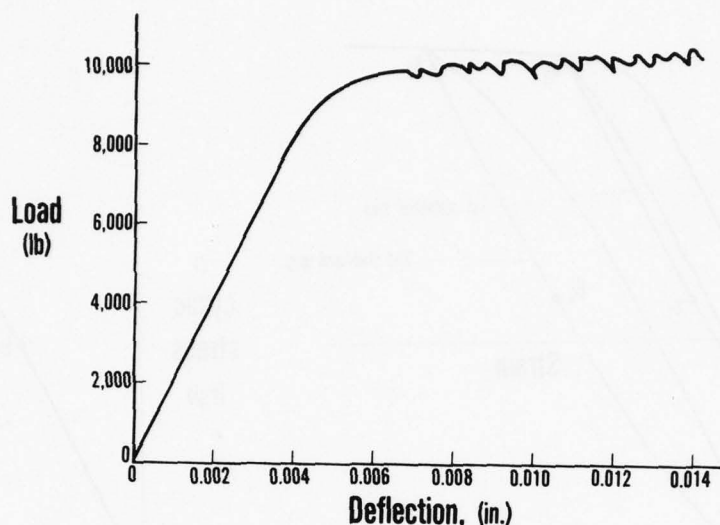


Figure A-5 Load-Deflection Tracing Showing Discontinuous Yielding of PWA 1057 at 900°F

Incremental step tests were used to characterize the cyclic stress-strain behavior of the two materials. Cycling was strain controlled at a fixed strain rate between selected strain limits until stabilized hysteresis loops were observed. Maximum strain limits were incrementally increased while maintaining the same minimum strain. Figure A-6a illustrates the technique. In both PWA 1216 and PWA 1057, stabilized hysteresis loops were obtained within a few cycles. Neither material exhibited cyclic hardening or cyclic softening. The cyclic stress-strain behavior was characterized by plotting the shapes of the hysteresis curves, i.e., curves A, B, and C for each test. This is illustrated in Figure A-6b. For PWA 1216, the shape of each hysteresis loop formed a single hysteresis curve (Figure A-7), while in PWA 1057, each strain range had its own characteristic curve shape (Figure A-8). The loci of tips of such curves were taken to represent the cyclic behavior of PWA 1057. The resulting curves are shown in Figure A-9.

Standard creep tests of PWA 1057 at 900°F were conducted using the specimen shown in Figure A-2. The results of these tests are shown in Figure A-10.

Two cyclic relaxation tests were also conducted using the specimen shown in Figure A-1. During these tests, the specimen was cycled between fixed strain limits with a 125 second "dwell" time imposed at the maximum strain of each cycle. While total stress range was unchanged during cycling (neither hardening nor softening) the peak stress, and consequently the mean stress was observed to change during cycling. These results are shown in Figure A-11. The stress relaxation was found to be approximated by equation A-1.

$$\sigma = 155 e^{-0.002 t}$$

where

$\sigma$  = the current stress (KSI)

$t$  = time spent at peak stress (hr)

(A-1)

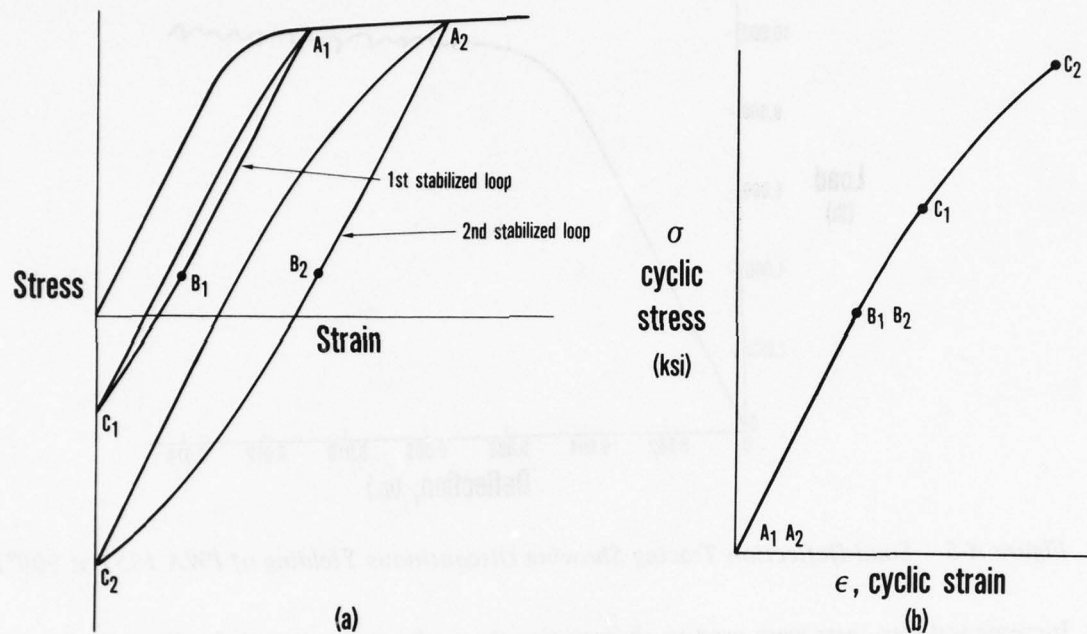


Figure A-6 Incremental Step Tests Used to Establish Hysteresis Curve

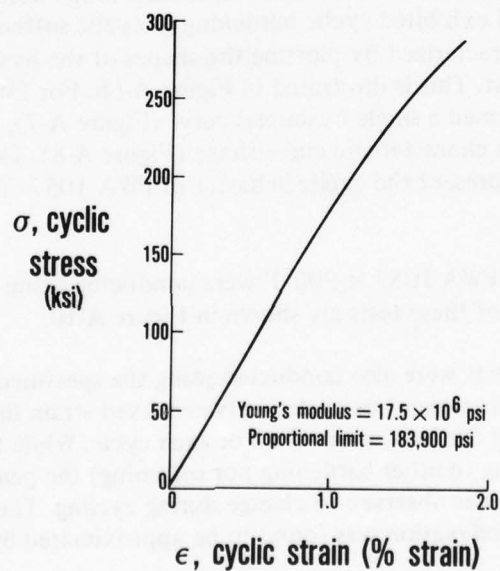


Figure A-7 PWA 1216 Hysteresis Curve Shape

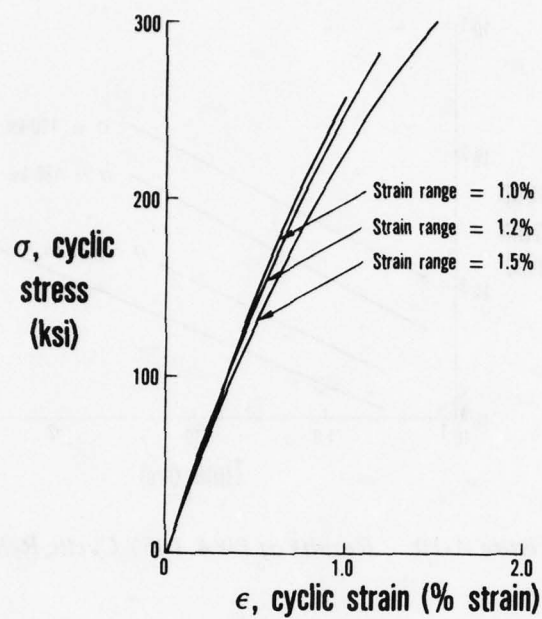


Figure A-8 PWA 1057 Hysteresis Curves Show Dependence Upon Strain Range

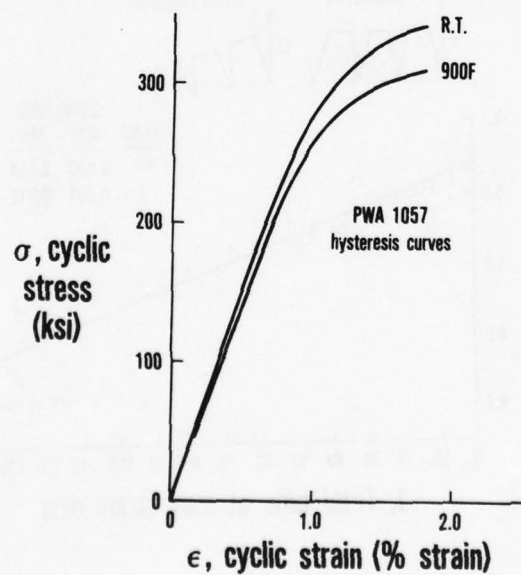


Figure A-9 PWA 1057 Hysteresis Curve Shapes



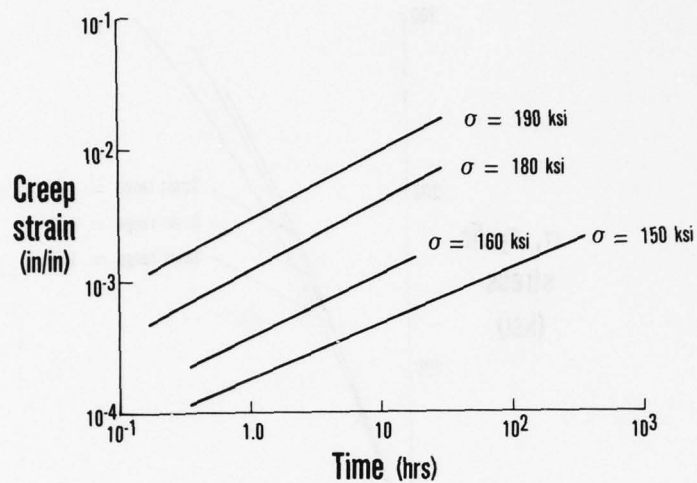


Figure A-10 Results of PWA 1057 Cyclic Relaxation Test

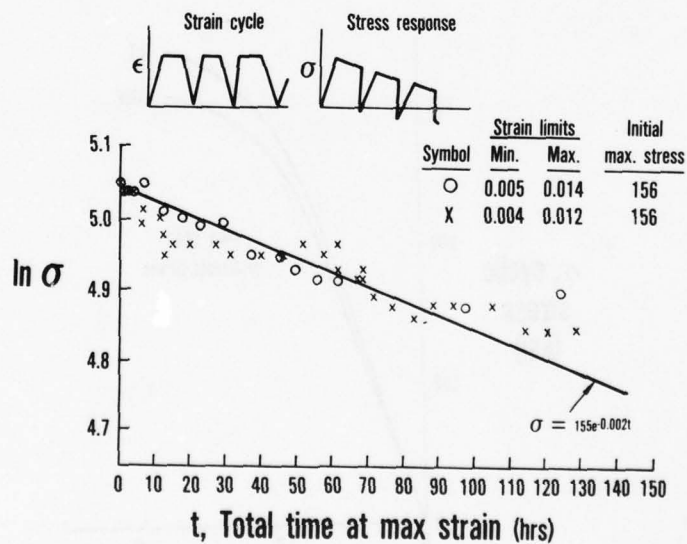


Figure A-11 Results of PWA 1057 Cyclic Relaxation Test

## APPENDIX B

### SURFACE LAYER ALGORITHM

The following procedure for calculating local surface mean stress recognizes the influences of residual surface stresses due to machining and cold working. The influence of residual stresses was found to be of prime importance in developing a fatigue life prediction model that encompassed both Strain Controlled (SC) and Bolt Hole (BH) specimens.

The bolt hole region can be viewed as a thin preworked surface layer having an initial stress state ( $\sigma_0, \epsilon_0$ ) lying atop a subsurface region of virgin material (Figure B-1). Because the residual machining stresses do not extend appreciably below the bolt hole surface, the bulk response of the region is not significantly altered by the prestressed surface layer and can therefore be modeled by the modified Neuber approach, as given in Section 4.0. Compatibility requires that both surface and subsurface strain excursions are identical. However, the stress-strain response of the two regions will be different since the surface layer has already experienced large plastic strains during machining, and is therefore responding according to the hysteresis curve shape, whereas the subsurface region is not.

Consequently, during the loading portion of the first cycle (A to B in Figure B-1), as the subsurface region strains to an amount  $\hat{\epsilon}$  (determined by the modified Neuber approach) along the monotonic stress-strain curve, the surface layer will experience an equal strain excursion along the hysteresis curve described in Appendix A. The local surface stress after the first loading is then given by

$$\sigma_{\max} = \sigma_0 + \sigma(\hat{\epsilon}) \quad (\text{B-1})$$

where  $\sigma(\hat{\epsilon})$  is the stress from the hysteresis curve at  $\hat{\epsilon}$ . Subsequent cyclic loading causes a strain excursion  $\Delta\epsilon$  in both the surface layer and subsurface region. The surface mean stress is then given by

$$\sigma_m = \sigma_0 + \sigma(\hat{\epsilon}) - \frac{1}{2} \sigma(\Delta\epsilon) \quad (\text{B-2})$$

The terms in (B-2) can be identified as the initial stress state, the first loading cycle stress excursion and one half the cyclic stress.

For the SC specimens which were electrochemically machined, or for an ideal bolt hole consisting of completely virgin material, the surface mean stress is

$$\sigma_m = \hat{\sigma}(\hat{\epsilon}) - \frac{1}{2} \sigma(\Delta\epsilon) \quad (\text{B-3})$$

where  $\hat{\sigma}(\hat{\epsilon})$  is the stress from the monotonic stress-strain curve at  $\hat{\epsilon}$ .

It should be noted that  $\sigma_{\max}$  of (B-1) is valid only for

$$\sigma_{\max} \leq \hat{\sigma}(\hat{\epsilon} + \epsilon_0) \quad (\text{B-4})$$

That is, the maximum local stress cannot be greater than that permitted by the monotonic stress-strain curve. For the materials considered in this document, (B-4) can be written approximately as

$$\sigma_{\max} \lesssim \hat{\sigma}(\hat{\epsilon}) \quad (\text{B-5})$$

If (B-5) is violated, e.g., for a particularly large first quarter cycle stress excursion, the surface mean stress will be given approximately by (B-3). In such a case, the effect of the surface layer initial stress state is essentially "wiped-out" and subsequent behavior of the surface layer will be identical to the subsurface behavior.

Comparison of (B-2) and (B-3) reveals that the local mean stress for a BH specimen and a SC specimen undergoing the same strain excursions differs by an amount  $\Delta\sigma_m$ :

$$\Delta\sigma_m = \hat{\sigma}(\hat{\epsilon}) - \sigma_0 - \sigma(\hat{\epsilon}) \quad (\text{B-6})$$

Thus, the residual stresses due to machining effectively shift the mean stress values for bolt holes relative to SC specimens, and it is clear that this shift is a function of the maximum load applied to the specimen.

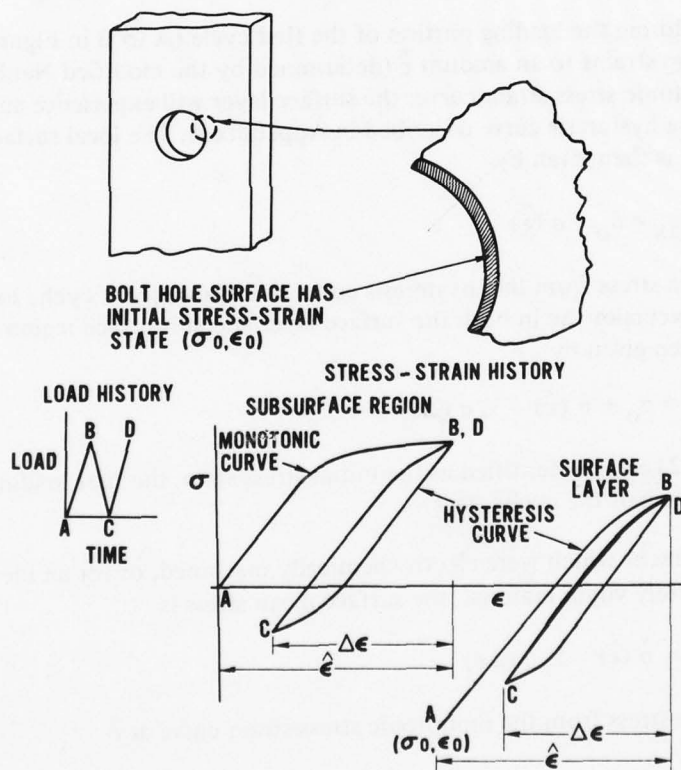


Figure B-1 Cyclic Loading of a Bolt Hole Specimen

## APPENDIX C

### MEAN STRESS RELAXATION MODEL

During repeated flights, a turbine disk bolt hole may be subjected to temperatures and stresses sufficient to cause time dependent material behavior in the hole. Because the bolt hole region is constrained by surrounding elastic material in the disk, the hole region can be viewed as a strain-controlled region. In this strain-controlled environment, the time dependent material response will result in stress relaxation.

The following procedure recognizes the composite influences of the various activities experienced during repeated applications of a complex mission. Any complex mission, Figure C-1, can be subdivided into separate activities, each of which will contribute to the relaxation of the bolt hole stresses. Consider the stress history during the  $i^{\text{TH}}$  activity of the first flight of the complex mission. The salient features of the activity are shown in Figure C-2. During the first complete cycle of the activity (a-b-c-d-e), the time averaged stress,  $\bar{\sigma}_{i0}$ , is given by

$$\bar{\sigma}_{i0} = \frac{\sigma_1 t_1 + \sigma_2 t_2}{t_1 + t_2} \quad (\text{C-1})$$

where  $\sigma_1, \sigma_2$  = the first cycle maximum and minimum stresses respectively

$t_1, t_2$  = "dwell" times at the maximum and minimum stresses respectively

A cruise activity such as the 2nd activity in Figure C-1 can be modeled by letting  $\sigma_2 = t_2 = 0$ .

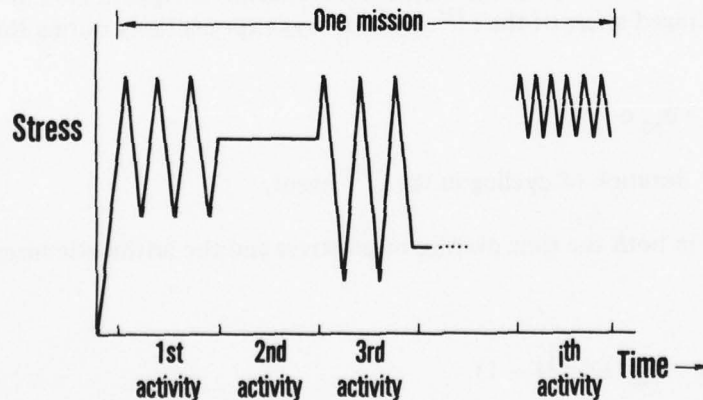


Figure C-1 The Component Activities in a Typical Mission



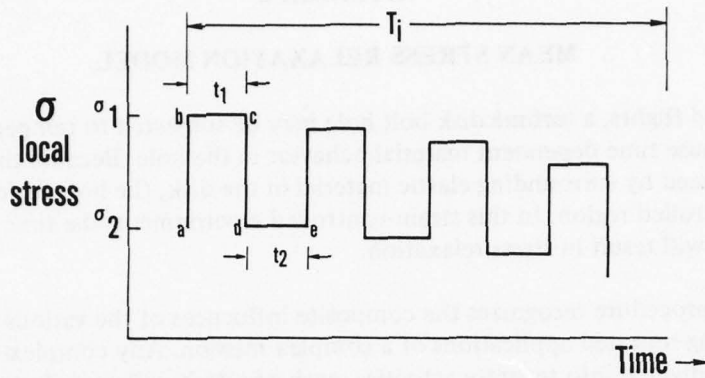


Figure C-2 Simplified History of the  $i^{TH}$  Mission Activity

Equivalently,

$$\bar{\sigma}_{io} = \sigma_{mi}^o - \frac{\Delta\sigma_i}{2} \left( \frac{t_2 - t_1}{t_2 + t_1} \right) \quad (C-2)$$

where  $\sigma_{mi}^o = \frac{\sigma_1 + \sigma_2}{2}$  = arithmetic mean stress during the first cycle

$$\Delta\sigma_i = \sigma_1 - \sigma_2$$

Based on the results of the cyclic relaxation tests reported in Appendix A, it will be assumed that the time averaged stress of the  $i^{TH}$  event decays exponentially during the first flight. That is

$$\bar{\sigma}_{i1} = \bar{\sigma}_{io} e^{-\alpha T_i} \quad (C-3)$$

where  $T_i$  = duration of cycling in the  $i^{TH}$  event.

Then the change in both the time average mean stress and the arithmetic mean stress after time  $T_i$  is

$$\Delta\sigma_{i1} = \bar{\sigma}_{io} (e^{-\alpha T_i} - 1) \quad (C-4)$$

Suppose the mission to be analyzed contains  $\eta$ , different activities. Then the total change in mean stress due to those  $\eta$  activities in the first flight,  $\langle \Delta \sigma \rangle_1$ , is given by

$$\langle \Delta \sigma \rangle_1 = \sum_{i=1}^{\eta} \Delta \sigma_{i1}$$

$$\langle \Delta \sigma_m \rangle_1 = \sum_{i=1}^{\eta} \bar{\sigma}_{i0} (e^{-\alpha T_i} - 1) \quad (C-5)$$

During the second flight of the mission, the arithmetic mean stress of the first cycle of an event  $i$  will be shifted by an amount  $\langle \Delta \sigma_m \rangle_1$  from the corresponding value in the first flight. Consequently,

$$\Delta \sigma_{i2} = (\bar{\sigma}_{i0} + \langle \Delta \sigma_m \rangle_1) (e^{-\alpha T_i} - 1) \quad (C-6)$$

and

$$\langle \Delta \sigma_m \rangle_2 = \sum_{i=1}^{\eta} \Delta \sigma_{i2}$$

$$\langle \Delta \sigma_m \rangle_2 = \sum_{i=1}^{\eta} (\bar{\sigma}_{i0} + \langle \Delta \sigma_m \rangle_1) (e^{-\alpha T_i} - 1) \quad (C-7)$$

In general, the mean stress relaxation during the  $j^{\text{TH}}$  mission is

$$\langle \Delta \sigma_m \rangle_j = \sum_{i=1}^{\eta} \Delta \sigma_{ij} \quad (C-8)$$

$$\langle \Delta \sigma_m \rangle_j = \sum_{i=1}^{\eta} (\bar{\sigma}_{i0} + \sum_{k=1}^{j-1} \langle \Delta \sigma_m \rangle_k) (e^{-\alpha T_i} - 1) \quad (C-9)$$

For convenience, let

$$A = \sum_{i=1}^{\eta} \bar{\sigma}_{i0} (e^{-\alpha T_i} - 1)$$

and

$$B = \sum_{i=1}^{\eta} (e^{-\alpha T_i} - 1)$$

Consider now, the relaxation during the j and (j-1) flights

$$\langle \Delta \sigma_m \rangle_j = A + B \left\{ \langle \Delta \sigma_m \rangle_1 + \langle \Delta \sigma_m \rangle_2 + \dots + \langle \Delta \sigma_m \rangle_{j-2} + \langle \Delta \sigma_m \rangle_{j-1} \right\} \quad (C-10)$$

$$\langle \Delta \sigma_m \rangle_{j-1} = A + B \left\{ \langle \Delta \sigma_m \rangle_1 + \langle \Delta \sigma_m \rangle_3 + \dots + \langle \Delta \sigma_m \rangle_{j-2} \right\} \quad (C-11)$$

Subtracting (C-11) from (C-10) gives a recursion formula for  $\langle \Delta \sigma_m \rangle_j$

$$\langle \Delta \sigma_m \rangle_j = (B + 1) \langle \Delta \sigma_m \rangle_{j-1} \quad (C-12)$$

And (C-12) can also be written as

$$\langle \Delta \sigma_m \rangle_j = (B + 1)^{j-1} \langle \Delta \sigma_m \rangle_1 \quad (C-13)$$

The total change at the end of N flights of the mission,  $\bar{\sigma}_R$ , is then

$$\bar{\sigma}_R = \sum_{j=1}^N \langle \Delta \sigma_m \rangle_j \quad (C-14)$$

$$\bar{\sigma}_R = \langle \Delta \sigma_m \rangle_1 \sum_{j=1}^N (B + 1)^{j-1} \quad (C-15)$$

(C-15) is simply a geometric progression and can be written as

$$\bar{\sigma}_R = \langle \Delta \sigma_m \rangle_1 \frac{(B + 1)^N - 1}{B} \quad (C-16)$$

or

$$\bar{\sigma}_R = \frac{\sum_{i=1}^{\eta} \bar{\sigma}_{i0} (e^{-\alpha T_i} - 1)}{\sum_{i=1}^{\eta} (e^{-\alpha T_i} - 1)} \left\{ \left[ 1 + \sum_{i=1}^{\eta} (e^{-\alpha T_i} - 1) \right]^N - 1 \right\} \quad (C-17)$$

This relaxation expression can be applied to simple cycle tests of specimens. For the simple rapid cycle test shown in Figure C-3a, (C-17) reduces to

$$\bar{\sigma}_R = \sigma_m^{\circ} (e^{-\alpha T} - 1) \quad (C-18)$$

At time T,

$$\sigma_m = \sigma_m^{\circ} + \bar{\sigma}_R$$

Thus, the mean stress of such a cycle would relax to zero, given sufficient time.

For the dwell cycle shown in Figure C-3b, (C-17) reduces to

$$\bar{\sigma}_R = (\sigma_m^{\circ} + \frac{\Delta\sigma}{2}) (e^{-\alpha T} - 1) \quad (C-19)$$

At time T,

$$\sigma_m = \sigma_m^{\circ} + \bar{\sigma}_R$$

Thus, the mean stress relaxes to the limit

$$\sigma_m = -\frac{\Delta\sigma}{2} \quad (C-20)$$

and the minimum stress in the cycle,  $\sigma_{\min}$ , relaxes by the same amount to

$$\sigma_{\min} = \sigma_2 - \sigma_m^{\circ} - \frac{\Delta\sigma}{2} \quad (C-21)$$

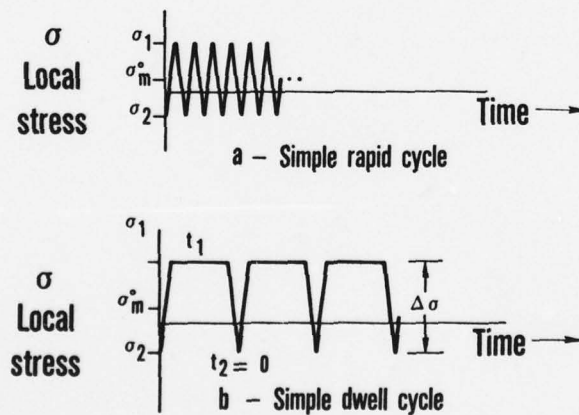


Figure C-3 Cyclic Test Characterization



However, it is obvious that  $\sigma_{\min}$  can never be less than the compressive strength of the material. Thus, (C-19) is valid so long as

$$\sigma_2 - \sigma_m - \frac{\Delta\sigma}{2} > \sigma_L \quad (\text{C-22})$$

where  $\sigma_L$  is the compressive strength of the material.

Similarly, (C-17) is valid so long as the minimum stress in the flight does not exceed the compressive limit,  $\sigma_L$ .

In summary, the relaxation due to N missions is

$$\bar{\sigma}_R = \frac{\sum_{i=1}^{\eta} \sigma_{i0} (e^{-\alpha T_i} - 1)}{\sum_{i=1}^{\eta} (e^{-\alpha T_i} - 1)} \left\{ \left[ 1 + \sum_{i=1}^{\eta} (e^{-\alpha T_i} - 1) \right]^N - 1 \right\} \quad (\text{C-23})$$

for  $\sigma_{\min} \geq \sigma_L$ .

## APPENDIX D

### STATISTICAL CONSIDERATIONS

#### MULTIVARIATE REGRESSION ANALYSIS

The form of the equation assumed to describe simple cycle LCF behavior is

$$N = A \Delta\epsilon^B 10^{C\sigma_m} \quad (D-1)$$

where  $N$  = fatigue life  
 $\Delta\epsilon$  = strain range  
 $\sigma_m$  = mean stress

The constants A, B and C are determined from a multivariate regression analysis. This section provides a brief description of such an analysis.

For each specimen test conducted, the fatigue parameters  $\Delta\epsilon$  and  $\sigma_m$  are known (either from direct measurement or from analysis) and the resulting fatigue life, N, (in this contract, the number of cycles to the appearance of a 1/32 inch crack) is observed. Many such tests are conducted, and the assumption made is that the typical behavior can be described by (D-1) with the proper values of A, B and C. These values are most easily found by considering the logarithmic form of (D-1)

$$\log N = \log A + B \log \Delta\epsilon + C\sigma_m \quad (D-2)$$

Equation (D-2) is now thought of as an equation to predict the fatigue life of each data point from the known loading conditions,  $\Delta\epsilon_i$  and  $\sigma_{mi}$ , of that data point. The difference between the actual fatigue life  $N_i$  and this predicted life is the error,  $E_i$ , in the prediction.

$$E_i = \log N_i - \log A - B \log \Delta\epsilon_i - C\sigma_{mi} \quad (D-3)$$

The constants log A, B, and C are found by minimizing the sum of the squares of the errors for the entire data set (n data points), i.e., by minimizing the expression

$$\sum^n [\log N_i - \log A - B \log \Delta\epsilon_i - C\sigma_{mi}]^2 \quad (D-4)$$

This is done by differentiating (D-4) partially with respect to log A, B, and C, equating these partial derivatives to zero, and solving three resulting equations for log A, B, and C.

#### EVALUATION OF DATA CORRELATION

Fatigue prediction systems quite frequently display a significant degree of scatter resulting from uncontrolled or unrecognized sources. Several of the major sources of scatter can be

listed as follows:

1. Inherent fatigue scatter
2. Heat-to-heat material variations
3. Fatigue model inadequacies
4. Inaccurate stress analyses
5. Variable machining procedures
6. Application to various components
7. Variations in component usage

With so many sources of variability, it is very difficult to judge the contributions of a single source. In this contract, these sources of scatter were limited to as few as possible. Only single heat codes of material were considered: H/C CAAZ in PWA1216 and H/C XNNZ in PWA1057. Only disk bolt holes under isothermal loading conditions were considered, and the variety of those loading conditions was limited through extensive surveys of actual component use. Machining procedures for each specimen type and the Ferris Wheel disks were controlled as nearly as possible. In addition, the most accurate state-of-the-art methods of stress analysis were employed. Consequently, the list of major sources of scatter was narrowed to the simple cycle and cumulative damage fatigue models themselves (Sections V and VI), the surface layer and relaxation algorithms (Appendix B and C) used in those fatigue models, and, of course, the inherent material fatigue scatter.

It is necessary to evaluate the fidelity of the various models and algorithms used to correlate the fatigue data. A statistical analysis of the correlation can be used in such an evaluation. In this contract, it is assumed that the fatigue data can be characterized by a two-parameter Weibull distribution<sup>14, 15</sup>. The Weibull distribution is given by the formula

$$F(N) = 1 - e^{-(N/\theta)^\beta} \quad (D-5)$$

where

N	= Random variable (life)
F(N)	= Cumulative probability of failure (the area under the distribution curve from n = 0 to N)
$\beta$	= Weibull slope (shape parameter)
$\theta$	= Characteristic life (life corresponding to 63.2 percent cumulative failure rate)

Figure D-1 illustrates two Weibull distributions, each having a characteristic life  $\theta = 40,000$  cycles but having different Weibull slopes,  $\beta$ , which define the amount of scatter in the distributions. For the distribution having  $\beta = 1.3$ , the B10 life (life at which 10 percent of the population would have failed) is 7500 cycles, indicating a fairly large degree of scatter. In contrast, the distribution with Weibull slope  $\beta = 5$  has significantly less scatter since its B10 life is 25,000 cycles.

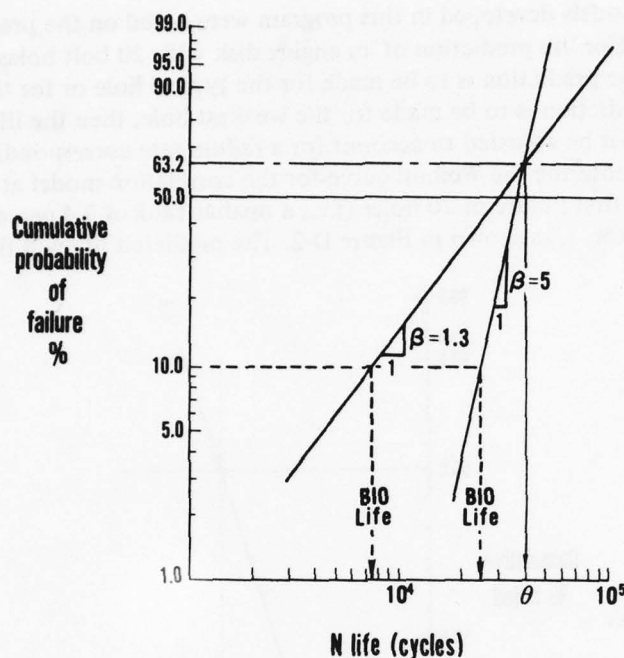


Figure D-1 Sample Weibull Distribution

The Weibull probability plot then can easily be used to compare the overall scatter produced by using a certain correlation model to the scatter that would have resulted from a hypothetical "perfect" correlation model. A perfect correlation model would predict the typical life of every test condition exactly. In such a model, the ratio of actual lives of specimens tested at a given condition to the typical life at that test condition ( $N_{act}/\bar{N}$ ) would describe a Weibull distribution with shape parameter,  $\beta_p$ . All models producing less than perfect correlation would have slopes smaller than  $\beta_p$  when the ratio of actual lives to lives obtained from the correlation model ( $N_{act}/N_c$ ) are plotted. It is desirable that  $\beta$  be as close as possible to  $\beta_p$ .

Certain other features of the Weibull plot can yield pertinent information about the correlation model being analyzed. The data points defining the Weibull line should be continuous: sharp "knees" or discontinuous subsets of data can signal poor correlation for certain data subsets. Likewise, the data should be evenly distributed on the Weibull line. If, for instance, all dwell cycle tests appear at low failure rates while all rapid cycle tests appear at a high failure rate, it would indicate that the correlation model was too optimistic for the dwell data.



## DISK FAILURE PREDICTION

The life prediction models developed in this program were based on the prediction of typical fatigue behavior. For life prediction of an engine disk with 20 bolt holes, it is necessary to specify whether the prediction is to be made for the typical hole or for the weakest hole in the disk. If the prediction is to be made for the weakest hole, then the life predicted by the typical model must be adjusted to account for a failure rate corresponding to one in 20. This can be done by entering the Weibull curve for the correlation model at a median rank corresponding to the first failure in 20 holes (i.e., a median rank of 3.4 percent<sup>15</sup>) and find the appropriate debit factor,  $f$ , as shown in Figure D-2. The predicted life will then be  $f \times N_c$ .

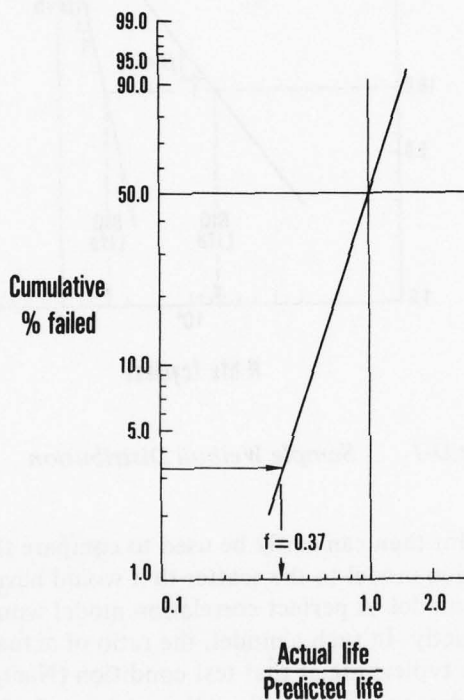


Figure D-2 Weibull Plot Used to Determine Life Debit Factor

It is usually desired to predict the number of cycles to failure (in the weakest bolt hole) for a large population of disks, each containing  $\eta$  bolt holes. To do this, an acceptable disk failure rate,  $F_D$ , must be specified. For example, it may be desired to predict the number of cycles required to cause one bolt hole to crack in 10 percent of the disks. The life debit factor,  $f$ , to be applied to the mean life prediction is determined as follows:

The Weibull distribution from testing of single bolt holes is given by equation D-6.

$$\text{where } F = 1 - e^{-(f/\theta)^\beta} \quad (D-6)$$

- $F$  = reliability rate in single bolt holes
- $f$  = life debit factor ( $= N_{act}/N_c$ )
- $\beta, \theta$  = shape factor and characteristic life of the bolt-hole specimen Weibull plot.

Now, for a disk with  $\eta$  bolt holes

$$1 - F_D = (1 - F)^\eta \quad (D-7)$$

where  $F_D$  is the disk failure rate.

$$1 - F_D = e^{-\eta(f/\theta)^\beta} \quad (D-8)$$

$$\ln(1 - F_D) = -\eta (f/\theta)^\beta$$

$$\ln \ln \left( \frac{1}{1 - F_D} \right) = \ln \eta + \beta \ln f - \beta \ln \theta$$

$$\ln f = \left[ \frac{1}{\beta} \ln \ln \frac{1}{1 - F_D} + \beta \ln \theta - \ln \eta \right]$$

$$f = \exp \left\{ \frac{1}{\beta} \left[ \ln \ln \frac{1}{1 - F_D} + \beta \ln \theta - \ln \eta \right] \right\} \quad (D-9)$$

## APPENDIX E

### COMPUTER PROGRAM

This computer program predicts component low cycle fatigue (LCF) life exhaustion as a function of user-defined material data base and mission analysis history and includes the effects of mission number and ordering of different flights. The program embodies the results of a research and development effort described in the main body of this document.

The program calculates the LCF life exhaustion due to multiple flights of user defined missions. Life exhaustion due to repeated flights of a single mission may be analyzed as well as the effect on life exhaustion due to a change in the mission usage. As many as three blocks of missions may be analyzed.

Each mission is described as a sequence of events selected from a "damage events library" chosen to reflect various flight activities. Each damage event requires specific user input (e.g., the maximum nominal stress level) as well as default values of parameters which describe the event completely.

Unless default parameters are over-ridden, they will reflect the usage of a specific engine disk: the TF30-P-100 fan disk if a "cold" analysis is specified, and the TF30-P-100 third-stage turbine disk if a "hot" analysis is specified. For all events, nominal stress level input must reflect appropriate thermally and mechanically induced stresses.

This computer program is limited to life predictions of isothermal engine disk bolt holes. Specification of a "cold" analysis implies that stress relaxation effects will not be analyzed. Specification of a "hot" analysis implies that relaxation effects will be modeled by a single exponential decay of all stresses. This decay rate and a lower bound for the minimum allowed stress,  $\sigma_L$ , must be supplied by the user.

Local bolt hole stresses and strains are computed internally using a Neuber calculation. Neuber strain correction curves are optional user input but are recommended especially for low strain hardening materials. A surface layer algorithm is implicit in the calculation of bolt-hole stress. User input must include initial stress state,  $\sigma_0$ . Component geometry is specified through an elastic stress concentration factor and the number of bolt holes in the disk being analyzed. The analysis will be performed for the disk failure form

$$N = A\Delta\epsilon^B 10^C \sigma_m$$

where  $N$  is the typical simple cycle life,  $\Delta\epsilon$  is strain range and  $\sigma_m$  is mean stress. The values  $A$ ,  $B$ , and  $C$  must be supplied along with a description of the fatigue scatter. The fatigue scatter is described by the Weibull distribution parameter,  $\beta$ , i.e., the slope of the Weibull distribution for specimen data.

Double-damage concepts are used in the prediction of the cumulative damage effects. The crack propagation model assumes that the material's crack growth behavior is described by

AD-A070 935

PRATT AND WHITNEY AIRCRAFT GROUP WEST PALM BEACH FL 6--ETC F/G 20/11  
STRUCTURAL LIFE PREDICTION AND ANALYSIS TECHNOLOGY.(U)  
DEC 78 T A CRUSE, T G MEYER

F33615-75-C-2063

UNCLASSIFIED

PWA-FR-10896

AFAPL-TR-78-106

NL

2 OF 2  
AD  
A070 935



END  
DATE  
FILMED  
8-79

DDC



the standard Paris law:

$$\frac{da}{dN} = C (\Delta K)^n$$

Program output is specific to disk failure rates and mission ordering specified by the user.

A listing of the program is presented on the following pages.

Warning: The data supplied in this program is for illustrative purposes only. The program is not to be used for component design.

```

C          DATA SET PLMAIN
COMMON /ID/ ID1, ID0, MAX, NMAX, MAXCV, ISWAP
COMMON /DATA/ CURVM(50,2), CURVH(50,2), KT, S(21,3), R(21,3)
2  , NUMMIS, SIGLOW, SIGZRO, NEVENT(3), E, NMONO, NHYST, NOCCUR(21,3)
3  , IHOT, NTPYE(21,3)
COMMON /LDATA/ A, B, C, D, XN, NTIMES(3), ALPHA
COMMON /CRCT/ CRMONO(50,2), NCR1, CRHYST(50,2), NCR2
COMMON /SRELAX/ ASUR, BSUR, CSUR, ASUB, BSUB, CSUB, REL1, REL2
COMMON /LEFT/ LIFESP
COMMON /SVLIFE/ XNA, RA, OVA
COMMON /ERROR/ IEKR
COMMON /REL1/ BETA, FRATE, NBOLT
REAL LIFESP
REAL KT
DIMENSION SURSVE(42,3,4), ICYCLE(21,3,3), IDAM(3), SLIFE(21,3,2)
DIMENSION IOFF(3)

C
C          READ INPUT DATA
C
C          IF(IERR.L1.0) GO TO 210
C          CALL INPUT
C
C          INITIALIZE CONSTANTS FOR STRESS HISTORY CALCULATIONS
C
C          ILIN=0
C          LIFESP=0.00
C          SURLST=SIGZRO
C          STRLST=0.0
C          SUBLST=0.0
C          JTIME=0
C          NTIMES(NUMMIS)=0
C
C          COMPUTE STRESS/STRAIN HISTORY
C
C          DO 200 MISS=1, NUMMIS
C          DO 5 J=1, 4
C          DO 5 JJ=1, 42
5  SURSVE(JJ, MISS, J)=0.0
  IF(MISS.EQ.1) GO TO 20
  STRLST=SURSVE(NUM, MISS-1, 1)
  SUBLST=SURSVE(NUM, MISS-1, 3)
  SURLST=SURSVE(NUM, MISS-1, 2)
20 CALL STRESS(MISS, STRLST, SUBLST, SURSVE, NUM, SURLST, ILIN)
C
C          DETERMINE STRESS CYCLES AND RELAXATION FACTORS
C

```

```

      CALL CYCLE(SURSVE,ICYCLE,IDAM,IOFF,MISS,NUM)
C
C   IF HOT FLIGHT RELAX STRESSES
C
      REL1=0.0
      REL2=0.0
      IF(MISS.EQ.NUMMIS) GO TO 35

30  IF(IHOT.EQ.2) CALL RELAX(SURSVE,MISS,NUM)
C
C   DO SIMPLE LIFE PREDICTION AND PROPAGATION DAMAGE DEBITS
C
35  CALL LIFE(SURSVE,ICYCLE,IDAM,SLIFE,IOFF,MISS)
C
C   LIFE EXHAUSTION CALCULATION
C
      CALL EXLIFE(SLIFE,ICYCLE,IDAM,MISS,JTIME)
      IF(MISS.LT.NUMMIS) GO TO 200
      JTIME=JTIME+1
C
C   NUMBER OF CYCLES PREDICTED NOT THE SAME AS LIFE USED TO
C   RELAX STRESSES ITERATION NEEDED
C
      DO 50 I=1,NUM
      SURSVE(I,MISS,2)=SURSVE(I,MISS,2)-REL1
      SURSVE(I,MISS,3)=SURSVE(I,MISS,3)-REL2
50  CONTINUE
      GO TO 30
200  CONTINUE
210  STOP
      END

      SUBROUTINE INPUT
      COMMON /ERROR/ IERR
      COMMON /IO/ IOI,IDO,MAX,NMAX,MAXCV,ISWAP
      COMMON /DAMAGE/ SDEF(6,2),RDEF(6,2),TIDEF(6,2),T2DEF(6,2)
      COMMON /DATA/ CURVM(50,2),CURVH(50,2),KT,S(21,3),R(21,3),NUMMIS,
2  SIGLOW,SIGZRO,NEVENT(3),E,NMONO,NHYST,NGCCUR(21,3)
3  ,IHOT,NTYPE(21,3)
      COMMON /LDATA/ A,B,C,D,XN,NTIMES(3),ALPHA
      COMMON /TIME/ T1(21,3),T2(21,3)
      COMMON /CRRCT/ CRMONO(50,2),NCR1,CRHYST(50,2),NCR2
      COMMON /RELI/ BETA,FRATE,NBOLT
C
C   IERR      -ERROR FLAG TO INDICATE FATAL INPUT ERROR
C   IOI       -LOGICAL UNIT FOR CARD READER
C   IDO       -LOGICAL UNIT FOR LINE PRINTER
C   MAX       -MAXIMUM NUMBER OF DAMAGE EVENTS
C   NMAX      -MAXIMUM NUMBER OF DATA POINTS FOR STRESS/STRAIN CURVES

```

```

C      NEVENT(I) -NUMBER OF EVENTS IN MISSION I
C      NTIMES    -NUMBER OF TIMES MISSION A IF FLOWN
C      MIS       -1 FOR MISSION A
C               2 FOR MISSION B
C      NTYPE(I,J) -TYPE OF DAMAGE EVENT FOR MISSION=J , ITH EVENT
C      NOCCUR(I,J)-NUMBER OF OCCURANCES OF EVENT
C      S(I,J)    -NOMINAL STRESS
C      R(I,J)    -STRESS RATIO
C      T1(I,J)   -TIME 1
C      T2(I,J)   -TIME 2
C      SDEF(N)   -DEFAULT VALUE OF NOMINAL STRESS OF NTH TYPE EVENT
C      RDEF(N)   -DEFAULT VALUE OF STRESS RATIO FOR NTH TYPE EVENT
C      T1DEF(N)  -DEFAULT VALUE OF TIME 1 FOR NTH TYPE EVENT
C      T2DEF(N)  -DEFAULT VALUE OF TIME 2 FOR NTH TYPE EVENT
C      IHOT = 1  COLD FLIGHT
C      IHOT 2  HOT FLIGHT
C
C      REAL KT
C      DIMENSION IPRINT(20,3,3),ICHCK(2),NTITLE(3,6)
C      DIMENSION IA(80),PRINT(3),TITLE(80)
C      DATA IBL/IH /,IASK/IH*/
C      DATA ICHCK/IHH,IHC/
C      DATA PRINT /IHA,IHB,IHC/
C      DATA NTITLE /4HTAKE,4H OFF,4H      ,4HTRIM,4H PAD,4H      ,
2 4HCRUI,4HSE  ,4H      ,4HCOMB,4HAT  ,4H      ,4HTOUC,
3 4HHC ,4HGG  ,4HBOMB,4H RUN,4H      /
C
C      ECHO INPUT DATA
C
C      WRITE(IDO,265)
1 READ(IDI,270)IA
  IF(EOF(IDI).GT.0.0) GO TO 5
  WRITE(IDO,280) IA
  WRITE(ISWAP,270)IA

  GO TO 1
5 WRITE(IDO,290)
  IDI=ISWAP
  REWIND IDI
  WRITE(IDO,1000)
  WRITE(IDO,1001)
  WRITE(IDO,1002)
  WRITE(IDO,1003)
  WRITE(IDO,1004)
1000 FORMAT(1H1,/,53X,24HSTATEMENT OF LIMITATIONS,/,/,9X,
2 43HTHIS COMPUTER PROGRAM IS LIMITED TO THE LIF,
3 52HPREDICTIONS OF ISOTHERMAL ENGINE DISK BOLT HOLES. ,
4 19HSPECIFICATION OF A ,/,8X,
5 43HCOLD ANALYSIS IMPLIES THAT STRESS RELAXAT,
6 33HION EFFECTS WILL NOT BE ANALYZED.,/,9X,
6 14HSPECIFICATION ,
7 29H OF A 'HOT' ANALYSIS IMPLIES .

```



```

      8 43H THAT RELAXATION EFFECTS WILL BE MODELED BY ,/,9X,
      9 43H A SINGLE EXPONENTIAL DECAY OF ALL STRESSES.)
1001 FORMAT(9X,43H MISSION DESCRIPTION MUST BE SELECTED FROM T,
      2 43H THE EVENTS LIBRARY. UNLESS EVENT PARAMETERS ,/,9X,
      3 27H ARE OVER-RIDDEN, THEY WILL ,
      4 45H REFLECT THE USAGE OF A SPECIFIC ENGINE DISK : ,/,9X,
      5 34H THE TF30P100 FAN DISK IF A 'COLD' ,
      6 38H ANALYSIS IS SPECIFIED AND THE TF30100 ,/,9X,
      7 43H THIRD TURBINE DISK IF A 'HOT' ANALYSIS IS S,
      8 38H SPECIFIED. NOMINAL STRESS LEVELS INPUT ,
      9 34H MUST REFLECT APPROPRIATE THERMALLY ,/,9X,
      1 43H AND MECHANICALLY INDUCED STRESSES. PROGRAM ,
      1 41H OUTPUT IS SPECIFIC TO DISK FAILURE RATES ,
      2 23H AND MISSION ORDERING BY ,/,9X,
      3 9H THE USER.)
1002 FORMAT(//,9X,43H THE LIFE EXHAUSTION MODEL USED IN THIS PROG,
      1 39H RAM ASSUMES THE FOLLOWING DESCRIPTIONS.,//,11X,
      2 54H 1. TYPICAL SIMPLE CYCLE FATIGUE LIFE, N, IS DESCRIBED BY,/,
      3 45X,40HN=A*(DELTA STRAIN)**B*10**(C*SIGMA MEAN) ,/)
1003 FORMAT(11X,41H 2. FATIGUE SCATTER IS DESCRIBED BY A WEIB,
      2 45H ULL DISTRIBUTION IN TERMS OF ITS SLOPE, BETA.,//,11X,
      3 73H 3. THE CRACK PROPAGATION BEHAVIOR IS DESCRIBED BY THE STANDARD,
      4 PARIS LAW.,//,14X,70H STRESS RATIO EFFECTS ARE ASSUMED TO BE INCLUD
      5 ED IN THE CALCULATION OF ,/,14X,41H THE ALTERNATING STRESS INTENSIT
      6 Y FACTOR. )
1004 FORMAT(//,11X,42H 4. MONOTONIC AND HYSTERESIS STRESS-STRAIN ,
      1 57H CURVES MUST BE INPUT FOR THE SINGLE TEMPERATURE AT WHICH ,
      2 16H THE ANALYSIS WILL,/,14X,13H BE PERFORMED.,//,11X,
      3 57H 5. THE STRESS RELAXATION MODEL ASSUMES THAT ALL STRESSES ,
      4 52H DECAY EXPONENTIALLY WITH A SINGLE DECAY RATE, ALPHA.,//,14X,
      5 51H WARNING : THE DATA SUPPLIED IN THIS PROGRAM IS FOR ,
      6 57H ILLUSTRATIVE PURPOSES ONLY. THE PROGRAM IS NOT TO BE USED,
      7 4H FOR,/,24X,17H COMPONENT DESIGN.)
      READ(IDI,270) TITLE
      READ(IDI,350) NUMMIS, IFLAG
350 FORMAT(I5,4X,A1)
      IHOT=0
      IF(IFLAG.EQ.1) IHOT=2
      IF(IFLAG.EQ.2) IHOT=1
      IF(IHOT.GT.0) GO TO 4
      IERR=-999
      WRITE(IDO,360)

360 FORMAT(1X,10(1H*),37H FATAL ERROR EITHER HOT OR COLD FLIGHT,
      218H MUST BE SPECIFIED )
      4 MISS=0
      IF(NUMMIS.LE.3) GO TO 10
      IERR=-999
      WRITE(IDO,300)
      READ MISSION DATA
C
C
      10 MISS=MISS+1
      READ(IDI,100) MEVENT(MISS), NTIMES(MISS)

```

```

      IF(NEVENT(MISS).LE.MAX) GO TO 20
      IERR=-999
      WRITE(IDO,900) NEVENT(MISS),MISS,MAX
900  FORMAT(1X,10(1H*),11HFATAL ERROR,15,22H EVENTS WERE INPUT FOR,15,
      2  8H MISSION,/,22X,12HA MAXIMUM OF,15,12H ARE ALLOWED)
20  N=NEVENT(MISS)
      DO 22 IJ=1,3
      DO 22 I=1,20
22  IPRINT(I,MISS,IJ)=IBL
      DO 30 J=1,N
      READ(IDI,110) NTYPE(I,MISS),DUMMY,5(I,MISS),R(I,MISS)
      T1(I,MISS),T2(I,MISS)
      NN=NTYPE(I,MISS)
      IF((NMAX-NTYPE(I,MISS))*NTYPE(I,MISS)) 21,21,25
21  IERR=-999
      WRITE(IDO,910) NTYPE(I,MISS),NMAX
910  FORMAT(1X,10(1H*),18HFATAL ERROR A TYPE,15,16H EVENT WAS INPUT,
      2  53H VALID EVENTS ARE GREATER THAN 0 AND LESS OR EQUAL TO,15)
25  IF(5(I,MISS).GT.0.0) GO TO 26
      WRITE(IDO,320)MISS,I
26  IF(T1(I,MISS).GT.0.0) GO TO 27
      IF(IHOT.EQ.2.AND.NN.EQ.4) GO TO 29
      T1(I,MISS)=T1DEF(NN,IHOT)
      IPRINT(I,MISS,2)=IASK
27  IF(T2(I,MISS).GT.0.0) GO TO 28
      IF(IHOT.EQ.2.AND.NN.EQ.4) GO TO 29
      T2(I,MISS)=T2DEF(NN,IHOT)
      IPRINT(I,MISS,3)=IASK
28  IF(R(I,MISS).GT.0.0) GO TO 129
      IF(IHOT.EQ.2.AND.NN.EQ.4) GO TO 29
      R(I,MISS)=RDEF(NN,IHOT)
      IPRINT(I,MISS,1)=IASK
      GO TO 129
29  WRITE(IDO,330)
      IERR=-999
129  NOCCUR(I,MISS)=IFIX((DUMMY/(T1(I,MISS)+T2(I,MISS)))+0.5)
      IF(NN.EQ.1.OR.NN.EQ.3) NOCCUR(I,MISS)=1
      IF(NN.EQ.2) NOCCUR(I,MISS)=IFIX(DUMMY+0.5)
30  CONTINUE
      IF(MISS.LT.NUMMIS) GO TO 10
C
C  CHECK THAT THERE IS A TAKE OFF AND LANDING FOR EACH MISSION
C
      DO 37 I=1,MISS
      N=NEVENT(I)
      DO 36 J=1,N
      IF(NTYPE(J,I).EQ.1) GO TO 37
36  CONTINUE

```

```

IERR=-999
WRITE(IDO,400)I
37 CONTINUE
C
C   ADD LANDING AT END OF EACH MISSION
C
DO 38 I=1,MISS
NEVENT(I)=NEVENT(I)+1
J=NEVENT(I)
R(J,I)=0.0
S(J,I)=0.0
T1(J,I)=0.0
T2(J,I)=0.0
NOCCUR(J,I)=0
38 CONTINUE
C
C   READ MATERIAL DATA
C
READ(IDI,120) KT,SIGLOW,ALPHA,SIGZRO,E
ALPHA=ABS(ALPHA)
C
C   READ RELIABILITY DATA
C
READ(IDI,115) BETA,FRATE,NBOLT
READ(IDI,120) A,B,C,D,XN
C   READ MONOTONIC CURVE
READ(IDI,100) NMONO,NCR1
IF(NMONO.LE.MAXCV) GO TO 40
IERR=-999
WRITE(IDO,920) NMONO,MAXCV
920 FORMAT(1X,10(1H*),11HFATAL ERROR,15,27H POINTS INPUT FOR MONOTONIC
2 35H STRESS STRAIN CURVE,12, 6H ALLOWED)
40 CONTINUE
READ(IDI,120) ((CURVM(I,J),J=1,2),I=1,NMONO)
IF(NCR1.NE.0) READ(IDI,120) ((CRMONO(I,J),J=1,2),I=1,NCR1)
C   READ HYSTERESIS CURVE
READ(IDI,100) NHYST,NCR2
IF(NHYST.LE.MAXCV) GO TO 45
IERR=-999
WRITE(IDO,930) NHYST,MAXCV
930 FORMAT(1X,10(1H*),11HFATAL ERROR,15,26H POINTS INPUT FOR HYSTERES
2 22HIS CURVE,15, 6H ALLOWED)
45 CONTINUE
READ(IDI,120) ((CURVH(I,J),J=1,2),I=1,NHYST)
IF(NCR2.NE.0) READ(IDI,120) ((CRHYST(I,J),J=1,2),I=1,NCR2)
C
C   ECHO MISSION DATA
C
IF(IHOT.EQ.1) WRITE(IDO,440) TITLE
IF(IHOT.EQ.2) WRITE(IDO,450) TITLE

```



```

WRITE(IDO,460)KT,NBOLT
460 FORMAT(10X,3HKT=,E15.4,/,10X,7HNBOLTS=,I10)
NL=NUMMIS-1
IF(NL.EQ.0.0) GO TO 806
DO 805 MISS=1,NL
WRITE(IDO,200) PRINT(MISS), NTIMES(MISS)
WRITE(IDO,430)
N=NEVENT(MISS)-1

DO 800 I=1,N
KP=NTYPE(I,MISS)
WRITE(IDO,210)I,(NTITLE(JP,KP),JP=1,3),NOCCUR(I,MISS),S(I,MISS),
2 IPRINT(I,MISS,1),R(I,MISS),IPRINT(I,MISS,2),T1(I,MISS),
3 IPRINT(I,MISS,3),T2(I,MISS)
800 CONTINUE
IF(IHOT.EQ.1) WRITE(IDO,380)
IF(IHOT.EQ.2) WRITE(IDO,390)
805 CONTINUE
806 N=NEVENT(MISS)-1
WRITE(IDO,220)PRINT(MISS)
WRITE(IDO,430)
DO 810 I=1,N
KP=NTYPE(I,MISS)
WRITE(IDO,210)I,(NTITLE(JP,KP),JP=1,3),NOCCUR(I,MISS),S(I,MISS),
2 IPRINT(I,MISS,1),R(I,MISS),IPRINT(I,MISS,2),T1(I,MISS),
3 IPRINT(I,MISS,3),T2(I,MISS)
810 CONTINUE
IF(IHOT.EQ.1) WRITE(IDO,380)
IF(IHOT.EQ.2) WRITE(IDO,390)

C
C ECHO MATERIAL DATA
C
WRITE(IDO,230)
WRITE(IDO,240) SIGLOW,ALPHA,SIGZRO,E,BETA,FRATE
E=E/1000.
WRITE(IDO,370)A,B,C,D,XN

C
WRITE(IDO,250)((CURVM(I,J),J=1,2),I=1,NMONO)
IF(NCR1.GT.0) WRITE(IDO,410)((CRMONO(I,J),J=1,2),I=1,NCR1)
WRITE(IDO,260)((CURVH(I,J),J=1,2),I=1,NHYST)
IF(NCR2.GT.0) WRITE(IDO,420)((CRHYST(I,J),J=1,2),I=1,NCR2)
WRITE(IDO,470)
RETURN
C FORMATS
100 FORMAT(2I5)
110 FORMAT(15,5X,5E10.0)
200 FORMAT(/,52X,7HMISSION,1X,A1,1X,11HDESCRIPTION,/,10X,
216HMISSION A OCCURS,15, 6H TIMES,/,10X,5HEVENT,5X,4HTYPE,4X,
310HOCCURANCES,2X,7HNOMINAL,8X,6HSTRESS,9X,6HTIME 1,9X,6HTIME 2,/,
440X,6HSTRESS,9X,5HRATIO)
210 FORMAT(10X,15,5X,3A4,13,5X,E10.4,3(5X,A1,E10.4))
220 FORMAT(1H1,/,52X,7HMISSION,1X,A1,1X,11HDESCRIPTION,/,10X,5HEVENT,

```



```

2 5X,4HTYPE,4X,10HOCURANCES,2X,7HNOMINAL,8X,6HSTRESS,9X,6HTIME 1,
3 9X,6HTIME 2,/,40X,6HSTRESS,9X,5HRATIO)
120 FORMAT(8E10.0)
230 FORMAT(1H1,/,10X,13HMATERIAL DATA,/)
240 FORMAT(10X,19HLOWER STRESS BOUND=,E15.4,1X,3HKSI,/,10X,
2 6HALPHA=,E15.4,1X,5H1/HRS,/,10X,15HINITIAL STRESS=,E15.4,1X,3HKS
3I,/,10X,2HE=,2PE15.4,1X,3HPSI,/,10X,5HBETA=,0PE15.4,/,
4 10X,18HDISK FAILURE RATE=,F10.2)
250 FORMAT(1H1,/,10X,28HMONTONIC STRESS/STRAIN CURVE,/,10X,6HSTRESS,9
2 X, 6HSTRAIN,/,11X,3HKSI,12X,5HIN/IN,/,50(5X,2E15.4,/)
260 FORMAT(1H1,/,10X,30HHYSTERESIS STRESS/STRAIN CURVE,/,10X,6HSTRESS
2 ,9X, 6HSTRAIN,/,11X,3HKSI,12X,5HIN/IN,/,50(5X,2E15.4,/)
265 FORMAT(1H1,13HECHO OF INPUT,/)
270 FORMAT(80A1)
280 FORMAT(1X,80A1)

320 FORMAT(1X,10(1H*),36HFATAL ERROR NOMINAL STRESS LEVEL NOT,
2 32H INPUT FOR MISSION,I5,1X,5HEVENT,I5)
330 FORMAT(1X,10(1H*),45HFATAL ERROR DAMAGE EVENT TYPE 4 HAS NO DEFAULT
2 21HT VALUES FOR HOT RUN.)
290 FORMAT(1X,12H END OF ECHO)
300 FORMAT(1X,10(1H*),38HFATAL ERROR MORE THAN 3 MISSIONS INPUT)
380 FORMAT(40X,37H*DEFAULT VALUE FOR TF30-P100 FAN DISK)
390 FORMAT(40X,41H*DEFAULT VALUE FOR TF30-P100 TURBINE DISK)
400 FORMAT(1X,10(1H*),35HFATAL ERROR NO TAKE OFF FOR MISSION,I5)
410 FORMAT(1H1,/,10X,36HCORRECTION CURVE FOR MONOTONIC CURVE,
1 /,10X,6HSTRAIN,9X,5HCFAC,
2 /,10X,5HIN/IN,
3 /,50(5X,2E15.4,/)
420 FORMAT(1H1,/,10X,36HCORRECTION CURVE FOR HYSTERESIS CURVE,
1 /,10X,6HSTRAIN,9X,5HCFAC,
2 /,10X,5HIN/IN,
3 /,50(5X,2E15.4,/)
115 FORMAT(2E10.0,I5)
430 FORMAT(40X,3HKSI,27X,3HHRS,12X,3HHRS/)
440 FORMAT(1H1,/,52X,21HCOLD MISSION ANALYSIS,/,25X,80A1,/)
450 FORMAT(1H1,/,52X,20HHOT MISSION ANALYSIS,/,25X,80A1,/)
370 FORMAT(1H1,/,10X,23HLIFE EQUATION CONSTANTS,/,
2 ,10X,2HA=,E15.4,/,10X,2HB=,E15.4,/,10X,2HC=,E15.4,
3 /,10X,22HCKACK GROWTH CONSTANTS,/,10X,2HD=,
4 E15.4,/,10X,2HN=,E15.4)
470 FORMAT(1H1,17X,27HRESULTS OF MISSION ANALYSIS,/,10X,7HMISSION,8X
2 ,10HCUMULATIVE,6X,9HNUMBER OF,/,25X,10HPERCENT OF ,
3 6X,7HFLIGHTS,/,25X,9HLIFE USED,/)
END

```

```

SUBROUTINE STRESS(MISS,STRLST,SUBLST,SURSVE,NUMLST,SURLST,ILIN)
COMMON /IO/ID1,IDO
COMMON /DATA/ CURVM(50,2),CURVH(50,2),KT,SS(21,3),RR(21,3),NUMMIS
2,SIGLOW,SIGZRO,NEVENT(3),E,NMONO,NHYST,NOCCUR(21,3)
3,IHOT,NTYPE(21,3)
COMMON /CRRCT/ CRMONO(50,2),NCR1,CRHYST(50,2),NCR2
REAL KT
DIMENSION SURSVE(42,3,4)

C
C THIS ROUTINE COMPUTES THE STRAIN HISTORY OF A MISSION
C
C INITIALIZE CONSTANTS
C
C ILIN=0 STRESS LEVEL ON LINEAR PORTION OF HYSTRESIS CURVE
C ILIN=1 ON NON-LINEAR PORTION
C
NUM=1
KWIPE=0
I=1
S3=0.0
S4=0.0
ISIGN=-1
ITIME=0
SURSVE(NUM,MISS,1)=STRLST
SURSVE(NUM,MISS,3)=SUBLST
SIGSUR=SURLST
SURSVE(NUM,MISS,2)=SIGSUR
1 S=SS(I,MISS)
R=RR(I,MISS)
ICHNGE=0
IF(S.GT.S4.AND.ISIGN.LT.0) ICHNGE=1
IF(S.LT.S4.AND.ISIGN.GT.0) ICHNGE=1
IF(ILIN.EQ.0.OR.ICHNGE.EQ.0) GO TO 200
NUMBCK=NUM
IF(ITIME.EQ.1.AND.NUM.EQ.1) NUM=NUMLST
STRLST=SURSVE(NUM,MISS,1)
SURLST=SURSVE(NUM,MISS,2)
SUBLST=SURSVE(NUM,MISS,3)
NUM=NUMBCK
S3=S4
ILIN=0
200 CONTINUE
C IF PART HAS NO PREVIOUS STRESS HISTORY SUBSURFACE FOLLOWS
C MONOTONIC STRESS STRAIN CURVE
C IF(I.EQ.1.AND.MISS.EQ.1.AND.ITIME.EQ.0)GO TO 5
GO TO 10
C FOLLOW MONOTONIC CURVE
5 DVDE=(KT*S)*(KT*S)/E
CALL INTERCURVM,NMONO,DE,DVDE,CRMONO,NCR1)
ILIN=1
SIGSUB=DVDE/DE
STRAIN=DE

```

```

      ISIGN=1
      IMONO=0
      ISIGN=1
      GO TO 20
C     FOLLOW HYSTERESIS CURVE FOR SUBSURFACE STRESS LEVEL
10    DVDE=(KT*(S3-S))**2/E
      ISIGN=1
      IF(S3.GT.S) ISIGN=-1
      CALL INTER(CURVH,NHYST,DE,DVDE,CRHYST,NCR2)
      ILIN=0
      IF(DE.GT.CURVH(1,1)) ILIN=1
      DSIGMA=DVDE/DE
      SIGSUB=SUBLST+ISIGN*DSIGMA
      STRAIN=STRLST+ISIGN*DE
      IF(SIGSUB.LT.SIGLOW) SIGSUB=SIGLOW
C     CHECK THAT MONOTONIC CURVE IS NOT VIOLATED
      IMONO=1
      CALL VLATE(CURVM,STRAIN,SIGSUB,IVIOL,NMONO)
      IF(IVIOL.LT.0) GO TO 5
C     HAS SURFACE LAYER BEEN PREVIOUSLY BEEN DESTROYED
20    IF(KWIPE.NE.0) GO TO 45
      IF(IMONO.GT.0) GO TO 30
C     SUBSURFACE FOLLOWED MONOTONIC STRESS/STRAIN THEREFORE SIGMASUR
C     IS SIG ZRO PLUS SIG HYST
      CALL INTERY(CURVH,NHYST,STRAIN,SIGSUR)
      SIGSUR=SIGSUR+SIGZRO
      GO TO 40
30    SIGSUR=SURLST+ISIGN*DSIGMA
      IF(SIGSUR.LT.SIGLOW) SIGSUR=SIGLOW
C     CHECK THAT MONOTONIC CURVE IS NOT VIOLATED
40    CALL VLATE(CURVM,STRAIN,SIGSUR,IVIOL,NMONO)
      IF(IVIOL.GE.0) GO TO 50
      KWIPE=1
45    SIGSUR=SIGSUB
50    IF(R.LE.0) GO TO 60
      DVDE=(KT*S*(1.0-R))**2/E
      CALL INTER(CURVH,NHYST,DE,DVDE,CRHYST,NCR2)
      ILIN=0
      IF(DE.GT.CURVH(1,1)) ILIN=1
      DV=DVDE/DE
      NUM=NUM+1
      SURSVE(NUM,MISS,1)=STRAIN
      SURSVE(NUM,MISS,2)=SIGSUR
      SURSVE(NUM,MISS,3)=SIGSUB
      SIGSUR=SIGSUR-DV
      IF(SIGSUR.LT.SIGLOW) SIGSUR=SIGLOW
      SIGSUB=SIGSUB-DV
      IF(SIGSUB.LT.SIGLOW) SIGSUB=SIGLOW
      STRAIN=STRAIN-DE
60    NUM=NUM+1
      SURSVE(NUM,MISS,1)=STRAIN
      SURSVE(NUM,MISS,2)=SIGSUR
      SURSVE(NUM,MISS,3)=SIGSUB

```





```

      B=ARRAY(NN-1,2)-XM*(ARRAY(NN-1,1))
      GO TO 80
75  XM=ARRAY(NN,2)/ARRAY(NN,1)
      B=0.0
80  XB=(SQRT(B*B+4.0*XM*XYB)-B)/(2.0*XM)
C
C      USE CORRECTION CURVE TO DETERMINE ACTUAL STRAIN FROM NUEBER
C      STRAIN PREDICTION
C
999  CFACT=1.0
      IF(ICRCT.GT.0) CALL INTERV(ICRCT,ICRCT,XB,CFACT)
      XB=XB*CFACT
      CALL INTERV(ARRAY,N,XB,Y)
      XYB=XB*Y
      RETURN
      END

SUBROUTINE INTERV(CURVE,N,X,Y)
  DIMENSION CURVE(50,2)
  COMMON /IO/ ID1,IDO
C
C      THIS ROUTINE FINDS Y GIVEN X USING CURVE (1,1) = X(I)
C      AND CURVE(I,2) = Y(I)
C
C      DETERMINE IF INTERPOLATION OR EXTRAPOLATION IS NEEDED
C
      NTOP=N
      IF(CURVE(N,1)-X) 40, 10, 20
10  Y=CURVE(NTOP,2)
      GO TO 999
C
C      INTERPOLATE
C
20  DO 25 I=1,N
      NTOP=I
      IF(X-CURVE(I,1)) 30, 10, 25
25  CONTINUE
      GO TO 40
30  IF(NTOP.EQ.1) GO TO 35
      Y=(CURVE(NTOP,2)-CURVE(NTOP-1,2))/(CURVE(NTOP,1)-CURVE(NTOP-1,1))
      2)*(X-CURVE(NTOP-1,1))+CURVE(NTOP-1,2)
      GO TO 999
C
C      ASSUME CURVE STARTS AT 0.0,0.0
C
35  Y=(CURVE(1,2)/CURVE(1,1))*X
      GO TO 999
C
C      EXTRAPOLATE TO SOLUTION
C
40  NTOP=N
      GO TO 30
999  CONTINUE
      RETURN
      END

```

```

BLOCK DATA
C BLOCK DATA ROUTINE TO SET DEFAULT VALUES OF I/O DEVICES AND DAMAGE
C EVENT DEFAULT VALUES
COMMON /ERROR/ IERR
COMMON /IO/ IDI,IDO,MAX,NMAX,MAXCV,ISWAP
COMMON /DAMAGE/ SDEF( 6,2),RDEF( 6,2),T1DEF( 6,2),T2DEF( 6,2)
DATA IDI,IDO /5,6/
DATA SDEF/12*0.0/
DATA T1DEF/.333,0.0166,.333,3*0.0166,.0333,.00833,.5,.0,.08333,.05
2 /
DATA RDEF/0.,.5,0.,.83,.29,.36,0.,.56,0.,0.,.16,.45/
DATA T2DEF/0.,.0166,0.,.0166,.0166,.0166,0.,.0166,0.,0.,.08333,.05
2 /
DATA MAX,IERR,NMAX,MAXCV,ISWAP
2 /20,3,6,50,1/
END

SUBROUTINE VLATE(CURVE,STRAIN,SIGSUB,IVIOL,NCURV)
C
C THIS ROUTINE DETERMINES IF GIVEN STRAIN & SIGSUR
C IF CURVE IS VIOLATED
COMMON /IO/ IDI,IDO,MAX,NMAX,MAXCV
DIMENSION CURVE(50,2)
XPRT=FLOAT(NCURV)
IVIOL=0
CALL INTERY(CURVE,NCURV,STRAIN,STRESS)
IF(SIGSUB.GT.STRESS) IVIOL=-999
XPRT=FLOAT(IVIOL)
RETURN
END

SUBROUTINE CYCLE(SURSVE,ICYCLE,IDAM,IOFF,MISS,NUM)
DIMENSION SURSVE(42,3,4),ICYCLE(21,3,3),IDAM(3)
DIMENSION IOFF(3)
C
C THIS SUBROUTINE DETERMINES STRESS CYCLES AND NUMBER OF TIMES
C THAT EACH IS CYCLED
C **BASED ON SUBSURFACE STRESS CYCLES
C
C ALSO CALCULATED ARE CONSTANTS FOR STRESS RELAXATION
C
C ICYCLE(I,MISS,J)
C J=1 POINTER TO SURSVE FOR BEG. STRESS
C J=2 POINTER TO SURSVE FOR END STRESS
C J=3 NUMBER OF CYCLES
C IDAM(MISS) COUNTS OF STRESS CYCLES IN A MISSION
C
COMMON /LDATA/ A,B,C,D,XN,NTIMES(3),ALPHA
COMMON /IO/ IDI,IDO
COMMON /DATA/ CURVM(50,2),CURVH(50,2),KT,S(21,3),R(21,3),NUMMIS
2 ,SIGLOW,SIGZRD,NEVENT(3),E,NMOND,NHYST,NOCUR(2,3)
3 ,IHOT,NTYPE( 21,3)
COMMON /SRELAX/ ASUR,BSUR,CSUR,ASUB,BSUB,CSUB,REL1,REL2

```

```

COMMON /TIME/TT1(21,3),TT2(21,3)
REAL KT
ASUR=0.0
BSUR=0.0
CSUR=1.0
ASUB=0.0
BSUB=0.0
CSUB=1.0
10 ISTR=0
   IEVENT=0
   IDAM(MISS)=0
20 ISTR=ISTR+1
   IF(IEVENT+1.GE.NEVENT(MISS)) GO TO 999
C
C   IS THIS THE END OF A DAMAGE EVENT
C
   IF(SURVE(ISTR,MISS,4).EQ.0.0) GO TO 20
C
C   INCREMENT DAMAGE CYCLE COUNTER
C
   IEVENT=IEVENT+1
   T1=TT1(IEVENT,MISS)
   T2=TT2(IEVENT,MISS)
   TRAT=(T2-T1)/(T1+T2)
   TI=(T1+T2)*SURVE(ISTR,MISS,4)
   ESTUFF=(1.0/EXP(ALPHA*TI))-1.0
C
C   DETERMINE EVENT TYPE AND CALCULATE NUMBER OF CYCLES
C
   N=NTYPE(IEVENT,MISS)
   IF(N.NE.4.AND.N.NE.5.AND.N.NE.6) GO TO 30
C
C   GET NUMBER OF CYCLES DIRECTLY FROM SURVE
C
25 SIGM=(SURVE(ISTR-1,MISS,2)+SURVE(ISTR,MISS,2))/2.
   DSIG=ABS(SURVE(ISTR-1,MISS,2)-SURVE(ISTR,MISS,2))
   SIGI=SIGM-(DSIG/2.0)*TRAT
   ASUR=ASUR+SIGI*ESTUFF
   BSUR=BSUR+ESTUFF
   CSUR=CSUR+ESTUFF
   SIGM=(SURVE(ISTR-1,MISS,3)+SURVE(ISTR,MISS,3))/2.0
   DSIG=ABS(SURVE(ISTR-1,MISS,3)-SURVE(ISTR,MISS,3))
   SIGI=SIGM-(DSIG/2.0)*TRAT
   ASUB=ASUB+SIGI*ESTUFF
   BSUB=BSUB+ESTUFF
   CSUB=CSUB+ESTUFF
   IF(N.EQ.2) GO TO 35
   IDAM(MISS)=IDAM(MISS)+1
   I=IDAM(MISS)
   ICYCLE(I,MISS,1)=ISTR-1
   ICYCLE(I,MISS,2)=ISTR
   ICYCLE(I,MISS,3)=FIX(SURVE(ISTR,MISS,4))
   GO TO 20

```

```

30 IF(N.NE.2) GO TO 40
   GO TO 25
35 CONTINUE
   IDAM(MISS)=IDAM(MISS)+1
   I=IDAM(MISS)
   ICYCLE(I,MISS,1)=ISTR-1
   ICYCLE(I,MISS,2)=ISTR
   ICYCLE(I,MISS,3)=1
   GO TO 20
40 IF(N.NE.1) GO TO 60

C
C   FIND VMAX AND VMIN OF MISSION
C
   IMAX=2
   IMIN=2
   ICT=2
45 ICT=ICT+1
   IF(ICT.GT.NUM) GO TO 50
   IF(SURSVE(ICT,MISS,2).LT.SURSVE(IMIN,MISS,2)) IMIN=ICT
   IF(SURSVE(ICT,MISS,2).GT.SURSVE(IMAX,MISS,2)) IMAX=ICT
   GO TO 45
50 IDAM(MISS)=IDAM(MISS)+1
   I=IDAM(MISS)
   IOFF(MISS)=I
   ICYCLE(I,MISS,1)=IMIN
   ICYCLE(I,MISS,2)=IMAX
   ICYCLE(I,MISS,3)=1
   SIGM=(SURSVE(IMAX,MISS,2)+SURSVE(IMIN,MISS,2))/2.0
   DSIG=ABS(SURSVE(IMAX,MISS,2)-SURSVE(IMIN,MISS,2))
   SIGI=SIGM-(DSIG/2.0)*TRAT
   ASUR=ASUR+SIGI*ESTUFF
   BSUR=BSUR+ESTUFF
   CSUR=CSUR+ESTUFF
   SIGM=(SURSVE(IMAX,MISS,3)+SURSVE(IMIN,MISS,3))/2.0
   DSIG=ABS(SURSVE(IMAX,MISS,3)-SURSVE(IMIN,MISS,3))
   SIGI=SIGM-(DSIG/2.0)*TRAT
   ASUB=ASUB+SIGI*ESTUFF
   BSUB=BSUB+ESTUFF
   CSUB=CSUB+ESTUFF
   GO TO 20
60 IF(N.NE.3) GO TO 20
   IF(IEVENT.EQ.1) GO TO 20
   NL=NTYPE(IEVENT-1,MISS)
   IF(NL.NE.1.AND.NL.NE.4.AND.NL.NE.5.AND.NL.NE.6) GO TO 20
   NN=NTYPE(IEVENT+1,MISS)
   IF(NN.NE.1.AND.NN.NE.4.AND.NN.NE.5.AND.NN.NE.6) GO TO 20
   IDAM(MISS)=IDAM(MISS)+1
   I=IDAM(MISS)
   ICYCLE(I,MISS,1)=ISTR
   ICYCLE(I,MISS,2)=ISTR+1
   ICYCLE(I,MISS,3)=1

```



```

SIGM=SURSVE(I STR,MISS,2)
SIGI=SIGM
ASUR=ASUR+SIGI*ESTUFF
BSUR=BSUR+ESTUFF
CSUR=CSUR+ESTUFF
SIGM=SURSVE(I STR,MISS,3)
SIGI=SIGM
ASUB=ASUB+SIGI*ESTUFF
BSUB=BSUB+ESTUFF
CSUB=CSUB+ESTUFF
GO TO 20
999 CONTINUE
RETURN
END

```

```

SUBROUTINE LIFE(SURSVE,ICYCLE,IDAM,SLIFE,IOFF,MISS)

```

```

THIS SUBROUTINE DOES SIMPLE CYCLE LIFE CALCULATION
USING SURFAC STRESS HISORY

```

```

SLIFE(I,MISS,1) - LIFE PREDICTION FOR ITH STRESS CYCLE OF MISSION
SLIFE(I,MISS,2) - PROPAGATION DAMAGE DEBIT

```

```

IOFF(MISS) - LOCATION OF TAKE-OFF CYCLE POINTERS IN CYCLE ARRAY

```

```

COMMON /IO/ IDI,IDO
COMMON /SVLIFE/ XNA,RA,DVA
COMMON /DATA/ CURVM(50,2),CURVH(50,2),KT,S(21,3),R(21,3),NUMMIS
2 ,SIGLOW,SIGZRO,NEVENT(3),E,NMONO,NHYST,NOCCUR(21,3)
3 ,IHOT,NTYPE(21,3)
COMMON /LDATA/ A,B,C,D,XN,NTIMES(3)
REAL KT
DIMENSION IOFF(3),SURSVE(42,3,4),ICYCLE(21,3,3)
DIMENSION IDAM(3),SLIFE(21,3,2)

```

```

A,B,C ARE USER INPUT CONSTANTS USED IN LIFE CALCULATIONS

```

```

LOG(N)=LOG(A)+B*LOG(DELT STRAIN)+C*STRESS MEAN WHERE N=LIFE

```

```

DETERMINE HOW MANY STRESS CYCLES IN MISSION

```

```

N=IDAM(MISS)

```

```

LOOP THROUGH STRESS CYCLES CALCULATING LIFE

```

```

DO 100 I=1,N
I1=ICYCLE(I,MISS,1)
I2=ICYCLE(I,MISS,2)
DSTR=ABS(SURSVE(I1,MISS,1)-SURSVE(I2,MISS,1))
SIGM=(SURSVE(I1,MISS,2)+SURSVE(I2,MISS,2))/2.
ARG=A*LOG10(A)+B*A*LOG10(DSTR)+C*SIGM
SLIFE(I,MISS,1)=10.**ARG

```

```

      IF(SLIFE(I,MISS,1).GE.1.0E6) SLIFE(I,MISS,1)=1.0E6
100 CONTINUE
C
C   CALCULATE PROPAGATION DAMAGE DEBIT
C
      IF(MISS.GT.1) GO TO 125
      ISUB=IOFF(MISS)
      XNA=SLIFE(ISUB,MISS,1)
      J1=ICYCLE(ISUB,MISS,1)
      J2=ICYCLE(ISUB,MISS,2)
      RA=AMIN1(SURSVE(J1,MISS,3),SURSVE(J2,MISS,3))/
2  AMAX1(SURSVE(J1,MISS,3),SURSVE(J2,MISS,3))
      DVA=SURSVE(J1,MISS,3)-SURSVE(J2,MISS,3)
      DVA=ABS(DVA)
125 CONTINUE
      DO 150 I=1,N
      I1=ICYCLE(I,MISS,1)
      I2=ICYCLE(I,MISS,2)
      XNB=SLIFE(I,MISS,1)
      RB=AMIN1(SURSVE(I1,MISS,3),SURSVE(I2,MISS,3))/
2  AMAX1(SURSVE(I1,MISS,3),SURSVE(I2,MISS,3))
      DVB=SURSVE(I1,MISS,3)-SURSVE(I2,MISS,3)
      DVB=ABS(DVB)
      SLIFE(I,MISS,2)=((1-(D-RB)*DVA)/(1-(D-RA)*DVB))**XN)*(XNA/XNB)
150 CONTINUE
999 CONTINUE
      RETURN
      END

      SUBROUTINE EX LIFE(SLIFE,ICYCLE,IDAM,MISS,JTIME)
      COMMON /LEFT/ LIFESP
      COMMON /DATA/ CURVM(50,2),CURVH(50,2),XKT,S(21,3),R(21,3),NUMMIS,
2  SIGLOW,SIGZRO,NEVENT(3),E,NMONO,NHYST,NOCCUR(21,3),
3  IHOT,NTYPE(21,3)
      COMMON /IO/ID1,ID0
      COMMON /LDATA/ A,B,C,D,XN,NTIMES(3)
      COMMON /RELI/ BETA,FRATE,NBOLT
      REAL LIFESP
      DIMENSION SLIFE(21,3,2),ICYCLE(21,3,3),IDAM(3),PRINT(3)
      DATA PRINT /1HA,1HB,1HC/
      NDAM=IDAM(MISS)
      XBOLT=FLOAT(NBOLT)
      RD=1.0-FRATE
      XNR=(1.0/BETA)*(ALOG(ALOG(1.0/RD))-ALOG(XBOLT)
2  -ALOG(ALOG(2.0)))
      XNR=EXP(XNR)
      IF(MISS.EQ.NUMMIS) GO TO 200
C
C   THIS IS NOT THE LAST MISSION CALCULATE REMAINING LIFE
C

```

```

XLIFE=0.0
DO 20 I=1,NDAM
  XLIFE=XLIFE+(FLOAT(ICYCLE(I,MISS,3))/(SLIFE(I,MISS,1)*
2SLIFE(I,MISS,2)))*NTIMES(MISS)/XNR
20 CONTINUE
  IF(XLIFE+LIFESP-1.0)30,40,50
30 LIFESP=XLIFE+LIFESP
  XPRT=(LIFESP)*100.
  WRITE(IDO,100)PRINT(MISS),XPRT,NTIMES(MISS)
  RETURN
40 WRITE(IDO,100)PRINT(MISS),XPRT,NTIMES(MISS)
  WRITE(IDO,110)
110 FORMAT(1X,23HLIFE HAS BEEN EXHAUSTED. )
  GO TO 999

C
C   LIFE USED UP BEFORE MISSION OVER CALCULATE APPROXIMATE LIFE
C
50 XLIFE=(XLIFE)/NTIMES(MISS)
  N=(1.0-LIFESP)/XLIFE
  WRITE(IDO,120)PRINT(MISS),N
120 FORMAT(1X,49HLIFE EXHAUSTED BEFORE SPECIFIED NUMBER OF MISSION,1X,
2 A1,1X,14HWERE COMPLETED,/,1X,13HAPPROXIMATELY,15,13H MISSIONS COU
232HLD BE FLOWN. REANALYSIS ADVISED.)
  GO TO 999

C
C   PREDICT HOW MANY MISSIONS CAN BE FLOWN
C
200 XLIFE=0.0
  DO 210 I=1,NDAM
    XLIFE=XLIFE+(FLOAT(ICYCLE(I,MISS,3))/(SLIFE(I,MISS,1)*SLIFE(2,MISS
2,2)))/XNR
210 CONTINUE
    N=(1.0-LIFESP)/XLIFE
    XPRT=100.
    IF(IHOT.EQ.1) GO TO 220
    IF(NTIMES(MISS).EQ.0.AND.JTIME.EQ.0) GO TO 950
    NT=NTIMES(MISS)-N
    IF(NT.GT.50) GO TO 950
220 N=(N+5)/10
    N=N*10
    WRITE(IDO,100)PRINT(MISS),XPRT,N
    GO TO 999
950 NTIMES(MISS)=N
  RETURN
100 FORMAT(13X,A1,11X,F8.2,7X,I10)
999 STOP
END

```

```

SUBROUTINE RELAX(SURSVE,MISS,NUM)
COMMON /SRELAX/ASUR,BSUR,CSUR,ASUB,BSUB,CSUB,REL1,REL2
COMMON /LDATA/ A,B,C,D,XN,NTIMES(3),ALPHA
COMMON /DATA/ CURVM(50,2),CURVH(50,2),XKT,S(21,3),R(21,3),NUMMIS,
2 SIGLOW,SIGZRO,NEVENT(3),E,NMONO,NHYST,NOCCUR(21,3),
3 IHOT,NTYPE(21,3)
COMMON /IO/ IDI,IDO
DIMENSION SURSVE(42,3,4),REL(2)

C
C THIS ROUTINE CALCULATES RELAXED STRESSES
C

NSAVE=NTIMES(MISS)
NFL=NTIMES(MISS)
DO 50 I=2,NUM
DO 50 J=2,3
1 REL(1)=(ASUR/BSUR)*(CSUR**NFL-1.0)
REL(2)=(ASUB/BSUB)*(CSUB**NFL-1.0)
J1=J-1
SIG=SURSVE(I,MISS,J)+REL(J1)
CALL INTERV(CURVM,NMONO,SURSVE(I,MISS,1),STRESS)
CALL VLATE(CURVM,SURSVE(I,MISS,1),SIG,IVICL,NMONO)
NFL=NFL-1
IF(NFL.EQ.0) GO TO 49
IF(IVICL.LT.0) GO TO 1
IF(SIG.LT.SIGLOW) GO TO 1
NFL=NFL+1
49 IF(NFL.LT.NSAVE) NSAVE=NFL
IF(NSAVE.EQ.0) GO TO 52
50 CONTINUE
52 NFL=NSAVE
55 IF(MISS.EQ.NUMMIS)NTIMES(MISS)=NFL
REL1=(ASUR/BSUR)*(CSUR**NFL-1.0)
REL2=(ASUB/BSUB)*(CSUB**NFL-1.0)
DO 60 I=1,NUM
SURSVE(I,MISS,2)=SURSVE(I,MISS,2)+REL1
SURSVE(I,MISS,3)=SURSVE(I,MISS,3)+REL2
60 CONTINUE
RETURN
END

```



# REFERENCES

1. *Structural Life Prediction and Analysis Technology Program Logic Manual*, Report No. FR-10895, Air Force Contract F33615-75-C-2063, October 30, 1978.
2. *Structural Life Prediction and Analysis Technology Input Manual*, Air Force Contract F33615-75-C-2063, October 30, 1978.
3. *Phase I Interim Technical Report; Structural Life Prediction and Analysis Technology*, Report No. FR-8396, Air Force Contract F33615-75-C-2063, February 28, 1977.
4. Neüber, H., "Theory of Stress Concentration for Shear Strained Prismatic Bodies With Arbitrary Nonlinear Stress Strain Law" *Journal of Applied Mechanics*, Transactions of the ASME, pp 544-550, December 1961.
5. Manson, S. S., "Application of a Double Linear Damage Rule to Cumulative Fatigue," NASA Technical Manual X-52226.
6. Miner, M. A., "Cumulative Damage Fatigue," *Journal of Applied Mechanics*, Volume 12, pp A159 - A164, 1945.
7. Schütz, W., "Schwingfestigkeit von vier Triebwerksoffen bei Betriebstemperatur, Low Cycle Fatigue," *Industrieanlagen - Betriebsgesellschaft mbH (IABG)*, IABG Auftrag Nr. 142 2645 01 (1975).
8. Chaboche, T. L., "Une Loi Differentielle Dendommagement de Fatigue avec Cumulation non Lineaire," *Revue Francaise de Mecanique*, No. 50-51, pp 71-84, 1974.
9. Wetzel, R. M., Editor, *Fatigue Under Complex Loading: Analyses and Experiments* The Society of Automotive Engineers, Inc., Warrendale, Pa., 1977.
10. Dowling, N. E., Brose, W. R. and Wilson, W. K., "Notched Member Fatigue Life Predictions by the Local Strain Approach," in *Fatigue Under Complex Loading: Analyses and Experiments*, The Society of Automotive Engineers, Inc., pp. 55-84, 1977.
11. Cruse, T. A., Gemma, A. E., Lacroix, R. F. and Meyer, T. G., "Surface Crack Life Prediction: An Overview, Part-Through Cracking," ASTM STP (to appear).
12. Forsyth, P. J. E., *The Physical Basis of Metal Fatigue*, pp. 31-32, American Elsevier Publishing Co., New York, 1969.
13. Manson, S. S., Freche, J. C. and Ensign, C. R., "Application of a Double Linear Damage Rule to Cumulative Fatigue," NASA TN D-3839, 1966.
14. Miller, I. and Freund, J. E., *Probability and Statistics for Engineers*, Prentice-Hall, Inc., Englewood Cliffs, N.J., 1965.
15. Lemon, G. H., "Statistical Consideration for Structural Reliability Analysis," in *Proceedings of the Colloquium on Structural Reliability: The Impact of Advanced Materials on Engineering Design*, ed. J. T. Swidlow, T. A. Cruise and J. C. Halpin, pp. 9-12, October 1972.

# DISTRIBUTION LIST

Detroit Diesel Allison  
Attn: Dr. M. Doner  
Indianapolis Operations  
P.O. Box 894  
Indianapolis, IN 46206

General Electric Co.  
Attn: Mr. A. Coles  
Mail Drop K-69  
Aircraft Engine Group  
Cincinnati, Ohio 45215

Garret AiResearch  
Attn: Mr. D. J. Tree  
402 S. 36th St.  
P. O. Box 5217  
Phoenix, AZ 85010

AFAPL/TBP  
Wright-Patterson Air Force Base, Ohio 45433  
Attn: Mr. D. Hill (15 cys)

ASD/YZEA  
Bldg. 125  
Wright-Patterson Air Force Base, Ohio 45433  
Attn: Mr. J. Ogg

AFFDL/FBE  
Wright-Patterson Air Force Base, Ohio 45433  
Attn: Mr. Frank Adams

AFML/LLN  
Wright-Patterson Air Force Base, Ohio 45433  
(1) Attn: Mr. D. E. Macha  
(1) Attn: Dr. W. H. Reimann

Naval Air Propulsion Test Center  
Mail Station PE-42  
Trenton, N. J. 08628  
Attn: Mr. G. Mangano

Mr. M. H. Hirschberg 49-1  
NASA Lewis Research Center  
21000 Brookpark Rd.  
Cleveland, Ohio 44135

Teledyne CAE  
Box 6971  
Toledo, OH 43612  
Attn: Mr. Tom D. Moyer

Boeing  
Box 3999  
MS 41-37  
Renton, WA 98124  
Attn: Dr. Magne N. Aarnes

Teledyne CAE  
Box 6971  
Toledo, OH 43612  
Attn: Mr. Robert Beck

Mar-Test  
45 Novner Dr.  
Cincinnati, OH 45215  
Attn: Dr. Joseph B. Conway

Matl's Research & Engrng  
Detroit Diesel Allison  
Box 894 - W5  
Indianapolis, IN 46206  
Attn: Dr. Mehmet Doner

Matl's Div MS-188M  
NASA-Langley  
Hampton, VA 23665  
Attn: Herbert F. Hardrath

J. Lane (SAVDL-EU-TAPP)  
Eustis Directorate  
AR&TL  
Fort Eustis, VA 23604

General Electric  
1C41-K1 Corp R&D Ctr  
Box 8  
Schenectady, NY 12301  
Attn: Dr. Louis F. Coffin, Jr.

P&WA - United Tech Corp  
Engineering Bldg - 3S3  
400 Main St  
E. Hartford, CT 06108  
Attn: Dr. Thomas A. Curse

General Electric  
Aircraft Engine Group K-59  
Cincinnati, OH 45215  
Attn: Anton Coles

University of Dayton  
Research Institute  
Rm 563 Kettering Bldg  
Dayton, OH 45469  
Attn: Dr. Joseph P. Gallagher

Univ of Ill  
321A Talbot Lab  
Urbana, IL 61801  
Attn: Prof JoDean Morrow

General Electric Mail Stop M-87  
MPTL - AEG  
Evendale, OH 45215  
Attn: Herbert G. Popp

Penn State Univ  
121 Hammond Blad  
University Park, PA 16802  
Attn: Prof Sam Zamrik

Southwest Research  
Assistant Director  
P.O. Drawer 28510  
San Antonio, TX 78284  
Attn: Dr. Clifford H. Wells

AiResearch  
402 S. 36th St.  
Phoenix, AZ 85034  
Attn: R. R. Van Nimwegen

CWRU  
619 Glennan Bldg.  
10900 Euclid Ave  
Cleveland, OH 44106  
Attn: Prof S. S. Manson

P&WA - United Tech Corp  
Box 2691, Loc B-08  
W. Palm Beach, FL 33402  
Attn: Marvin C. VanWanderham

P&WA - United Tech Corp  
Box 2691, Loc B-08  
W. Palm Beach, FL 33402  
ATTN: John A. Harris

AiResearch  
111 S. 34th St  
Box 5217  
Phoenix, AZ 85010  
Attn: Nick M. Hughes

NASA - Lewis Research Ctr  
MS 105-1  
Cleveland, OH 44135  
Attn: Chief, Matl's Appl Br

NASA - Lewis Research Ctr  
MS 105-1  
Cleveland, OH 44135  
Chief, Fracture Branch

Techn Info Ctr  
AEG  
General Electric Co  
Cincinnati, OH 45215

Library  
Detroit Diesel Allison  
340 White Rover Pkwy  
Indianapolis, IN 46206

Technical Library  
AR&TL  
Fort Eustis, VA 23604

General Electric - Mgr EM&LM  
Mail Drop K-221  
Evendale, OH 45215  
Attn: Dr. Len Beitch

P&WA - United Tech Corp  
Box 2691, Loc B-08  
W. Palm Beach, FL 33402  
Attn: Chuck Annis

ASD/YZEA  
Attn: D. Anderson  
Wright-Patterson Air Force Base, OH 45433

AFAPL/STINFO  
WPAFB, OH 45433

AFAPL/CCN  
WPAFB, OH 45433

AFAL/TSR  
WPAFB, OH 45433

Air University Library  
Maxwell AFB, Ala. 36112

DDC/DDA (2)  
CAMERON STATION  
ALEXANDRIA, VA. 22314